Schweizerische Eidgenossenschaft
Confédération suisse
Confederazione Svizzera
Confederaziun svizra

Eidgenössisches Departement für Umwelt, Verkehr, Energie und Kommunikation UVEK
Département fédéral de l'environnement, des transports, de l'énergie et de la communication DETEC
Dipartimento federale dell'ambiente, dei trasporti, dell'energia e delle comunicazioni DATEC

Bundesamt für Strassen
Office fédéral des routes
Ufficio federale delle Strade

Research Package on Bridge-deck Waterproofing Systems: EP5-Mechanisms of Blister Formation

Forschungspaket Brückenabdichtungen: EP5 - Mechanismen der Blasenbildung

Paquet de recherché étanchéité de ponts : EP5 - mécanismes de formation de cloques

KTH, Division of Highway Engineering
Prof. Dr. Manfred N. Partl
Biruk Hailesilassie

Forschungsprojekt VSS 2006/515_OBF auf Antrag des Schweizerischen Verbandes der Strassen-und Verkehrsfachleute (VSS)

November 2014 **1503**

Schweizerische Eidgenossenschaft
Confédération suisse
Confederazione Svizzera
Confederaziun svizra

Eidgenössisches Departement für Umwelt, Verkehr, Energie und Kommunikation UVEK
Département fédéral de l'environnement, des transports, de l'énergie et de la communication DETEC
Dipartimento federale dell'ambiente, dei trasporti, dell'energia e delle comunicazioni DATEC

Bundesamt für Strassen
Office fédéral des routes
Ufficio federale delle Strade

Research Package on Bridge-deck Waterproofing Systems: EP5-Mechanisms of Blister Formation

Forschungspaket Brückenabdichtungen: EP5 - Mechanismen der Blasenbildung

Paquet de recherché étanchéité de ponts : EP5 - mécanismes de formation de cloques

KTH, Division of Highway Engineering
Prof. Dr. Manfred N. Partl
Biruk Hailesilassie

VSS 2006/515_OBF auf Antrag des Schweizerischen Verbandes der Strassen-und Verkehrsfachleute (VSS)

November 2014 **1503**

Impressum

Forschungsstelle und Projektteam

Projektleitung
Prof. Dr. Manfred N. Partl

Mitglieder
Hailesilassie Biruk

Federführende Fachkommission

Fachkommission 5: Bautechnik

Gesamtprojektleiter

Remy Gubler

Begleitkommission

Präsident, Gesamtprojekt
Hans Hürzeler

Mitglieder, Gesamtprojekt
Heinz Aeschlimann
Harry Fehlmann
Kurt Frei
Jean-Christoph Putallaz
Hans Wahlen
Jean-Marc Waeber

Präsident, Einzelprojekt
Angst Dr. Christian

Mitglieder, Einzelprojekt
Michel Pittet
Reto Bühler
Yvan Ramel
Max Seeberger
Felix Solcà

Antragsteller

Schweizerischen Verbandes der Strassen-und Verkehrsfachleute (VSS)

Bezugsquelle

Das Dokument kann kostenlos von http://www.mobilityplatform.ch heruntergeladen werden

Inhaltsverzeichnis

Zusammenfassung

Kurzzeit-Blasen können beim Einbau von heissem Gussasphalt infolge feuchter Luft im Inneren von Asphalt Mischung entstehen. Solche Blasen werden in der Praxis häufig durch Aufstechen der Blasen mittels einer Stahlstange zur Druckentlastung eliminiert. Diese bedenkliche Vorgehensweise ist allgemein Ausdruck von Qualitätsproblemen bei Material oder Einbau. Da es praktisch unmöglich ist, den gesamten Druck durch Aufstechen von Blasen abzubauen, können einzelne Blasen während dem Abkühlen quasi „eingefroren" werden, wobei die eingeschlossene Luft als Auslöser für die Bildung von Langzeit-Blasen wirken kann, die sukzessive unter Betriebsbedingungen wachsen können. Die vorliegende Forschungsarbeit gliedert sich in zwei Teile. Im ersten Teil wird die Blasenbildung unter Gussasphalt auf Betonuntergrund untersucht. Der zweite Teil ist der Blasenbildung unter Dichtungsbahnen gewidmet.

Hauptziel des ersten Teils ist die Entwicklung eines Finite-Element-Modelles, welche das Wachstum von Blasen unter dem Aspekt der Langzeitblasenbildung simuliert. Dies beinhaltet die Untersuchung des Blasenwachstums im Labor mittels Finite-Element-Modellierung im Vergleich zur Schubverformungs-Theorie erster Ordnung an dicken Platten unter besonderer Berücksichtigung von Gussasphalt. Dazu gehört auch der Einfluss zyklischer Veränderungen von Temperatur und Blasendruck auf das Blasenwachstum (viskoelastische dicke Platte) bei linearer Variation von Temperatur und Druck. Als Grundlage für künftige weitere Forschung wird zusätzlich ein vereinfachtes Modell zur Beschreibung des Blasenwachstums bei konstantem Blasenradius unter Berücksichtigung der viskoelastischen Eigenschaften von Gussasphalt eingeführt.

Die zeitabhängige vertikale Verformung von Gussasphalt-Blasen hängt von drei Faktoren ab: Den Materialcharakteristika für die Modellierung, der Temperatur des Gussasphalts im Zeitpunkt der Belastung sowie der Geschwindigkeit des Druckaufbaus in der Blase. Es wurde festgestellt, dass das vertikale Blasenwachstum von Gussasphalt deutlich stärker von der Geschwindigkeit der Temperaturänderung als vom Blasendruck beeinflusst wird. Dabei zeigten Simulationsberechnungen der Blasenbildung über einen Zeitraum von 12 Stunden, dass sowohl ein langsam aufgebrachter, gleichförmig verteilter Blasendruck als auch eine langsame Temperaturänderung geringere vertikale Deformationen bewirken. Bei konstantem Blasendruck (p_0=7.12 •10^{-06} MPa) aufgebrachter zyklischer Temperaturänderung wird das vertikale Blasenwachstum stark von der Temperaturabhängigkeit des Materials beeinflusst. Ein konstanter Gasdruck im Blaseninneren kann daher bei steigender Temperatur deutliches Blasenwachstum verursachen. Demgegenüber ist bei konstanter Temperatur (T=25 °C) und zyklischem Blasendruck das Blasenwachstum deutlich geringer, da die Steifigkeit von Gussasphalt ausreicht, um Änderungen des Blasendruckes zu widerstehen. Bei Berücksichtigung des Gussasphaltgewichts in den Simulationsberechnungen wäre das Blasenwachstum sogar noch kleiner.

Durch Simulation aufeinanderfolgender Heiz- und Kühlzyklen wurde festgestellt, dass sich die täglichen Temperaturschwankungen deutlich auf das Blasenwachstum in Asphaltbelägen auswirken. Während der Entlastung, wenn Blasendruck und Temperatur abnehmen, wachsen Blasen mit geringerer Geschwindigkeit weiter. Gemäss Simulationsberechnungen können Blasen kontinuierlich unter wechselnden Belastungsbedingungen während mehrerer Tage wachsen.

Der zweite Teil und Schwerpunkt dieser Arbeit galt der Untersuchung und Modellierung der adhäsiven Blasenausbreitung zwischen einer orthotropen Polymerbitumen-Dichtungsbahn (PBM) und Beton. Dies schliesst die Formulierung eines elastischen Modells ein, welches die Ausbreitung des adhäsiven Haftverlustes bei Blasenbildung infolge kontrollierten Drucks zwischen PBM und Betonplatten beschreibt (d.h. Riss-Modus I gemäss Bruchmechanik). Das Modell beruht auf der Annahme, dass die PBM als orthotropes Material angenähert werden kann, welches einem ebenen Spannungszustand unterliegt. Ein weiteres Ziel war die Bestimmung der Energie für eine elliptische adhäsive Bla-

senausbreitung. Um dies zu erreichen, wurde zunächst das orthotrope Materialverhalten einer SBS modifizierten Dichtungsbahn im ebenen Zugspannungszustand mittels biaxialer Zugversuche bestimmt. Eine solche Belastung erlaubt nämlich die Berücksichtigung eines biaxialen Spannungszustandes, wie er sich während der Blasenbildung einstellt. Die gemessenen Spannungs-Dehnungsdaten wurden mittels orthotroper elastischer Gleichung analysiert, um die Materialeigenschaften in Längs- und Querrichtung zu bestimmen. Schliesslich wurden Blasen-Tests auf Betonplatten durchgeführt, um die adhäsive Blasenausbreitung infolge konstanten kontrollierten Drucks zwischen PBM und der Betonplatte experimentell zu studieren. Als Ergebnis wurde ein neues Modell vorgeschlagen, welches es ermöglicht, die entsprechende Energie für die adhäsive Blasenausbreitung zu bestimmen.

Die durchgeführten Arbeiten zeigten, dass biaxiale Tests ein nützliches Mittel sind, um die mechanischen Eigenschaften orthotroper Polymerbitumen-Dichtungsbahnen unter mehrachsigem ebenen Spannungszustand zu erfassen und die elastischen Materialcharakteristika zur Berechnung der elliptischen adhäsiven Blasenwachstumsenergie zu bestimmen. Unter Annahme eines ebenen Spannungszustandes führen die orthotropen Eigenschaften von PBM zu einer elliptischen Rissausbreitungsfront, die sich entsprechend von jener des klassischen kreisförmigen Blasenwachstums unterscheidet. Nimmt man ferner an, dass die Adhäsion zwischen Betonuntergrund und PBM gleichförmig ist, folgt daraus, dass die Vertikalspannung an der elliptischen Rissausbreitungsfront konstant sein muss, damit die elliptische Form der Blasenausbreitungsfront und damit die elliptische Rissausbreitung beibehalten werden kann.

In der Realität dürfte das Blasenwachstum auf Dampfdruck unter der PBM zurückzuführen sein. Daher ist die Dichtungsbahn einer mehrachsigen Beanspruchung ausgesetzt. Im Gegensatz zum sog. Membran Adhäsion Test (MAT) der technischen Universität in Delft, wobei die Dichtungsbahn einem einachsigen Spannungszustand ausgesetzt ist und das Haftverhalten nur in einer Richtung untersucht wird, weist der Blasentest den Vorteil auf, dass die Blasenbildung unter Berücksichtigung des multiaxialen Spannungszustands simuliert wird und die Energie der Blasenausbreitung auch in orthotropen Fällen bestimmt werden kann. Da in diesen Fällen die Materialeigenschaften in Längs- und Querrichtung unterschiedlich sind, kann somit eine Anwendung des MAT Tests für orthotrope Dichtungsbahnen zu unterschiedlichen Resultaten führen. Blasenwachstum-Prüfungen mit konstantem Wasserdruck ergaben, dass die Blasenausbreitung in Längs- und Querrichtung proportional zum Verhältnis der Elastizitätsmoduli in den entsprechenden Richtungen ist. Die Ellipsengleichung für den Elastizitätsmodul senkrecht zur adhäsiven Bruchfront erwies sich im Falle der Blasenbildung als gute Näherung für die komplexe Orthotropie-Gleichung. Die elliptische Modulgleichung vereinfacht nämlich die Lösung des Problems ohne Verlust der orthotropen Materialeigenschaften des allgemeinen ebenen Spannungszustands. Zu beachten ist auch, dass die Vertikalkomponente der Normalspannung an der Rissausbreitungsfront konstant und unabhängig von der Richtung im Material ist. Mit diesen Erkenntnissen und unter der Annahme linear elastischen Verhaltens war es somit möglich, eine Näherungsgleichung für die Energie der adhäsiven Rissausbreitung bei dünnen PBMs zu entwickeln.

In einem weiteren Schritt wurde die Energie der Blasenausbreitung mit der Schälzugmethode gemäss Schweizer Norm und der Bruchenergie aus der Literatur verglichen. Drei verschiedene PMB-Arten wurden untersucht, einschliesslich eines Vergleiches einachsiger und biaxialer Tests zur Bestimmung des Elastizitätsmoduls der Dichtungsbahnen. Auch wurde der Einfluss der Verschiebungsgeschwindigkeit und Temperatur auf die Adhäsionsbruch-Energie für den Schälzugversuch untersucht. Ein anderes Ziel bestand darin, ein neues Modell für die Energie der adhäsiven Blasenausbreitung mit den in der Literatur angegebenen Gleichungen für die Bruchenergie bei Schälzug zu vergleichen. Damit sollte die Rissausbreitung bei Blasenbildung auf der Betonoberfläche mit dem Schälzugtest in Verbindung gebracht werden. Dies nicht zuletzt auch darum, um zwischen den Hafteigenschaften verschiedener Dichtungsbahnen, namentlich ihres Widerstandes gegen Blasenbildung, unterscheiden zu können, ohne die zeitraubende und aufwändige Prüfung der Blasenausbreitung unter Druck mit digitalen Bildanalyseverfahren durchführen zu müssen. Die Untersuchung erstreckte sich auf die Prüfung einer als SBS-1 bezeichneten Dichtungsbahn unter einachsigem Zug bei 23°C, 40°C und 55°C und Verschiebungsgeschwindigkeiten in Längsrichtung von 50mm/min, 75mm/min und 100mm/min. Die einachsige Prüfung von SBS-1 bei 23°C und 50mm/min wurde mit der biaxialen Prüfung verglichen, um festzustellen, ob beide Prüfbedingungen ähnliche Spannungs-Dehnungs-Kurven und Elastizitätsmoduli liefern. Jeweils drei Prüfkörper wurden uniaxialer und biaxialer Beanspruchung ausgesetzt. Anschliessend wurden einachsige Prüfungen an SBS-1, SBS-2 und APP Dichtungsbahnen bei 23°C und 50mm/min in Längs- und Querrichtung zur Bestimmung des jeweiligen Elastizitätsmoduls durchgeführt. Zusätzlich wurden mit der Dichtungsbahn SBS-1 bei 23°C, 40°C und 55°C Schälzugprüfungen mit Geschwindigkeiten von 50mm/min, 75mm/min und 100mm/min durchgeführt, um den Einfluss von Temperatur und Verschiebungsgeschwindigkeit auf die Bruchenergie bei Schälzug zu untersuchen. In Längsrichtung wurde zudem die Schälzugenergie bei 23°C für SBS-1, SBS-2 und APP Dichtungsbahnen bestimmt. Ferner wurden Blasenprüfungen bei 23°C unter kontrolliertem Druck bei SBS-1, SBS-2 und APP durchgeführt. Der Druck wurde auf 0.2 MPa eingestellt. Blasenhöhe und Blasenausbreitung in Längs- und Querrichtung wurden mittels 3D Bildanalysesystem ermittelt. Schliesslich wurde die Energie der Blasenausbreitung mit der Bruchenergie der Schälzugprüfungen verglichen.

Allfällige Blasenbildung findet meist durch Akkumulierung von Dampfdruck zwischen Dichtungsbahn und Gussasphalt oder unter der PBM statt. Somit erzeugt der Druck einen multiaxialen Spannungszustand in der PBM, die ja orthogonale Materialeigenschaften aufweist. Die Ergebnisse der Bruchenergie der Schälzugprüfung aller drei Dichtungsbahnen lassen erkennen, dass die Energie der Blasenausbreitung im Bereich der Schälzugenergie liegt. Ein Vergleich der Bruchenergien beider Prüfungen zeigt, dass das entwikkelte Modell sowohl Ausbreitung als auch Wachstum von Blasen gut zu beschreiben vermag. Dessen ungeachtet bleibt jedoch festzustellen, dass die Durchführung von Blasenprüfungen zu Untersuchung der Verbundeigenschaften von PBMs schwierig und zeitraubend sein kann, da die Modellparameter, die das Ergebnis beeinflussen können, mit besonderer Sorgfalt zu bestimmen sind. Mittels Schälzugprüfung in Kombination mit einachsigen Prüfungen ist es möglich, die ermittelten Schälzugkräfte bezüglich Bruchenergie von PBM's bei Schälzug zu interpretieren. Dank der Korrelation zwischen den Bruchenergien von Schälzug und Blasentest ist es also möglich, die Anfälligkeit gegenüber Blasenausbreitung mittels Schälzug zu bewerten. Da die Bruchenergie bei Schälzug nur eine sehr geringe Beeinflussung von der Geschwindigkeit der Ausbreitungsgeschwindigkeit erfuhr, kann dies als Bestätigung dafür gewertet werden, dass die Vergleichbarkeit der Schälzug- und Blasenwachstums-Energie weniger durch die Verformungsgeschwindigkeit als durch die Prüftemperatur beeinflusst wird.

Die ermittelten Elastizitätsmoduli der PBMs der vorliegenden Untersuchung weisen darauf hin, dass im Falle von SBS die biaxiale Zugprüfung und der normierte einachsige Zugversuch im elastischen Bereich vergleichbare Spannungs-Dehnungs-Kurven liefern. Tatsächlich verlief die äquivalente Spannungs-Dehnungs-Kurve der biaxialen Prüfung ähnlich wie die einachsige Spannungs-Dehnungskurve in Längsrichtung. Daraus wurde geschlossen, dass zur Bestimmung des Materialverhaltens im elastischen Bereich biaxiale Prüfungen keinen Vorteil gegenüber einachsigen Prüfungen bieten.

Résumé

Des cloques, dites « cloques à court-terme », apparaissent lors de la mise en oeuvre d'asphalte coulé à chaud et sont dues à l'air humide piégé dans le mélange bitumineux. Dans la pratique, de telles cloques sont souvent enlevées en les perçant au moyen d'une tige en acier afin de libérer la pression. Cette pratique douteuse est généralement le signe d'un problème de qualité qui est en lien soit avec le matériau soit avec la mise en œuvre. Etant donné qu'il est pratiquement impossible de libérer toute la pression en perçant les cloques, certaines de ces dernières, notamment parmi les plus petites, peuvent se retrouver en quelque sorte « gelées » pendant le processus de refroidissement et l'air piégé peut agir en tant que déclencheur de la formation de cloques, dites 'cloques à long-terme', qui ont graduellement tendance à se croître sous conditions de service. Le présent travail de recherche comporte deux parties. En premier lieu, la formation de cloques sous la couche d'asphalte coulé posée sur le support en béton est examinée. La seconde partie est consacrée à la formation de cloques sous les membranes d'étanchéité.

Le principal objectif de la première partie de l'étude est de développer un modèle d'éléments finis simulant la croissance d'une cloque, en se concentrant sur la formation de cloques à long-terme. Cette tâche comprend l'analyse en laboratoire de la croissance d'une cloque à l'aide d'une simulation utilisant les éléments finis, en se focalisant sur la formation de cloques dans l'asphalte coulé ainsi que sur la théorie de la déformation de premier ordre sous cisaillement des plaques épaisses. L'analyse inclut également l'influence des fluctuations de température et de pression sur la croissance d'une cloque (plaque épaisse viscoélastique) pour des variations linéaires de température et de pression. A titre de base pour de futures recherches, il est en outre établi un modèle simplifié pouvant simuler la croissance d'une cloque de rayon constant, en considérant les propriétés viscoélastiques de l'asphalte coulé.

Dépendante du temps, la déformation verticale des cloques se formant dans les asphaltes coulés est fonction de trois facteurs : la caractérisation du matériau dans le modèle, la température de l'asphalte coulé au moment de l'application de la charge et la vitesse d'application de la charge sur le matériau. Il a ainsi été constaté que la déformation verticale de l'asphalte coulé dépend bien plus de la vitesse du changement de température appliqué que de la pression appliquée. Au cours d'une simulation effectuée sur une durée de douze heures, les calculs effectués ont montré qu'une pression lentement et uniformément appliquée aussi bien qu'une lente variation de température provoquaient de plus petites déformations verticales. Dans le cas de l'application d'une pression constante (p_0=7.12 $\cdot 10^{-06}$ MPa) et d'une température variable, la dépendance du matériau à la température avait une importance significative sur la déformation verticale de la cloque. Ceci indique qu'une pression constante du gaz à l'intérieur de la cloque peut, lorsque la température croît, produire une augmentation importante de la croissance de la cloque. Lorsque la température est constante (T=25°C) et que la pression varie de manière cyclique, la croissance de la cloque est par contre bien moindre que dans le cas précédent, du fait que l'asphalte coulé possède une rigidité suffisante pour résister aux changements de pression. En fait, la déformation serait même inférieure si le poids de l'asphalte coulé était inclus dans la simulation.

Une simulation de cycles consécutifs de chauffage et de refroidissement a permis de remarquer que les variations journalières de la température ambiante ont une influence considérable sur la croissance des cloques dans les revêtements en asphalte. En phase de déchargement, lorsque la pression et la température diminuent, la cloque continue à croître à une vitesse inférieure. Les calculs effectués lors de la simulation indiquent que la cloque peut croître de manière continue durant plusieurs jours sous conditions répétées de chargement.

Dans la seconde partie de l'étude, l'objectif principal était d'analyser et de modéliser la propagation d'une cloque adhésive entre une membrane orthotrope en bitume modifié avec du polymère (PBM) et le béton. Cette étape inclut la formulation d'un modèle élastique qui décrit la propagation de la perte d'adhérence d'une cloque adhésive PBM (c'est-

à-dire le mode I de fracturation mécanique), en appliquant une pression contrôlée entre le PBM et les plaques en béton. L'hypothèse faite pour la formulation du modèle est que la membrane PBM est assimilée à un matériau orthotrope, soumis à un état de contraintes dans le plan. L'objectif consiste également à déterminer l'énergie nécessaire à la propagation elliptique d'une cloque adhésive. Pour atteindre ces objectifs, le comportement mécanique orthotrope, sous contrainte de tension dans le plan, d'une membrane en bitume modifié avec du polymère SBS a en premier lieu été déterminé à partir des données d'essais biaxiaux. L'application d'une charge de traction biaxiale permet l'examen de l'état de contrainte biaxiale qui règne durant la croissance de la cloque. Les données de contrainte-déformation mesurées ont donc été analysées en utilisant l'équation élastique orthotrope afin de déterminer les propriétés du matériau dans le sens longitudinal et transversal. Enfin, des tests de cloquage ont été réalisés sur des plaques de béton pour étudier expérimentalement la propagation d'une cloque adhésive, en appliquant une pression d'eau contrôlée et constante entre la PBM et les plaques de béton. Le résultat en est la proposition d'un nouveau modèle permettant de déterminer l'énergie correspondante de propagation de la cloque adhésive.

Le résultat des travaux réalisés dans le cadre de cette étude est que les tests biaxiaux servant à déterminer les propriétés mécaniques de membranes orthotropes en bitume modifié avec du polymère (PBM) sous état de contraintes multiaxiales dans le plan sont utiles pour caractériser les propriétés des matériaux élastiques afin de calculer l'énergie de propagation elliptique d'une cloque adhésive. La propriété orthotrope de contrainte plane du matériau PBM induit une propagation des fissures dans la cloque ayant un front elliptique, un mode de propagation différent du cas général de la croissance circulaire d'une cloque. Dans l'hypothèse d'une adhérence uniforme entre le support en béton et la PBM, la contrainte verticale dans la membrane doit être constante sur tout le pourtour de la fissure elliptique pour que soit conservée la forme elliptique du front de propagation de la cloque, à défaut de quoi la propagation elliptique de la fissuration ne seraient pas possibles.

Dans la réalité, la croissance de la cloque pourrait se produire en raison de la pression de vapeur créée sous la PBM. La membrane est par conséquent exposée à un état de contrainte multiaxial. Contrairement au Test d'Adhérence de la Membrane (MAT) proposé par la TU Delft, qui soumet la membrane à un état de contrainte uniaxial et analyse le comportement à l'adhérence dans une direction, le test de cloquage présente l'avantage de simuler la formation de la cloque en considérant un état de contrainte multiaxial et de permettre de déterminer l'énergie de propagation de la cloque également dans les cas orthotropes. L'utilisation de l'essai MAT pour des matériaux orthotropes peut conduire à des résultats différents puisque les propriétés du matériau dans le sens longitudinal et transversal diffèrent. Les tests de cloquage réalisés sous une pression d'eau constante ont montré que la propagation de la cloque dans les directions longitudinale et transversale est proportionnelle au rapport du module d'élasticité dans les directions respectives. L'équation elliptique pour le module d'élasticité perpendiculaire au front adhésif elliptique de rupture s'est, dans le traitement de la formation des cloques, avérée comme étant une bonne approximation de l'équation complexe orthotrope. L'équation de module elliptique simplifie en fait l'analyse du problème, sans que soient perdues les propriétés générales du matériau dans le cas d'un état de contraintes dans le plan. La composante verticale de la contrainte normale à l'endroit du front de propagation de la fissure est constante et indépendante de l'orientation dans le matériau. A l'aide de ces conclusions et en admettant l'hypothèse d'un comportement élastique linéaire, il est possible de fournir une équation approximative pour l'énergie de propagation d'une cloque adhésive dans le cas de membranes minces PMB.

Dans un deuxième temps, l'énergie analytique de propagation de la cloque a été comparée à l'essai de pelage standard décrit dans les normes suisses et à l'énergie de rupture adhésive telle qu'elle ressort de la littérature. Trois types de membranes en bitume modifié avec du polymère (PBM) ont été utilisés pour cette étude. L'étude comprend la comparaison entre le test uniaxial et le test biaxial afin de déterminer le module d'élasticité des membranes. L'influence de la vitesse de déplacement et de la température sur l'énergie de la rupture adhésive est également étudiée dans le test de pelage. L'autre objectif est de comparer un nouveau modèle permettant de déterminer l'énergie de propagation d'une cloque adhésive avec les équations de l'énergie de fracture pour le pelage que l'on retrouve dans la littérature. Cela permet en finalité de comprendre la propagation des fissures de la cloque à la surface du béton et de la mettre en relation avec le test de pelage. Cela permet également de faire la distinction entre les propriétés adhésives de différents types de membranes et leur résistance à la formation de cloques, sans devoir procéder aux longs et compliqués essais sous pression de propagation des cloques au moyen de techniques de corrélation d'images numériques. L'étude inclut des essais sur une membrane d'étanchéité SBS-1, en effectuant un essai de traction uniaxiale à 23°C, 40°C et 55°C en combinaison avec des vitesses de déplacement de 50, 75 et 100 mm / min dans la direction longitudinale. L'essai uniaxial effectué pour la SBS-1 à une température de 23°C et une vitesse de déplacement de 50 mm / min est comparé à un test bi axial, afin de vérifier si les conditions sous lesquelles sont effectués les deux tests livrent des courbes de contrainte-déformation et des modules d'élasticité similaires. Trois échantillons ont à chaque fois été testés, à la fois en uniaxial et en biaxial. L'essai uniaxial est ensuite réalisé sur des membranes d'étanchéité SBS- 1, SBS -2 et APP à une température de 23°C et une vitesse de déplacement de 50 mm / min dans les directions longitudinales et transversales, afin de déterminer le module d'élasticité dans les directions respectives. De plus, le test de pelage a été effectué pour une membrane d'étanchéité SBS-1 à des températures de 23°C , 40°C et 55°C et des vitesses de déplacement de 50, 75 et 100 mm/min, afin de comprendre l'influence de la température et de la vitesse de déplacement sur l'énergie de rupture lors du pelage. Un essai de pelage a été effectué dans la direction longitudinale, à une température de 23°C, sur des membranes SBS- 1, SBS-2 et APP pour déterminer l'énergie de rupture lors du pelage. Le test de cloquage est réalisé sur des membranes d'étanchéité SBS-1, SBS-2 et APP à 23 ° C, sous pression contrôlée. La pression est réglée à 0,2 MPa durant le test. La hauteur de la cloque et la propagation de la fissuration dans les directions longitudinales et transversales sont mesurées en utilisant le système de corrélation d'images 3D. Enfin, l'énergie de propagation de la cloque est comparée à l'énergie de rupture obtenue lors de l'essai de pelage.

Dans la plupart des cas, le cloquage se produit vraisemblablement suite à une accumulation de pression de vapeur entre la PBM et l'asphalte coulé ou sous la PBM. La pression crée donc un état de contrainte multiaxial dans la PBM, qui possède la propriété d'un matériau orthotrope. Pour les trois membranes, les résultats relatifs à l'énergie de rupture obtenus à partir de l'essai de pelage ont montré que l'énergie de propagation de la cloque se situe dans la zone de l'énergie de rupture par pelage. La comparaison de l'énergie de fracture entre les deux méthodes a indiqué que le nouveau modèle fonctionnait bien pour la modélisation de la croissance et de la propagation de la cloque. La conduite de l'essai de cloquage, afin d'analyser la propriété adhésive de la PBM, peut néanmoins être difficile et prendre du temps car une attention certaine doit être portée aux différents paramètres qui existent dans le modèle et qui peuvent influer sur le résultat. En effectuant l'essai de pelage et l'essai uniaxial, il est possible d'interpréter la force de pelage en termes d'énergie de rupture par pelage de la PBM. La prise en compte de la corrélation entre l'énergie de rupture obtenue avec l'essai de pelage respectivement avec l'essai de cloquage rend par conséquent possible l'emploi de l'essai de pelage en tant que méthode d'investigation pour la propagation d'une cloque. Du fait que l'énergie de propagation de la fissure lors du pelage dépend très peu de la vitesse d'accroissement de la fissure, il se confirme que la comparaison entre l'énergie de fracture lors du pelage et l'énergie de propagation de la cloque sont moins influencées par la vitesse de déplacement lors du pelage que par la température à laquelle est réalisé l'essai.

Les modules d'élasticité de la PBM déterminés dans cette étude indiquent que, dans le cas de SBS, l'essai de traction biaxial et l'essai standard de traction uniaxial livrent des courbes contrainte-déformation comparables dans le domaine élastique. La courbe contrainte-déformation équivalente pour un essai biaxial était en fait similaire à la courbe contrainte-déformation uniaxiale dans le sens longitudinal. En conséquence et dans l'objectif de déterminer le comportement du matériau dans le domaine élastique, aucun avantage majeur n'a été trouvé dans l'emploi d'essais biaxiaux par rapport à celui d'essais uniaxiaux.

Summary

Short-term blisters occur during placing of hot mastic asphalt and result from humid air trapped in the asphalt mixture. These blisters are often removed in practice by punching a steel stick into the blister of the mixture to release pressure. This bad practice indicates a quality problem either in the material or construction process. Since it is practically impossible to release all pressure by punching through the blisters, some of the smaller blisters may get “frozen” during the cooling process and the trapped air may be the trigger for the formation of long term blisters that may gradually grow under service condition. This research work includes two parts, in the first part blister formation under the mastic asphalt layer is investigated alone. In the second part blister formation under the water proofing membrane is studied.

The primary objective of the first part of the study is to develop a finite element model, which simulates blister growth with focus on long term blistering. This includes investigation of blister growth in the laboratory with finite element simulation focusing on blistering of mastic asphalt and first order shear deformation of thick plates. It includes also investigating the influence of temperature and pressure fluctuation on blister growth (viscoelastic thick plate) for linearly varying temperature and pressure. In addition to this, a simplified model is established which can simulate blister growth for constant blister radius, considering the viscoelastic properties of the mastic asphalt, as a basis for future research.

The time dependent vertical deflection in mastic asphalt blisters depends on three factors: material characterization of the model, temperature of the mastic asphalt at the time of loading and the rate at which the load is applied to the material. It was found that vertical deflection of mastic asphalt is much more depending on the rate of the applied temperature than on the applied pressure. A 12 hour simulation showed that slower applied uniformly distributed pressure and temperature produces smaller vertical deflection. For constant pressure (p_0=7.12 $\cdot 10^{-06}$ MPa) and fluctuating temperature, the temperature dependency of the material had a great influence on the vertical deflection of the blister. This indicates that constant gas pressure inside the blister can produce significant amount of blister growth with increasing temperature. On the other hand, for constant temperature (T=25 °C) and fluctuating pressure, the blister growth is much less than in the previous case. This is due to the fact that the mastic asphalt has enough stiffness to resist pressure changes. In fact, deflection would even be less if the weight of the mastic asphalt was incorporated in the simulation.

From simulation of the consecutive cycles of heating and cooling, it was noticed that the daily temperature variations have a significant influence on blister growth in asphalt pavement. During the unloading process, i.e. when pressure and temperature decrease, the blister still grows at a slower rate. The simulation indicates that the blister can grow continuously under repeated loading conditions over subsequent days.

In the second part, the main objective was to investigate and model adhesive blister propagation between an orthotropic PBM and concrete. This includes formulating an elastic model which describes propagation of PBM adhesive blister debonding (i.e. fracture mechanical cracking mode I) by applying controlled pressure between the PBM and the concrete plates. The model is formulated assuming the membrane as orthotropic plane stress material. The objective also includes determining the energy for elliptical adhesive blister propagation. In order to achieve these objectives, first, the orthotropic mechanical behavior of an SBS polymer modified bitumen membrane under in-plane tension stress was determined from biaxial test data. The biaxial tensile loading allows consideration of the biaxial stress condition that exists during blister growth. Hence, the measured stress-strain data were analyzed using the orthotropic elastic equation to find the material properties in the longitudinal and transversal direction. Finally, blister tests were performed on concrete plates for studying adhesive blister propagation by applying controlled constant pressure between the PBM and the concrete plates and for proposing a

new model that allowed determining the corresponding adhesive blister propagation energy

From this study it was found that the biaxial tests for determining the mechanical properties of an orthotropic polymer modified bitumen membrane (PBM) in multi-axial plane stress state are useful to characterize the elastic material properties for calculating elliptical adhesive blister propagation energy. The plane stress orthotropic property of the PBM material creates blister crack propagation with an elliptical propagation front other than in the general case of circular blister growth. Under the assumption of uniform adhesion between the concrete substrate and the PBM, the vertical stress in the membrane must be constant around the elliptical crack front in order to keep the elliptical shape of the blister propagation front; otherwise elliptical adhesive crack propagation would not be possible.

In reality, blister growth might occur due to vapor pressure created beneath the PBM. Hence, the membrane is exposed to multi-axial stress state. Unlike the membrane adhesion test (MAT) by TU Delft, which captures the uniaxial stress state of a membrane and adhesive bonding behavior in one dimension, the blister test has the advantage of simulating the multi-axial stress state during blister formation, thus helping to determine blister propagation energy also in orthotropic cases. Applying the MAT test for orthotropic materials may produce different results since the material properties in the longitudinal and transversal direction are different. Blister tests with constant water pressure showed that the blister propagation in the longitudinal and transversal direction is proportional to the ratio of the moduli of elasticity in the respective direction. The elliptical equation for the elastic modulus normal to the elliptic adhesive failure front is a good approximation to the complex orthotropic equation in dealing with blistering. The elliptical modulus equation simplifies the analysis of the problem without losing the general orthotropic plane stress material properties. The vertical component of the normal stress at the crack failure front is constant and independent of the orientation of the material direction. With these finding and under the assumption of linear elastic behavior it is possible to provide an approximate equation for the adhesive blister propagation energy for thin PMBs.

Moreover the analytical blister propagation energy was compared with a standard peeling test method, as described in the Swiss standards, and the adhesive fracture energy from literature. Three different types of polymer modified bitumen membranes (PBMs) were used for this investigation. The investigation includes the comparison between the uniaxial and biaxial test for determining the modulus of elasticity of the membranes. Influence of the displacement rate and temperature on adhesive fracture energy is also investigated for the peeling test. The other objective was to compare a new model that allows determining the adhesive blister propagation energy with the fracture energy equations for peeling as proposed in literature. Finally, this helps to understand the blister crack propagation on top of the concrete surface and it's relation to the peeling test. It also helps to distinguish the adhesive properties of different types of membranes and their resistance to blister formation without conducting the time consuming and complicated pressurized blister propagation tests with digital image correlation techniques. The investigation includes testing of SBS-1 waterproofing membrane using uniaxial tension test at 23°C, 40°C and 55°C in combination with 50, 75 and 100 mm/min displacement rate in the longitudinal direction. The uniaxial test performed for SBS-1 at 23°C and 50 mm/min displacement rate is compared with the biaxial test to check if the two testing condition give similar stress-strain curves and moduli of elasticity. Three specimens each were tested in a uniaxial and biaxial experiment. After this, the uniaxial test is performed for SBS-1, SBS-2 and APP waterproofing membranes at 23°C and 50 mm/min displacement rate in the longitudinal and transversal direction to determine the modulus of elasticity in the respective direction. In addition to this, peeling test is performed for SBS-1 waterproofing membrane at 23°C, 40°C and 55°C in combination with 50, 75 and 100 mm/min displacement rate in order to understand the influence of the temperature and the displacement rate on the peeling fracture energy. Peeling test is done in the longitudinal direction at 23°C for SBS-1, SBS-2 and APP water proofing membranes to determine the peeling fracture energy. Blister test is performed on SBS-1, SBS-2 and APP waterproofing membranes at 23°C by applying a controlled pressure. The pressure was set to 0.2 MPa during the testing period. Blister height and crack propagation in the longitudinal and transversal direction is measured using 3D image correlation system. Finally the blister propagation energy is compared with the fracture energy from peeling tests.

In most cases blistering occurs possibly by steam pressure accumulation in between PBM and mastic asphalt or beneath the PBM. Hence the pressure creates a multi axial stress state in to the PBM which has an orthotropic material property. The results from peeling fracture energy of all the three membranes indicated that the blister propagation energy is within the range of peeling fracture energy. The fracture energy comparison between the two methods indicated that the blister propagation model approach works well for modeling blister growth and propagation. Nevertheless, conducting blister test to investigate the adhesive property of the PBMs can be difficult and time consuming since care has to be devoted to the parameters that exists in the model, which can influence the result. By conducting the peeling test and uniaxial test, it is possible to interpret the peeling force in terms of peeling fracture energy of the PBM. Therefore taking in to account the correlation between the fracture energy between the peeling and blister test, it is possible to use a peeling test as investigation method for blister propagation. Since the peeling crack propagation energy had very little dependency on the crack growth rate, this confirms that comparison between the peeling fracture energy and blister propagation energy is less influenced by the displacement rate than the testing temperature.

The moduli of elasticity of the PBM determined in this study indicated that in case of SBS, the biaxial extension and standard uniaxial tension test produce comparable strain-stress curve in the elastic range. The equivalent stress-strain curve from a biaxial experiment was similar to longitudinal direction uniaxial stress-strain curve. As a result, no major advantage was found in using the biaxial test over the uniaxial test to determine the material behavior in the elastic range.

1 Introduction

Bridges play a major part of a functional infrastructure. Increasing the durability of bridge infrastructure means less repair and therefore less materials and energy consumption. This has a direct positive impact on the general sustainable development of our society. Repair of bridges is extremely costly and can create congestions with environmental consequences and financial draw-backs for the users. Hence, loss of structural long-term integrity of bridges through corrosion is a mayor issue for road authorities from a safety, economic, environmental and sustainability point of view. Typically, these failures are often caused by interaction problems between the different materials of the waterproofing system itself as well as adhesion loss between mastic asphalt and the other waterproofing components of the system [1]. In many cases, this corrosion is triggered by blisters under the hot mix asphalt bridge deck pavement and secretly evolving during weather exposure until it is often detected too late. Applying hot mastic asphalt on concrete bridge decks with flexible polymer-bitumen waterproofing sheets may negatively affect the bond between concrete base and waterproofing sheet due to formation of blisters. These bonding imperfections are initially not visible because of the leveling effect of mastic asphalt. They indicate, weak areas promoting horizontal water penetration and are therefore putting at risk durability and functionality of the system at a later stage of life time. As countermeasure, a good bond in the interface between the pavement and the concrete bridge deck structure must be achieved during construction.

The main reason for blister formation is a pressure produced by air and water vapor under the pavement [2] .Blisters can be also caused by the expansion of hot humid air in the concrete after torching of the membrane with open gas flame. The other reason for blister formation can be the presence of unbounded areas created due to poor workmanship [3]. Blistering also can be caused by thermal buckling of pavement[4]. Blister can also be found between surface and base course of asphalt pavement as indicated in Fig.1.1 (c). [5] mentioned that blister were detected using an IR thermography as shown in Fig. 1.1 (b). The blister were found at a depth of 40mm below the surface of the pavement. Blistering can occur as well in asphalt plug joints due to debonding of the connecting PBM strip from the concrete surface[1]. During service period lateral water infiltration below the PBM strip may occur, leading to blistering or deboning of the asphalt plug joint (APJ-filling). [1] mentioned that blister growth in asphalt pavements is temperature-dependent. Examples of blisters formed in strömbron-bridge in Stockholm is shown in Fig. 1.1 (a).

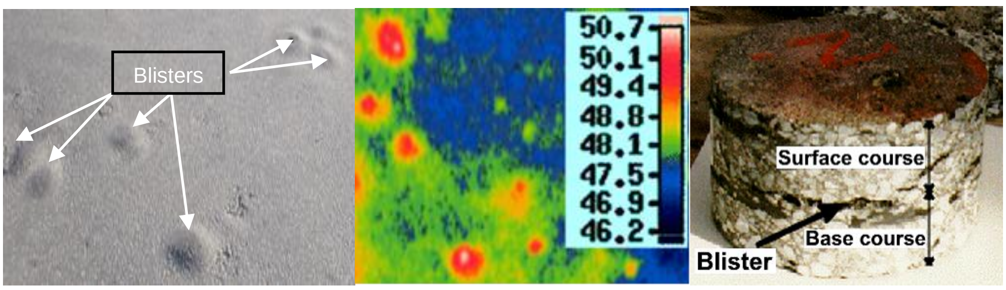

(a) (b) (c)

Fig 1.1 (a) Examples of blisters formed in strömbron -bridge, Stockholm, May, 2010 (b) Thermogram of blisters (max. diameter ca. 120mm) on a mastic asphalt surface course (scale in °C) (c) asphalt core with blister formed between surface and base course

Thermal compatibility tests performed in reference [6] has shown that the mastic asphalt pouring temperature on the surface of the waterproofing membrane has an influence on the formation of blisters. The temperature on the surface of the PBM can reach up to 180 °C during pouring temperature of 220°C mastic asphalt as shown in Fig.1.2. A gas released assumed to be a major cause which led to small bubbles in the contact surface of the mastic to the membrane. The amount and appearance of the bubbles in the contact surface of the mastic depends on the pouring temperature of the mastic; at mastic asphalt (MA) temperature up to 200 °C blisters was not observed however at a poring temperature higher than 210 °C many short- term blisters were observed (partl, 2001).

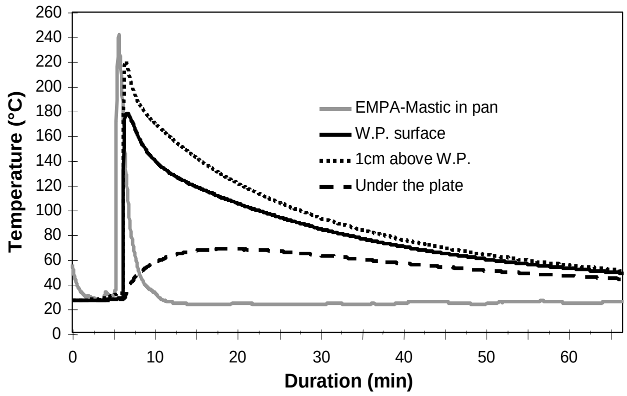

Fig. 1.2 Temperature measurements during pouring of mastic asphalt at 220°C on the water proofing membrane

Blister growth in asphalt pavement can depend on the temperature [5]. An effort has been made by [6] to measure the blister growth naturally on the pavement. As an example it is indicated in Fig. 1.3 (a) that, the blister can grow close to 3 mm in few minutes. During the blister growth, as indicated in Fig 1.3 (b), the temperature fluctuation on the blistered surface and non-blistered surface including the change of temperature on the blistered surface and non-blistered surfaces (bars) are plotted as a function of time of day [5]. The air temperatures are also indicated on the Fig. 1.3 (b). The results showed that the maximum temperature difference between blistered and non-blistered surfaces was 5°C when the temperatures of blistered surfaces reached approximately 55°C. Carefully applying the PBM without partial burning and overheating and activation of the mastic asphalt by heating before installation of the PBM is important to increase the adhesion property [1].

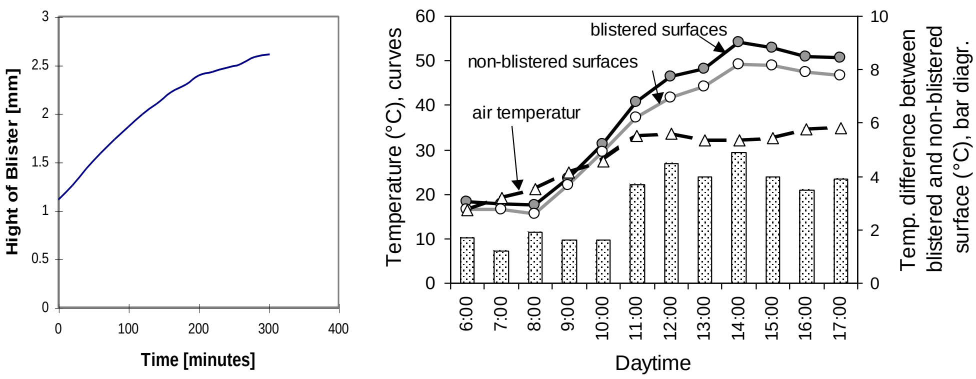

(a) (b)

Fig.1.3 (a) Natural blister growth on pavement (b) Surface and air temperatures during daytime (curves); temperature difference between blistered and non-blistered surface (bars) (Oba and Partl)

The blister test is a method to study the crack propagation of thin layer of adhesive from the substrate by injecting a liquid or a gas in to the orifice of the substrate. Applying a controlled pressure of liquid or gas in to the membrane or the adhesive will inflate at the beginning until the critical pressure for propagation is reached, after wards the propagation commences. The pressure and blister profile are used to extract the interfacial fracture energy, believed to be a fundamental property of the interface. [7] mentioned that the Interfacial Fracture Energy (IFE) is a fundamental property of the interface that can be used to predict sealant-aggregate fracture. The relationship between the applied pressure and blister deflection was used by [8] to determine the energy dissipated during debonding of the crack sealant. Interfacial debonding propagation arises from two superimposed stress fields. One is due to specimen deformation while the other is from the stress concentration around the orifice of the substrate [8]. To address the blister growth in terms of crack propagation of isotropic thin elastic membranes interface on substrate[7] used the energy changes that occur when the film deboned around the edge of a circular orifice plate effectively increasing the window's radius by a tiny increment *da* as indicted in Fig. 1.4. The energy used during the bulging of the blister before the blister propagation was assumed to have a pressurized, circular thin film modelled as a section (or cap) of a thin-walled spherical pressure vessel having uniform equi-biaxial stress and curvature [7]. The energy release rate, *G* which accounts for removing the membrane from a substrate is defined in Eq. (1.1). The formulated equation to calculate the blister propagation energy of elliptical debonding is presented in Eq. (1.2).

$$G = \frac{1}{2\pi a} \frac{\partial \left(W_{applied} - U_{strain} \right)}{\partial a} \Bigg|_P \tag{1.1}$$

Blister growth can occur only if *G* is equal to or greater than the energy required per unit area to separate the film from the substrate.

$$G = \frac{4k_1 + 5k_2 \left(\frac{h}{a} \right)^2}{4\left(k_1 + k_2 \left(\frac{h}{a} \right)^2 \right)} \frac{k_v}{\pi} ph \tag{1.2}$$

$$k_v = \frac{V}{a^2 h}; \quad k_1 = c_1 \sigma_0 t; \quad k_2 = c_2 Mt$$

Where k_v is the volume parameter, c_1 and c_2 are parameters which account for the shape of the window, *M* is the biaxial modulus of the membrane, *t* is the thickness of the membrane, *h* is the blister height, *a* is the blister radius, *P* is the pressure, σ_o is the stress at the crack front.

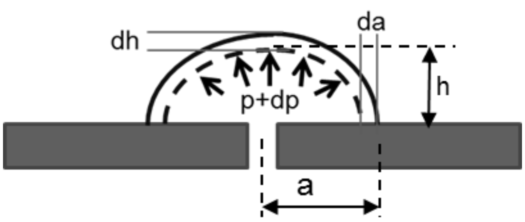

Fig. 1.4 Schematic of an ideal circular blister growth for modeling crack propagation [7]

Similar equation has been used by [7] to measure the work of adhesion between a thin flexible film on a rigid substrate. In contrast to the conventional blister loaded by constant fluid pressure, that leads to catastrophic effect during blister propagation, the new test proposed by [9] is driven by an internal expansion of a fixed mass of working gas which leads to stable crack growth. [9] employed the exact geometry of an inflated blister for the first time determined by Hencky [10] and was later adopted in many other literatures. [11] use recently the hencky series equation to investigate the blister propagation including, bubbles formed when placing a Graphene membrane on a substrate due to gas molecules trapped underneath.[1] indicated that the adhesive interactions are accounted via an energy balance involving the strain and adhesion energies and the study was confined to relatively large grapheme bubbles for height larger than 10 nm (h>10 nm). In the pressurized blister test, an atomic force microscope (AFM) was used to measure the shape of the bulged graphene membrane in Nano scale, which was parameterized by its maximum deflection [11].

1.1 Research aims

Given this background, the objective of this research is explanation of the scientific basis for better understanding and modelling the formation of blisters between the bridge deck and the dense asphalt, as well as waterproofing membranes on concrete bridge decks.in addition to this helps to distinguish the adhesive properties of different types of membranes and their resistance to blister formation. To achieve the research aims, experimental and analytical investigation on the basis of a model system of practical relevance and as close to reality as possible was used.

1.2 Research outline

The first part of the research was focused on investigation of asphalt blistering on concrete palate. The investigation incudes blister growth in laboratory using a controlled pressure and temperature. Viscoelastic thick plate model was developed using Abacus to simulate the influence of temperature and pressure fluctuation on blister growth (chapter 1). The second part of the thesis contains to sections, the first one focus on experimental and analytically modelling of blister propagation on orthotropic plate this includes testing of polymer modified membranes (PBM) using a biaxial testing condition (chapter 2). The second section focus on the comparing the analysis method described in section one to standard peeling test method, as described in Swiss standard and determine the fracture energy from literatures. As indicted in Fig. 1.5. The second part comprises of testing the PBM in uniaxial tension test to characterize the material property for peeling fracture energy. The biaxial extension test is used to determine the model parameters for blister test. More over the modulus of elasticity from the uniaxial and biaxial tension tests are compared including the fracture energies from peeling and blister test (chapter 3).

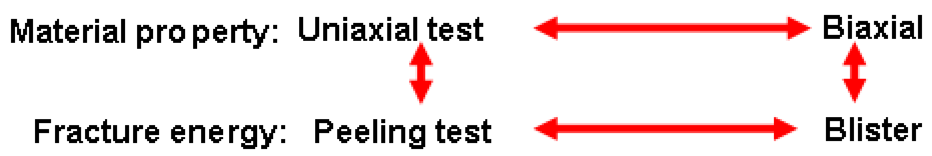

Fig. 1.5 Schematic of testing methods and relation to fracture energy determination method

2 Blister formation on mastic asphalt

The primary aim of waterproofing layers under a bridge-deck pavement is to protect the structural concrete from penetrating water and de-icing chemicals. As shown in Fig. 2.1, such a waterproofing system often consists of a polymer-modified bitumen membrane (PBM) that is glued to the concrete surface by an adhesive-bonding agent or by welding with a torch. Generally, the bridge-deck pavement consists of two layers of mastic asphalt (MA), composed of aggregate with a maximum aggregate size of 8 mm, 11 mm, or 16 mm and a 6.5 % by weight binder of 20/30 penetration grade to survive extreme traffic conditions [1]. In addition to this, epoxy sealing, acrylate, or polyurethane is used as a waterproofing layer on concrete bridge decks. MA has virtually no air voids. Therefore, it contributes to the waterproofing properties of the system. In general, bituminous waterproofing membranes on bridges have a thickness of 5 mm. They are typically made of styrene–butadiene–styrene polymer-modified bitumen that is carried by glass fiber and polyester fabrics in the center of the sheet. Usually, the upper surface is treated with talcum, sand, and granules for ultraviolet radiation protection. High-quality waterproofing membranes have good thermal stability, flexibility at low temperature, and good adhesion to the concrete surface.

Failure of the adhesive bond between a concrete surface and a waterproofing membrane PBM can occur because of the lack of strength of the concrete or insufficient adhesion and cohesion of the bituminous membrane layer. In addition to this, the welding process can affect the strength of the concrete.

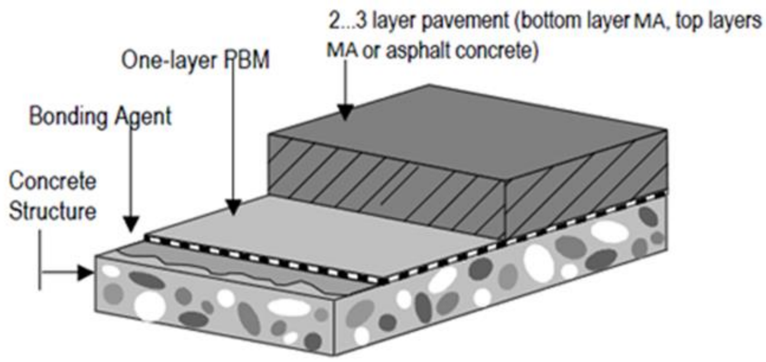

Fig. 2.1 Scheme of a concrete bridge deck waterproofing system [1].

Heating can lead to tension in the upper surface followed by cracking or detachment. Various techniques can be used to improve the adhesion, such as sandblasting and water jetting, etc. Possible use of low-viscosity epoxy resin as bonding agent and seal against humidity may be helpful [12].Reasons for blister formation

Mechanical properties, dimensional change with temperature, permeability, the ability to vent gas, etc., are major issues concerning blistering of water proofing membranes. The main reason for blister formation is attributed to pressure produced by air and water vapor under the pavement [2]. Blisters can be caused by the expansion of hot humid air in the concrete after torching of the membrane with open gas flame.

Short-term blisters occur during placing of hot mastic asphalt and result from humid air trapped in the asphalt mixture. These blisters are often removed in practice by punching a steel stick into the blister of the mixture to release pressure. This bad practice indicates a quality problem either in the material or construction process. Since, it is practically impossible to release all pressure by punching through the blisters, some of the smaller blisters may get “frozen” during the cooling process and the trapped air may be the trigger for the formation of long term blisters that may gradually grow under service condition. Reference [4] suggested that blisters on concrete with asphalt overlay are caused by thermal buckling of the pavement slab.

Waterproofing sheets on roofs may also show blister formation. In a broad analysis of blister phenomena [3], the authors indicate that blisters can only develop in initial voids or unbound areas because of poor membrane application during construction. After such blister initiation, gas expansion inside the blister can cause blisters to grow. When the temperature rises, obviously, the pressure increases. However, from actual pressure measurements within blisters, it was found that the pressure is much lower than calculated for totally entrapped gases [3]. Because of temperature fluctuation in the surrounding environment, air is forced out during day time and sucked in during night time. It is supposed that temperature variation leads to breathing or pumping action which changes the blister volume.

2.1 Objectives

The primary objective of this study is to develop a finite element model, which simulates blister growth with focus on long term blistering. This includes investigation of blister growth in the laboratory with finite element simulation focusing on blistering of mastic asphalt and first order shear deformation thick plate theory. It includes also investigating the influence of temperature and pressure fluctuation on blister growth (viscoelastic thick plate) for linearly varying temperature and pressure. In addition to this, a simplified model is established which can simulate blister growth for constant blister radius, considering the viscoelastic properties of the mastic asphalt, as a basis for future research.

2.2 Methodology

Generally, shell elements are used in models, where the thickness is significantly smaller than the other dimensions. Shells with a thickness of more than about 1/15 of the span of the shell are considered as thick shells, otherwise as thin shells [13]. In this report, the exact bending solution from the classical plate theory [14] and the Mindlin plate theories [15] are used. These theories are applied to calculate the out-of-plane displacement-pressure relationship of thin and thick solid isotropic plates respectively.

In case of thick plates, where the shear deformation is significant, shear deformation plate theories can be applied. There are numerous shear deformation plate theories available, the simplest of which is the first-order shear deformation plate theory (FSDT) also known as the Mindlin plate theory. The deflection equation of the first-order shear deformation plate theory can be expressed in terms of the corresponding quantities of the classical plate theory for axisymmetric bending of isotropic circular plates as shown in eqn. (2.1) [15]. A Similar equation was used by Fini et. al. [16] to calculate the out-of-plane displacement for a thick circular plate (see Fig. 2.2) under axisymmetric uniform pressure with built in edge constraint.

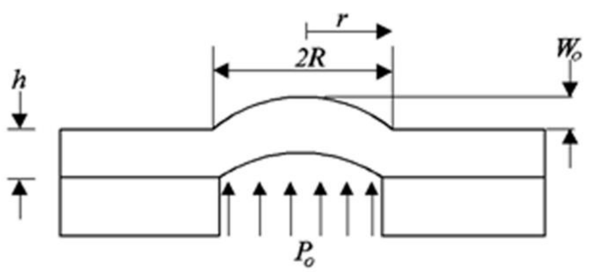

Fig. 2.2 Scheme of a pressurized blister plate

$$w_o = \frac{p_o}{64D}(R^2 - r^2)^2 + \frac{p_o R^2}{4SGh}\left(1 - (\frac{r}{R})^2\right)^2 \qquad (2.1)$$

Where:

P_0	=	pressure
R	=	distance from the center of the thick circular plate
R	=	radius of the thick circular plate
H	=	thickness of the thick circular plate
w_o	=	displacement at a distance r from the center of thick circular plate
S	=	shear correction factor (5/6 for thick circular plate)
D	=	flexural rigidity of the plate, $D = \frac{Eh^3}{12(1-v^2)}$
G	=	shear modulus of the plate, $G = \frac{E}{2(1+v)}$
E	=	modulus of elasticity
v	=	Poisson's ratio

2.3 Finite element model: geometry and loading

The bending properties of different meshing elements have been studied with linear elastic analysis and then the dimensions and boundary condition of the viscoelastic model were defined. The C3D20R (continuum three dimensional twenty node reduced) element was selected for its good agreement with the linear elastic analytic solution for the vertical deflection of a thick plate. This model had 56 elements and all elements were arranged in a single layer. The linear elastic model for blister formation in a thick plate was used as reference for the viscoelastic finite element simulation in this chapter.

In this particular case, a three dimensional half circular model was considered. As long as the symmetry conditions hold at the edges, the radial symmetry in the pressurized circular plate allows any size of pie slices or segments to be used in the model. A three dimensional finite element (3-D FE) model was developed using ABAQUS™ Version 6.8.

Modeling blister growth in mastic asphalt has been done by Michalski [17] and blister formation in thermo viscous material was studied by Rogosch [18]. In this report, a three-dimensional model is established to simulate the time dependent vertical blister deflection of a thick plate for different types of loading amplitudes.

The geometric finite element model setup of the 3-D plate is shown in Fig. 2.6(b), where the entire contact area between the plate and supporting substrate is constrained in all degrees of freedom ($u_X = u_Y = u_Z = 0$, where u_X, u_Y and u_Z are displacement in x, y and z-axis respectively and $u_{RX} = u_{RY} = u_{RZ} = 0$, where u_{RX}, u_{RY} and u_{RZ} are rotational displacements in x, y and z-axis respectively). This condition of support represents full adhesion to a rigid substrate beyond the area of the interface. Symmetry plane x-z has a degree of freedom $u_y=0$. A uniform pressure load of 0.03 MPa is applied over the entire region (blister radius) of the circular half plate. The pressure load applied in this model is the same as the pressure used in the laboratory test which is described below. A constant average temperature of 59 °C is used in the finite element simulation model. This temperature is measured during the experiment as mentioned in section 5.

2.4 Test development

Digital image correlation experiment technique gives the possibility to measure displacement and deformation fields at the surface of objects under any kind of loading condition. The post processing software uses the images taken at different loading times to construct the impression of the distribution of vertical deflection in the measured object. This system can be used in bubble inflation tests to measure the strains on the surface of the bubble [19]. In this case, the blister growth is measured with a 3D digital image correlation system (Limes Vic3D-4Mp) where two cameras were used to measure the out of plane deflection of the mastic asphalt see Fig. 2.3(b). Mastic asphalt thickness of 25 mm at temperature of 250 °C was applied to a concrete plate 500 mm*500 mm. Since it was intended to study the blister growth due to bending and stretching of mastic asphalt, it was important to avoid interfacial fracture between the layer of mastic asphalt and concrete by keeping the blister radius constant. Therefore, an aluminum clamping plate having a hole with a diameter of 250 mm was used at the top of the mastic asphalt and ordinary white and black paint spray was used to produce a speckle pattern on the surface of the mastic asphalt as shown in Fig. 2.3(a). Water pressure was injected through the concrete plate to produce a pressure for blister growth. The pressure was controlled with a manometer and the pressure was kept constant at 0.03 MPa during the testing period. The temperature inside the blister was recorded using a thermo element and the average temperature inside the mastic asphalt was found to be 59 °C. The measured vertical deflection data are presented in Fig. 2.9.

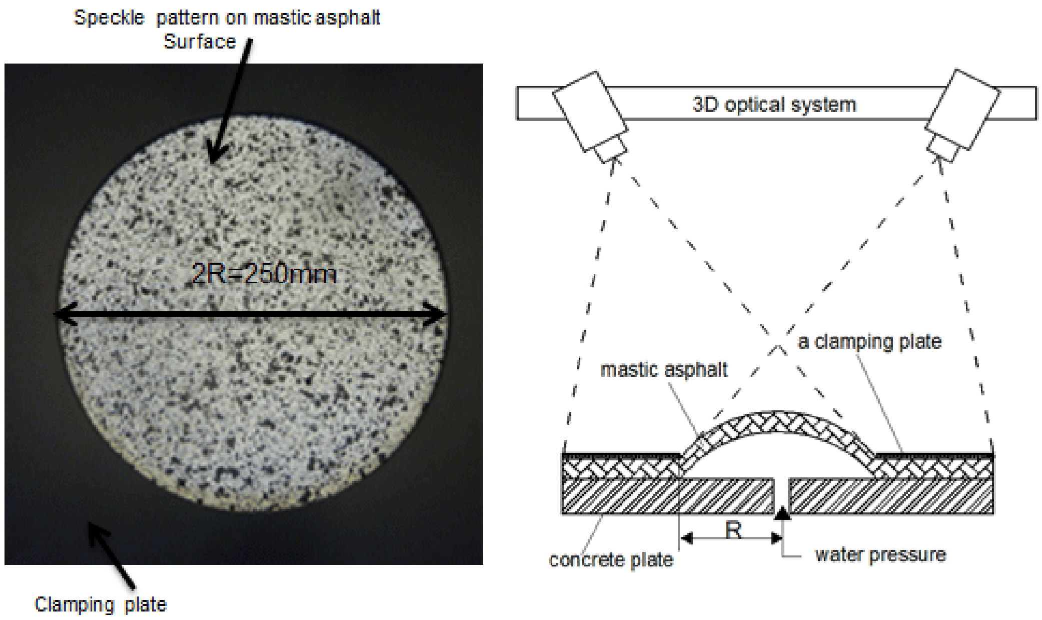

(a) (b)

Fig. 2.3 (a) Top view of the mastic asphalt sample after spraying paint to produce speckle image (b) the blister test devise (Vic3D- 4Mp)

2.5 Viscoelastic Material characterization

Fig. 2.4 describes the steps followed to determine the Prony series parameters as input for the finite element model. After performing the creep compliance test with IDT test, the master curve is constructed using a sigmoidal function; then the master curve (experimental data) is fitted to a power law function. Using this power law function and Laplace transform, the relaxation modulus in power law representation is determined and approximated by a four parameter Prony series as input for the finite element calculation. Details of the work are shown below.

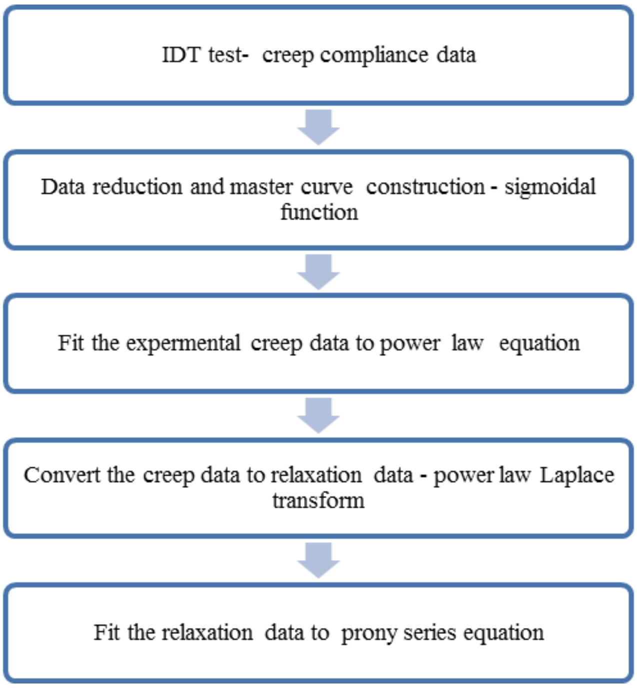

Fig. 2.4 Scheme of a material characterization for the finite element model.

2.6 Creep compliance test

In order to predict the blister response accurately, proper characterization of the mastic asphalt is needed. The viscoelastic properties of mastic asphalt are measured using either simple creep tests (time domain) or complex modulus tests (frequency domain). In this study, time domain indirect tensile test results are used to describe the viscoelastic properties of the material in ABAQUS. In case of indirect tensile tests (IDT), a static constant load was applied along the vertical diametrical axis of a temperature controlled cylindrical specimen for a specified period of time (100 or 1000 s) while measuring the horizontal deformation. The load was controlled such that the upper linear-elastic limit of the specimen, typically 100…500 µstr (micro strain), was not exceeded (see reference [20]).

In this report, the dimensions of the indirect tensile specimens were 100 mm in diameter and 49.8 mm in height. These specimens were cored from mastic asphalt slabs. Each specimen was tested at 5 °C, 15 °C and 25 °C temperatures. A load was applied to cause a horizontal strain in the order of 100 µstr, so that the electric noise during data acquisition process became insignificant. During the loading period, horizontal deformations were measured on both sides of the specimens using four extensometers.

Different theoretical assumptions are commonly used for evaluating IDT results. Homogeneity, isotropy, Poisson’s ratio, coefficient of thermal contraction and the estimation of relaxation modulus from the creep compliance are important issues in the IDT analysis [21].

Huang [22] suggested that the Poisson's ratio for most asphalt mixtures ranges between 0.3 and 0.4. It is stated that it can be appropriate to assume the Poisson's ratio value rather than determining it from actual tests since the effect of Poisson’s ratio is not significant. Hence, for simplicity, Poisson's ratio is often assumed to be time independent in spite of the fact that this is not the case in reality [23].

2.7 Data reduction

In this research, creep compliance is calculated as a function of horizontal deformations. A detailed review of the measurement and analysis system is presented in [24]. All correction factors are considered to depend on Poisson's ratio. With this adjustment, the creep compliance was obtained as follows.

$$D(t) = \frac{\frac{H_{TRIM}(t)}{L_G} \cdot 1.071 \cdot C_{BX}}{\frac{2P}{\pi w d}(C_{sx} + 3\nu \cdot C_{SY})} \qquad (2.2)$$

Where:

D(t) = creep compliance,1/GPa

ν = Poisson's ratio

P = creep load, N

C_{BX} = horizontal bulging correction factor

C_{SX} = horizontal stress correction factor

C_{SY} = vertical stress correction factor

D = diameter of the specimen, mm

L_G = length between gage point centers, mm

W = thickness of the specimen, mm

H_{TRIM} (t) = trimmed average horizontal deformation, mm

The trimmed average horizontal deformation is calculated by ranking each of the horizontal arrays according to their deflection values in considering a window around the middle of the test (46-50 s). After ranking, the horizontal deflection with the highest and the lowest measurement values are removed from the data analysis and four of these results are used out of the six measurements to determine the creep compliance; for details see [24]. Creep compliance is calculated with eqn. (2.2) from the row data of IDT for three different temperatures (5 °C, 15 °C and 25 °C) as indicated in Table 2.1.

Tab 2.1 Creep compliance from IDT

	Measured creep compliance, 1/GPa		
Time, s	Log (D) at 5, °C	log (D) at 15, °C	Log(D) at 25, °C
1	$3.70 \cdot 10^{-02}$	$8.14 \cdot 10^{-01}$	$6.92 \cdot 10^{0}$
2	$1.34 \cdot 10^{-01}$	$7.13 \cdot 10^{-01}$	$1.53 \cdot 10^{01}$
5	$2.59 \cdot 10^{-01}$	$1.57 \cdot 10^{0}$	$2.35 \cdot 10^{01}$
10	$4.26 \cdot 10^{-01}$	$2.19 \cdot 10^{0}$	$3.73 \cdot 10^{01}$
20	$7.72 \cdot 10^{-01}$	$3.79 \cdot 10^{0}$	$6.07 \cdot 10^{01}$
50	$1.33 \cdot 10^{0}$	$6.17 \cdot 10^{0}$	$8.46 \cdot 10^{01}$
100	$2.01 \cdot 10^{0}$	$1.97 \cdot 10^{01}$	$9.79 \cdot 10^{01}$
200	$2.91 \cdot 10^{0}$	$3.22 \cdot 10^{01}$	$1.21 \cdot 10^{02}$
500	$4.68 \cdot 10^{0}$	$5.78 \cdot 10^{01}$	$1.85 \cdot 10^{02}$
1000	$6.50 \cdot 10^{0}$	$8.60 \cdot 10^{01}$	$2.58 \cdot 10^{02}$

2.8 Master curve representation

As shown in eqn. (2.3), the sigmoidal function in combination with the WLF (Williams-Landel-Ferry) equation may be used to construct master curves. Shifting to an arbitrary temperature (in case of this investigation 5 °C) is done by solving for the shifting factors with the parameters of the sigmoidal function by least square method.

The different parameters of eqn. (2.3), as determined from non-linear representation analysis with the curve fitting toolbox of Matlab, are indicated in Table 2. 2. R-square is the square of the correlation between the response values and the predicted response values. The master curve constructed from eqn. (2.3) is shown in Fig. 2.5(a) and will be used in ABAQUS™ to define the thermorheologically simple behavior of the mastic asphalt.

$$log(D) = b_1 + \frac{b_2}{1 + e^{\left[a_1 + a_2\left(log(t) + \frac{c_1\,(T - T_{ref})}{c_2 + (T - T_{ref})}\right)\right]}} \tag{2.3}$$

Where:

D	=	creep compliance,1/GPa
T	=	time of loading, s
T_{ref}	=	reference temperature, K
T	=	temperature, K
b_1	=	minimum value of D
b_2	=	span between maximum and minimum value of D

a_1 and a_2 = parameters describing the shape of the sigmoidal function

c_1 and c_2 = WLF (Williams-Landel-Ferry) constants

Tab 2.2. Sigmoidal parameters and the WLF constants

b_1 ,MPa	b_2, MPa	a_1	a_2	c_1	c_2	R-square
$3.70\cdot10^{-02}$	$6.98\cdot10^{03}$	2.097	-0.908	1520	11750	0.976

2.9 Power law analytical form of interconversion

The power law analytic form of interconversion is used to predict the relaxation modulus from measured creep compliance data and as input for characterizing asphalt mixtures in ABAQUS. It is evident that creep and stress relaxation phenomena are caused by the same linear viscoelastic properties. For linear viscoelastic material, this interconversion can be done by applying Laplace transform.

$$\varepsilon(s) = sD(s)\sigma(s) \tag{2.4}$$

Where, s is the Laplace transform variable, ε and σ are strain and stress respectively

$$\sigma(s) = sE(s)\varepsilon(s) \tag{2.5}$$

Where, E is the relaxation modulus

Hence, $E(s)=\frac{1}{s^2\ D(s)}$ (2.6)

According to eqn. (2.6), the relaxation modulus can be calculated from the creep compliance. Hence, it is easier to express the creep compliance by the power law function.

$D(t)=At^n$ (2.7)

Where t is time and D(t) is creep compliance (1/GPa)

In this report, the experimental creep data are limited to the linear part of the sigmoidal function with maximum slope. Hence, instead of using a sigmoidal function, the data is approximated by a power function for easier interconversion of the creep data to the relaxation modulus. The power law equation fitted to the creep compliance data for an arbitrary reference temperature of 5 °C is expressed by eqn. (2.7) as shown in Fig. 2.5(a) with, $A=7.71\cdot10^{-02}$ 1/GPa and $n=6.88\cdot10^{-01}$. Transforming eqn. (2.7) in to the Laplace domain and substituting into eqn. (2.6) leads to the following eqn. (2.8) after back transforming the equation in to the time domain. The result is shown in Fig. 2.5(b).

$$E(t)=t^{-n}\frac{1}{\Gamma(n+1)A\Gamma(n+1)} \quad (2.8)$$

Where A and n are constants and $\Gamma(n+1)$ is the gamma function.

2.10 Relaxation modulus determination

For numerical analysis in ABAQUS™, the power law representation of the relaxation modulus was fitted and replaced by a four element Prony series according to eqn. (2.9) as shown in Fig. 2.5(b). The fit with Prony series for a reference temperature of 5 °C is shown in Fig. 2.5(b). The fit is not exactly identical to the power law representation because, for simplicity, only four elements were used. However, for this investigation, four Maxwell elements are considered to be sufficient. The relaxation times of the four Maxwell elements and the Prony series parameters are presented in Table 2.3.

$$E(t)=\sum_{i=1}^{N+1} E_i e^{\frac{-t}{t_{ri}}} \quad (2.9)$$

Where E(t) is the relaxation modulus, E_i are Prony series spring constant parameters for the relaxation modulus master curve (spring constants or moduli), t_{ri} are the relaxation times for each Maxwell element.

Tab 2.3 Prony series parameters at reference temperature 5 °C.

Prony series relaxation time, s				Prony series spring constants, MPa			
tr_1	tr_2	tr_3	tr_4	E_1	E_2	E_3	E_4
747.384	$186.358\cdot10^{03}$	$9.183\cdot10^{03}$	29.146	90.89	3.457	18.84	32.69

For 3-D multi axial stress state, it is convenient to describe the stress state with deviatoric and dilatational components. A detailed description is given in [25], a generalized solid Maxwell model is used in ABAQUS™ to characterize these two stress state components. The bulk relaxation modulus follows from eqn. (2.10) and the shear relaxation modulus from eqn. (2.11)

$$K(t) = K_0\left(1 - \sum_{i=1}^{n} K_i\left(1 - e^{-\frac{t}{t_{ri}}}\right)\right) \qquad (2.10)$$

$$G(t) = G_0\left(1 - \sum_{i=1}^{n} G_i\left(1 - e^{-\frac{t}{t_{ri}}}\right)\right) \qquad (2.11)$$

Where G is shear modulus, K is bulk modulus, t is actual time, t_{ri} are relaxation times, G_0 and K_0 are instantaneous shear and bulk elastic moduli, G_i and K_i are Prony series parameters.

Assuming constant Poisson's ratio in the analysis simplifies the problem. This assumption was made in spite of the fact that Poisson's ratio in viscoelastic materials is generally time dependent. The time dependent Poisson's ratio of viscoelastic materials can increase or decrease depending on the bulk and shear relaxation with time [23]. However, since the modeling of blister in this study was assumed to remain in the small strain regime, this simplification was considered acceptable. A time independent Poisson's ratio of 0.35 was assumed for mastic asphalt, and introduced in eqns. (2.12) and (2.13) to relate time dependent relaxation modulus to the time dependent bulk and shear relaxation modulus.

$$K(t) = \frac{E(t)}{3(1-2v)} \qquad (2.12)$$

$$G(t) = \frac{E(t)}{2(1+v)} \qquad (2.13)$$

As shown in Fig. 2.5(b), the power function of the relaxation modules was used for determining the parameters of the Prony series for the generalized Maxwell model by curve fitting. Since the master curve is constructed for the reference temperature of 5 °C, the Prony series parameters represent the time dependent shear and volumetric behavior of the material at this particular temperature. The Prony series parameters for 25 °C are determined by shifting the creep compliance data to the reference temperature of 25 °C and by applying a similar procedure as mentioned above. Table 2.4 lists the Prony series parameters at 5 °C.

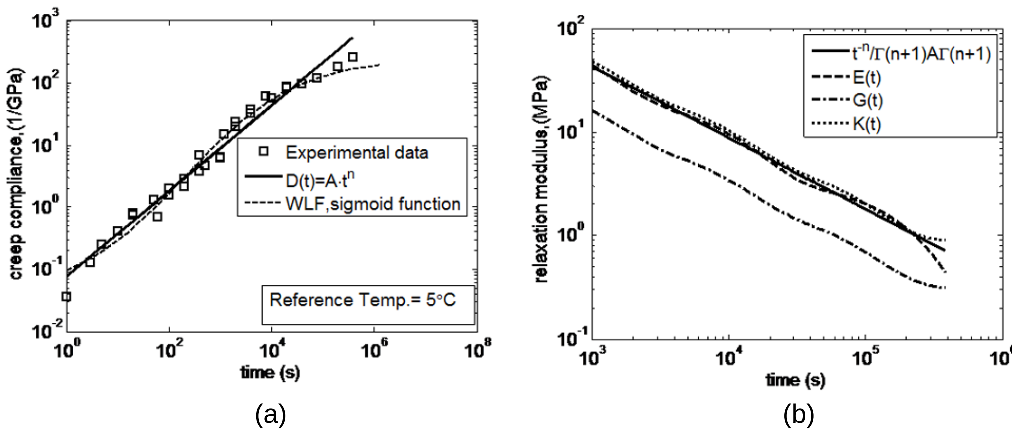

Fig. 2.5 (a) Approximation of the creep behavior of mastic asphalt with a power function, Prony series and master curves for mastic asphalt at reference temperature 5 °C (WLF (Williams-Landel-Ferry), sigmoid function); (b) Shear and bulk relaxation modulus variation with time at 5 °C.

Tab 2.4.Shear and bulk relaxation modulus Prony series parameters at 5 °C used for modeling

Instantaneous modulus , MPa	N	Gi, MPa	Ki, MPa	t_{ri}, s
79.81	1	1.605	4.757	10
79.81	2	42.09	39.92	44.62
79.81	3	29.21	82.91	200.60
79.81	4	6.598	20.54	26874.5

2.11 Closed form solution for viscoelastic creep

In any solid body subjected to external loading or displacement, the resulting stress and strain must simultaneously satisfy three basic equations; the equilibrium equations; the kinematic equations; and the constitutive equations. Viscoelastic stress analysis problems are more difficult to solve than elasticity problems since time dependency requires the solution of the differential equations of the constitutive law. If the boundary conditions and the temperature remain invariable, the time variable in the equations can be removed by transforming the equation into the Laplace transform domain as shown earlier.

In this section, the elastic solution shown in eqn. (2.1) is used to determine the deflection of the thick plate. As shown below, for constant Poisson's ratio, eqn. (2.1) is transformed to the equivalent elastic solution with the Laplace domain variable 's'.

$$w_0(s)=\frac{3(1-v^2)}{16sE(s)h^3}p(s)(R^2-r^2)^2+\frac{p(s)R^2(1+v)}{2sE(s)Sh}\left(1-(\frac{r}{R})^2\right) \tag{2.14}$$

Rearranging the above expression with eqn. (2.6) results in the following relation

$$w_0(s)=\left(\frac{3(1-v^2)}{16h^3}(R^2-r^2)^2+\frac{R^2(1+v)}{2Sh}\left(1-(\frac{r}{R})^2\right)\right)p(s)sD(s) \tag{2.15}$$

In order to make the conversion back from the Laplace domain to the time domain Maple software is used. The shear relaxation modulus, the corresponding relaxation times and the Poisson's ratio are used and converted into the creep eqn. (2.16). The parameters of eqn. (2.16) are shown in table 2.5. The vertical deflection of the thick plate is calculated based on the analytic eqn. (2.17).

$$D(t)=D_o+\sum_{i=1}^{N}D_i(1-e^{\frac{-t}{t_{ri}}}) \tag{2.16}$$

Tab 2.5. Prony series parameters at reference temperature 5 °C

D_0 , MPa	N	D_i, MPa	t_{ri}, s
0.02729318695	1	$5.68528967271\cdot10^{-03}$	317.5685434
	2	$29.35788435\cdot10^{-03}$	10.52481012
	3	$0.1712212104\cdot10^{-03}$	19.48316577
	4	$29.592292201577\cdot10^{-03}$	1.935661701

$$w_0(t)=\left(\frac{(3(1-v^2)}{16h^3}(R^2-r^2)^2+\frac{R^2(1+v)}{2Sh}\left(1-(\frac{r}{R})^2\right)\right)p_0D(t) \qquad (2.17)$$

Where w_o is vertical deflection of the thick plate (mm)

2.12 Temperature and pressure influence in blister growth

The thermal environmental conditions have significant impact on stability and long term performance of a pavement during its life span. Daily temperature variations influence the

deformation of asphalt pavement significantly. A linear viscoelastic 3D finite element model is more realistic than a linear elastic model because it considers time dependent behavior of the mastic asphalt and temperature effects on material property. The 3D finite element simulation will therefore be used to study blister growth (vertical deflection) of a mastic asphalt pavement plate subjected to diurnal heating and cooling temperature fluctuation. During day time of sunny days, heat energy transfer by interaction between pavement and its surroundings exists. This interaction consists of the radiation balance and exchange by convection which comprises solar radiation, thermal radiation heat flux and convection heat flux at the pavement surfaces or at the bottom of the bridge deck [26].

The 3D finite element model in this study was developed based on the following assumption. The bridge deck pavement lies directly on the bridge deck, i.e. no PBM (polymer bitumen membrane) sheet is applied, the radius of the blister will remain constant, which prohibits horizontal blister growth, i.e. the adhesion between the mastic asphalt and concrete (rigid substrate) has sufficient strength to prevent debonding. The pavement is idealized as thick plate. The mastic asphalt is considered to be homogenous, isotropic and linear viscoelastic. The asphalt pavement's temperature fluctuation is the same in the whole cross section of the pavement. The pressure build up inside the blister is only caused by gas pressure; vapor pressure and off-gassing pressures are not considered. The blister cavity is assumed to be closed; therefore there is no exchange of gas between inside and outside of the blister. The analysis assumes constant Poisson's ratio.

C3D20R Elements were used and one single layer was used to model the blister. Linear quasi-static analysis was used to model time dependent material response such as creep and recovery. ABAQUS™ allows controlling time incrementation automatically or directly by specifying the time. As long as the output results of the simulation are compared with closed form solution the fixed time incrementation of 0.8 second was applied in the analysis. The pressure load applied in this model was estimated from ideal gas law eqn. (2.18).

$$\frac{p_1V_1}{T_1}=\frac{p_2V_2}{T_2} \qquad (2.18)$$

Where p_1 and p_2 are initial pressure (0.1MPa at 273.15 K) and the required pressure, V_1 and V_2 are initial volume and final volume of the blister, T_1 and T_2 are initial Temperature (273.15 K) and final temperature.

It was assumed that the initial volume is equal to 268.083 mm^3 (which corresponds to radius of 800 mm and blister height $1{\cdot}10^{-04}$ mm) and the final volume is $4.02{\cdot}10^{06}$ mm^3 (for radius of 800 mm and blister height 1.5 mm). The pressures at 5 °C and 25 °C are calculated based on the input variables described in eqn. (2.18).

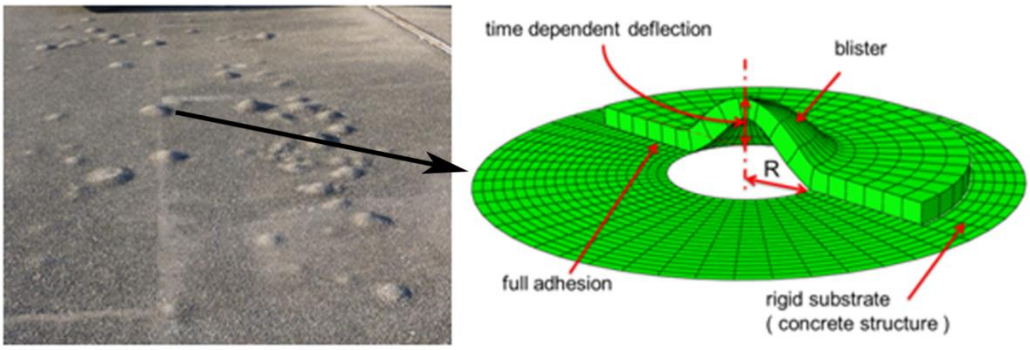

(a) (b)

Fig. 2.6 (a) Observed blisters (b) Schematic three-dimensional model setup for blister growth simulation

The thick plate modeling consisted of 80 mm thick asphalt layer with a constant blister radius of 800 mm. Hence the ratio of the width to height was 1/10, identical to that of the laboratory produced blister.

In order to assess blister growth for 12 h (1/2 day) under uniformly applied pressure, an initial temperature of 15 °C was selected at start of the analysis and the temperature of the mastic asphalt was assumed to increase linearly up to 25 °C at different rates, as shown in Fig. 2.7(a). In addition, it was assumed that the temperature inside the blister was rising simultaneously as in the asphalt layer. In this way, gas pressure in the blister corresponded directly to the temperature history as shown in Fig. 2.7(b).

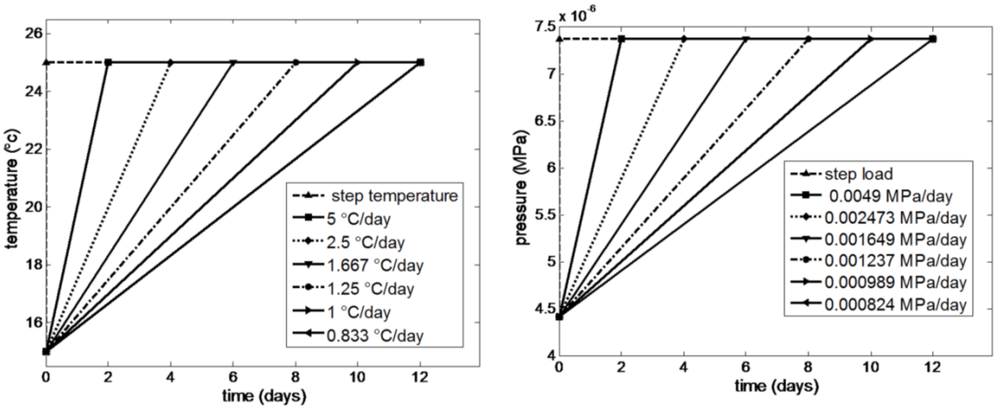

(a) (b)

Fig. 2.7 (a) Temperature history and (b) Pressure history for different rate (1/2day)

Moreover, actual temperature measurements on and within the blister as reported in [6] is shown in Fig. 2.8(a). The temperature inside the blister was measured by putting a temperature probe in the mastic asphalt whereas the temperature on the surface was measured by fixing the temperature probe using a transparent tape. Since the surface temperature was exposed to air convection it appeared that, the highest temperature was measured inside the blister. These temperature measurements were considered as basis to assess the significance of the daily temperature and pressure variations on the blister growth for one week, a history with repeated temperature and pressure cycles was investigated. For simplicity it was assumed that one cycle consisted of a linear increase within 12 hours and a linear decrease within the following 12 hours, as shown in Fig. 2.8(b). As indicated in section 6.2, IDT test is conducted and a master curve for temperature range between 5 °C to 25 °C is determined. Since the mastic asphalt property is determined for the above specified temperature, the temperature in the finite element simulation was assumed to vary moderately between 15 °C and 25 °C. The corresponding pressure history was defined using eqn. (2.18), in a similar way varying from 7.12 $\cdot 10^{-06}$ MPa to 7.37 $\cdot 10^{-06}$ MPa within one day. This frequency of temperature variation was chosen based on earlier experience [6] in a different case as shown in Fig. 2.8(b).

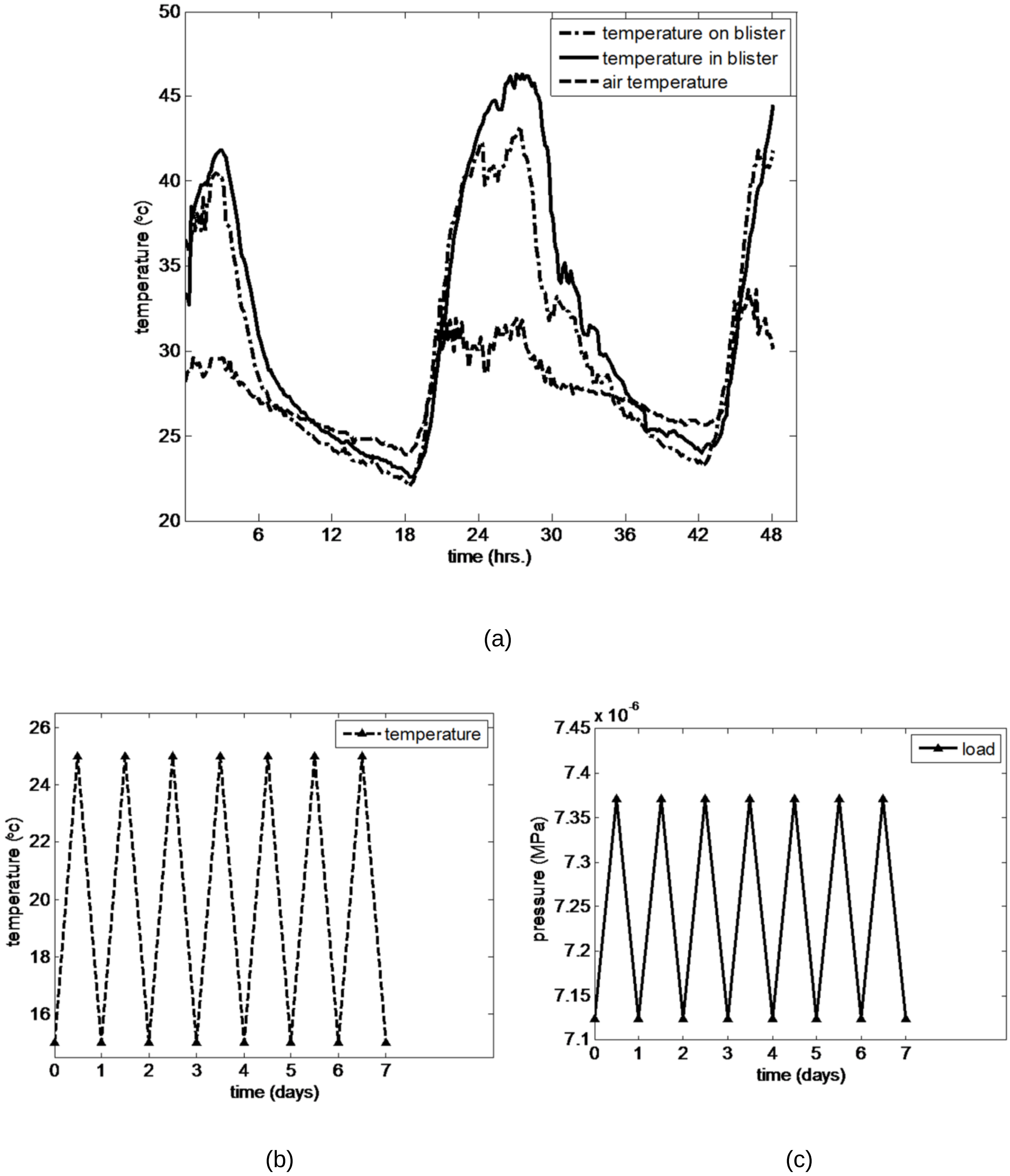

Fig. 2.8 (a) Temperature measurement in a blister on a bridge deck [6] as compared to idealized (b) Temperature and (c) Pressure history (one week) assumed for this study

2.13 Results and discussion

Three samples of mastic asphalt were tested as described in section 5 and the average deflection found from the 3D digital image correlation software profile measurement was compared with the finite element simulation and the analytic solution as shown in Fig. 2.9(a) and (b). The standard deviation in Fig. 2.9(d) was calculated from the image correlation measurement by taking different sections on 2D vertical deflection contour plot shown in Fig. 2.9(c).

The blister growth estimated with the viscoelastic model produced different deflections depending on the pressure and temperature rate. The pressure and temperature histories from Fig. 2.7 resulted in vertical deflections shown in Fig. 2.10(a). The step function temperature and pressure produced higher vertical deflection (1.7332 mm) compared to other types of temperature and pressure histories. The minimum vertical deflection was 1.0304 mm.

In order to assess only the effect of temperature increase in the mastic asphalt, the temperature histories shown in Fig. 2.7(a) were applied while keeping the pressure ($7.37\ 10^{-06}$ MPa) in the blister constant for 12 h. The result in Fig. 2.10(b) indicates that temperature increasing rate has significant effect on the deflection of the plate. The entire deflection in the mastic asphalt was almost completely due to change in temperature. The deflections found from temperature variation were similar to those from simultaneous temperature and pressure variation as shown in Fig. 2.10(b). The maximum deflection was 1.7332 mm for temperature and pressure step function and the minimum deflection of 1.0380 mm was produced by the slowest temperature and pressure rate.

Moreover, the results shown in Fig. 2.11(a) is found when the temperature was constant throughout the thickness (25 °C) and a linearly varying load history shown in Fig. 2.7(b) was applied. This result shows that the rate at which the pressure increases has no significant influence on the vertical deflection of the mastic asphalt. The deflection found from pressure variation is clearly different to the deflection from simultaneous variation of temperature and pressure as shown in Fig. 2.11(b). The maximum vertical deflection obtained was 1.7332 mm and the minimum vertical deflection was 1.7148 mm.

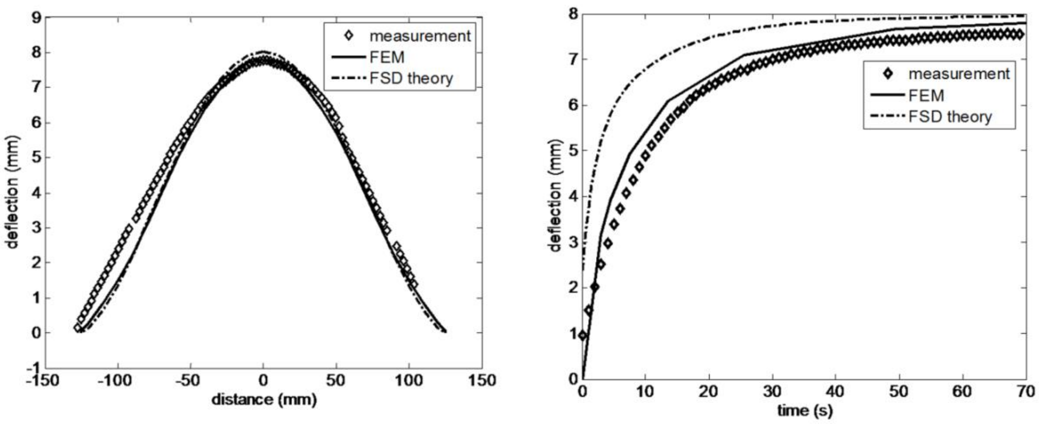

(a) (b)

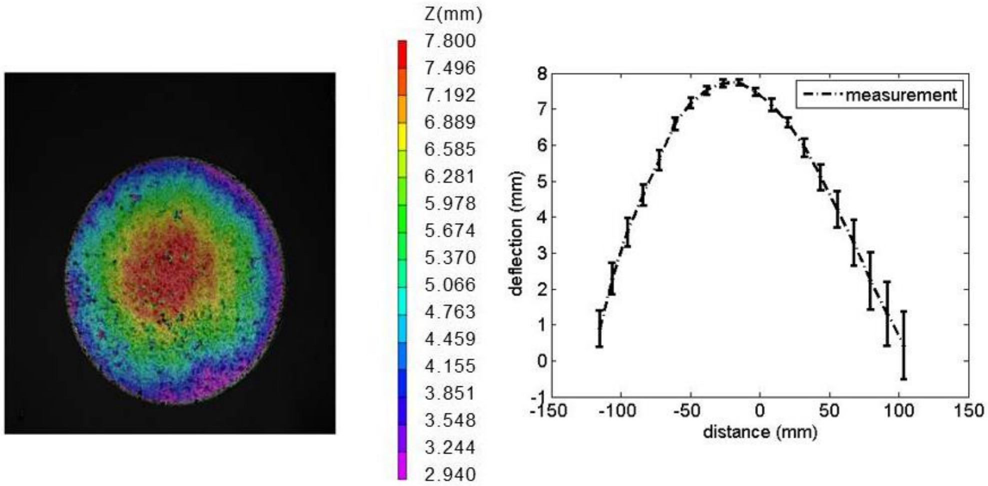

(c) (d)

Fig. 2.9 Comparison of mastic asphalt plates with finite element method (FEM) simulation, first order shear deformation (FSD) plate theory and measurement from image correlation; (a) vertical deflection profile (b) maximum vertical defection as a function of time (c) image correlation 2D plot of vertical deflection after 70 s of measurement (d) vertical deflection with standard deviation

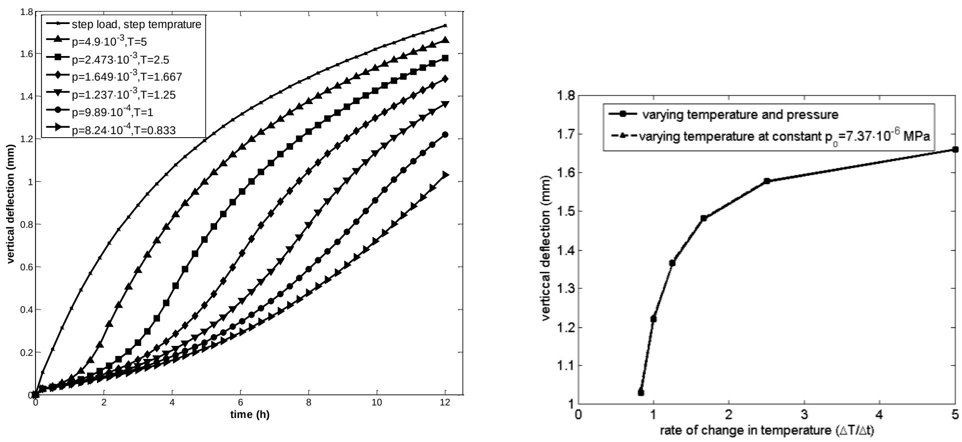

(a) (b)

Fig.2.10 (a) Vertical deflection at the center of the plate when both temperature (T, °C/day) and pressure (P, MPa/day) rate are involved (12 h) (b) Rate of change in temperature vs. vertical deflections at the center of the plate

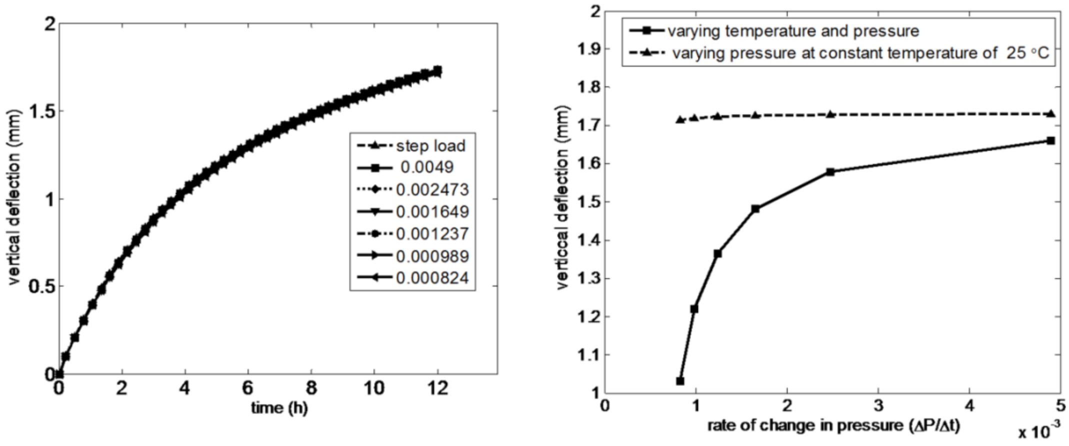

(a) (b)

Fig. 2.11 (a) Vertical deflection at the center of the plate for different pressure rates (MPa/day) at constant temperature of 25 °C (12h) (b) Rate of change in pressure vs vertical deflections at the center of the plate

In Fig. 2.12 the vertical deflection from pressure and temperature fluctuation in one week is presented. The highest deflection of 1.2877 mm was found for repeated simultaneously varied temperature and pressure. In case of fluctuating temperature and constant pressure ($7.124 \cdot 10^{-06}$ MPa corresponding to a temperature of 15 °C) a vertical deflection of 1.2228 mm was found. Pressure fluctuation had no significant influence, as shown previously, and results in the lowest deflection of 0.02521 mm. Moreover, Fig. 2.12 clearly shows that, repeated temperature and pressure cycles may well produce continuous blister growth. The blister growth tends to slow down when more cycles are applied. This corresponds to observations in practice as shown Fig. 2.6(a).

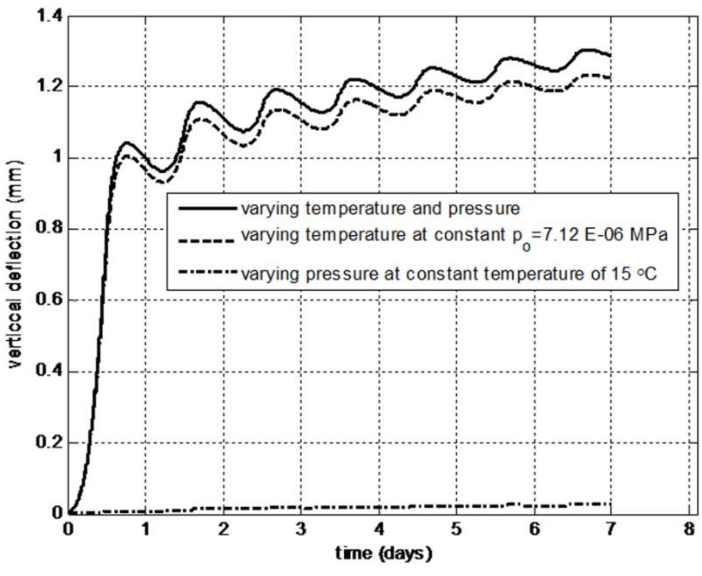

Fig. 2.12 Vertical deflection at the center of the plate for repeated temperature and pressure cycles for 7 days (cycles of linear increment with 12 hours and a linear decrement within the following 12 hours).

3 Adhesive Blister Propagation Energy of Water Proofing Membrane

In most countries, waterproofing systems used on concrete bridge decks or roofs of buildings are generally based on orthotropic bituminous membranes; amongst these, styrene–butadiene–styrene copolymer (SBS) and atactic polypropylene (APP) polymer modified bituminous membranes are being used in most applications. One of the main technical concerns is the formation of blisters under the membrane caused by a complex mechanism governed by bottom-up pressure and loss of adhesion. This report intends to contribute in understanding this mechanism by mechanical elastic modeling and experimental investigation. In order to study the material properties of SBS membranes under the in-plane complex stress state, the orthotropic mechanical behavior of a polymer modified bitumen membrane (PBM) was determined from biaxial test data. Hence, the measured stress–strain data were analyzed using the orthotropic equation to find the material properties in the longitudinal and transversal direction. Finally, blister tests were performed on concrete plates for studying adhesive blister propagation by applying controlled pressure between the PBM and the concrete plates. It was found that the ratio of the longitudinal to transversal adhesive blister propagation is comparable to the ratio of the modulus of elasticity in the longitudinal to transversal direction. Due to the orthotropic material property of the PBM, elliptical adhesive blister propagation was observed and a new model proposed for determining the energy for elliptical adhesive blister propagation.

Blistering on bridge decks is a common phenomenon that may occur either between the dense asphalt layers and the waterproofing layer[6, 27], or between the waterproofing layer and the structural bridge deck element [28]. This report focuses on blistering of waterproofing layers made of orthotropic polymer modified bitumen membranes (PMB), which are frequently used as flexible sheets for waterproofing on concrete bridge decks to prevent water infiltration through the pavement. The application process and the material properties determine functionality of PBMs and the strength of adhesion to the concrete, both having a significant impact on the life span of concrete bridges. The main reason for blister formation is attributed to pressure produced by air and water vapor under the pavement[2]. Blisters can be caused by the expansion of hot humid air in the concrete after torching of the membrane with open gas flame.

Generally, PBM's are composed of one or two reinforcing carrier layers that are coated on both sides with polymer-bitumen sealing material. The polymer-bitumen sealing material is a mixture of bitumen, mineral fillers and polymers. Polymers are almost exclusively modified either with an elastomer, i.e. styrene-butadiene-styrene copolymer (SBS), or with a plastomer, i.e. atactic polypropylene (APP). A typical SBS-PBM contains 10 to 15 Mass-% SBS-copolymer and 30 to 40 Mass-% filler whereas an APP-PBM contains about 25 to 30 Mass-% APP-polymer and 10 to 30 Mass-% filler [28] The nominal standard thickness of a PMB for waterproofing of bridge decks is 5mm. PBMs are normally attached to the concrete surface by heat welding with a flame or hot air. The peak temperatures in the steam at welding may be about 400°C if hot air is used and about 600-800°C if a gas torch is used [29] These temperatures are high enough to damage the polymer and, if applied excessively, change properties and functionality of the PMBs [29]. Insufficient adhesion and cohesion of the bituminous layer in the membrane and lack of strength of the concrete are the main causes for failure of the adhesive bond between concrete surface and PBM. In addition to this, the welding process can affect the strength of the concrete, i.e. heating can lead to tension in the upper surface followed by cracking or spalling. Low-viscosity epoxy resin as bonding agent, sandblasting and water jetting the concrete plate, etc. can be used to improve the adhesion [1]. Several adhesion test are proposed and standardized, such as pull-off [30], pealing and shear tests[31]. However, these tests are generally not acknowledged to capture the risk of adhesive blister formation in a reliable and realistic way[6].

Other than in the membrane adhesion test (MAT) test, which have been introduced to characterize the adhesive characteristics of the various membranes [32], the blister test allows to characterize the adhesive propagation of blister in a 3D testing situation and in a more realistic pressure controlled than a deformation controlled way. Interfacial debonding propagation arises from two superimposed stress fields. One is due to specimen deformation while the other is from the stress concentration around the orifice of the substrate [8]. The blister test can be modeled as crack propagation along the interface between the hot-poured crack sealant and substrate. The relationship between the applied pressure and blister deflection was used by reference [8] to determine the energy dissipated during debonding of the crack sealant.

3.1 Objective of the study

The main objective of the study is to investigate and model adhesive blister propagation between an orthotropic PBM and concrete. This includes formulating an elastic model which describes propagation of PBM adhesive blister debonding (i.e. fracture mechanical cracking mode I) by applying controlled pressure between the PBM and the concrete plates. The model is formulated assuming the membrane as orthotropic plane stress material. The objective also includes determining the energy for elliptical adhesive blister propagation.

In order to achieve these objectives, first, the orthotropic mechanical behavior of an SBS polymer modified bitumen membrane under in-plane tension stress was determined from biaxial test data. The biaxial tensile loading allows consideration of the biaxial stress condition that exists during blister growth. Hence, the measured stress-strain data were analyzed using the orthotropic elastic equation to find the material properties in the longitudinal and transversal direction. Finally, blister tests were performed on concrete plates for studying adhesive blister propagation by applying controlled constant pressure between the PBM and the concrete plates and for proposing a new model that allowed determining the corresponding adhesive blister propagation energy.

3.2 Biaxial tension test

Typically, mechanical tests are force-displacement tests for determining the relationship between stress and strain in a material. This can be done either by imposing a displacement on the material and measuring the resulting mechanical force (a displacement-controlled test), or by applying a mechanical force and measuring the displacement (a force-controlled test). In order create a test for measuring mechanically reliable material properties, the mechanical characteristics and possible failure mechanisms of the material as well as geometrical design of the specimens must be taken into account. This is also true for a successful biaxial tension strength tests with cruciform specimens (Fig. 3.1(a)) which requires maximization of the region of the uniform biaxial strain, minimization of the shear strains in the biaxial loaded test zone, minimization of the strain concentration outside the test zone and specimen failure in the biaxial loaded test zone [33]. In order to obtain an optimum shape of the cruciform specimen linear elastic finite element model with COMSOL multi-physics commercial software was used. The cruciform specimen was designed to reduce the stress concentration on the edge of the material and to create uniform stress and strain condition in the central part of the cruciform specimen. A homogeneous tensile stress in the center of the specimen for large deformation was achieved by cutting slits in each arm of the specimen.

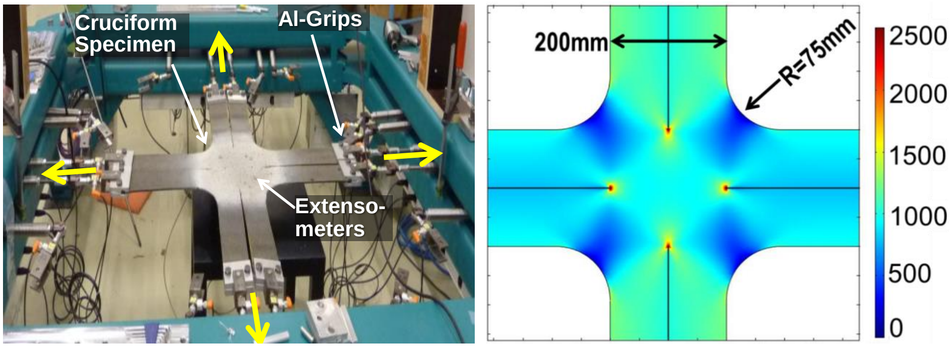

(a) (b)

Fig. 3.1 Biaxial tension test: a) experimental setup, b)Finite element Von Mises stress distribution

A cruciform shaped PBM specimen had a total size of 1000 mm x 1000 mm and central part of 200 mm width. Slits were cut in each arm of the specimen to distribute a tensile deformation at the center of the specimen. Displacement controlled testing condition was set to apply the displacement at a rate of 40 mm/min. Strains in longitudinal and transversal direction in the center of the cruciform specimen were measured with two needle extensometers attached to the center of the specimen. The maximum engineering strain measured was 3.9 %. All the experiments were done to 1:1 loading ratio at room temperature of 23°C.

A linear elastic finite element model (FEM) of the cruciform specimen was used to determine the stress causing the strain measured in the center of the specimen. However, a correction factor is required because of the non-uniform stress distribution in the cruciform sample [34]. From the FEM modeling of the cruciform specimen, it was found that the stress is not completely uniform throughout the specimen. For this reason a correction factor for the stress in the center of the specimen was determined from finite element modeling and found to be 0.94, assuming a Poisson's ratio value (v_{xy} and v_{yx}) of 0.3. From the measured strains and forces in the longitudinal, i.e. production direction of the PBM, and transversal direction as shown in Fig. 3.2(a), the moduli of elasticity in the longitudinal (E_y) and transversal direction (E_x) were determined using Eq. (3.1)

$$\begin{bmatrix} \varepsilon_x \\ \varepsilon_y \end{bmatrix} = \begin{bmatrix} 1/E_x & -v_{yx}/E_y \\ v_{xy}/E_x & +1/E_y \end{bmatrix} \begin{bmatrix} \sigma_x \\ \sigma_y \end{bmatrix} \qquad (3.1)$$

where, ε_x and σ_x are strain and stress in the transversal direction, ε_y and σ_y are strain and stress in the longitudinal direction; v_{xy} and v_{yx} are Poisson's ratio value. From Eq. (3.1) the moduli of elasticity were found to be E_y =10.4 MPa and E_x =7.8 MPa respectively.

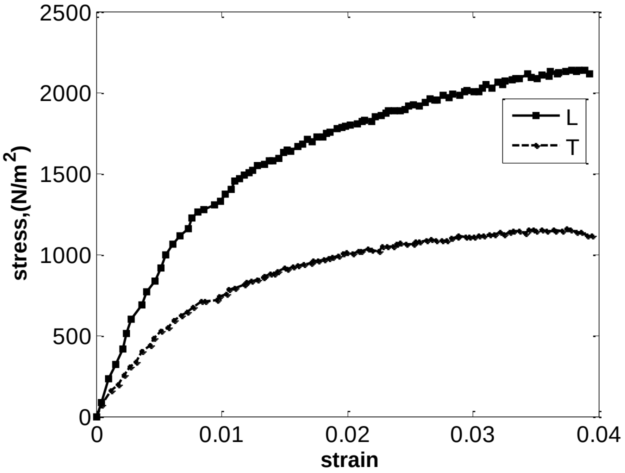

Fig. 3.2 Typical measured biaxial stress-strain curve at 23°C (L: longitudinal, T: transversal)

3.3 Blister test

Sand blasted square concrete plates of 500 mm*500 mm were prepared to investigate the adhesive blister propagation. Each plate contained a central hole for a 17mm diameter steel pipe as water pressure inlet from the bottom of the plate. In order to increase the bond between the concrete and the PBM membrane, a primer of SBS modified bitumen dissolved in toluene was applied on the concrete surface prior to welding the PBM, as shown on Fig. 3.3(a). Afterwards, an open gas torch without air supply into the nozzle was used to weld the membrane on each concrete plate, as shown in Fig. 3.3(b). In doing so, the distance between the membrane surface and the flame as well as the speed of torching was given great care for achieving uniform welding and reducing the most unfavorable heat effect. To create a debonding area that represents an initial crack at the interface between PBM and the concrete substrate, a 17-mm-diameter silicon paper film disk was placed at the bottom of PBM. Next, the PBMs were sprayed with paint to create a spackle pattern as shown in Fig. 3.3(c). The specimens were conditioned at 23 °C room temperature for more than 24 h and the temperature in the PBM layer was checked using thermocouple prior to testing. The pressure was controlled with a manometer and the pressure was increased at 3.3kPa/s for 60 s until it reached 0.2MPa and then kept constant at 0.2 MPa during the testing period. Water instead of gas was used for safety reason, fully aware that in reality water pressure would not cause blister propagation. Digital image correlation experimental technique as described in [34] was used to measure the adhesive blister propagation. This experimental technique allows to measure deformation fields at the surface of objects under any kind of loading condition [19]. As shown in Fig. 3.4 (b), a 3D camera (Limess Vic3D-4Mp) was installed for measuring the adhesive blister propagation in the longitudinal (da_y) and transversal (da_x) direction of the PBM, as defined in Fig. 3.4 (a), together with the change in blister height (dh), as defined in Fig. 3.4(b). Results of blister profile section taken in the longitudinal and transversal direction from the center of blister are shown in Fig. 3.5 (a) and Fig. 3.5 (b). The profiles were determined in one second intervals. Post processing software (Vic-3D 2009) was used to construct the 3D views and contour maps of the vertical deflection of the blisters from the images taken during loading, as presented in Fig. 3.3 (d) and 4 (a). In addition to this, the blister height and radius with time measured during the adhesive blister propagation was determined according to Fig. 3.6(a) and (b). Bulging of the blister was observed during the first 60 sec loading period of the experiment and the change in blister radius remained zero during the pressure increment period of 60 sec while the blister height reached up to 6.8 mm as shown in Fig. 3.6 (a) and (b). In these experiments one image per second was used to measure the blister growth of the PBM membrane. Since the growth rate was slow, this image rate was sufficient. At the end of each experiment the final blister height was measured using a ruler to check with the data from the digital image correlation. It is found that the estimated error between digital image correlation and the measured value is 3.75%.

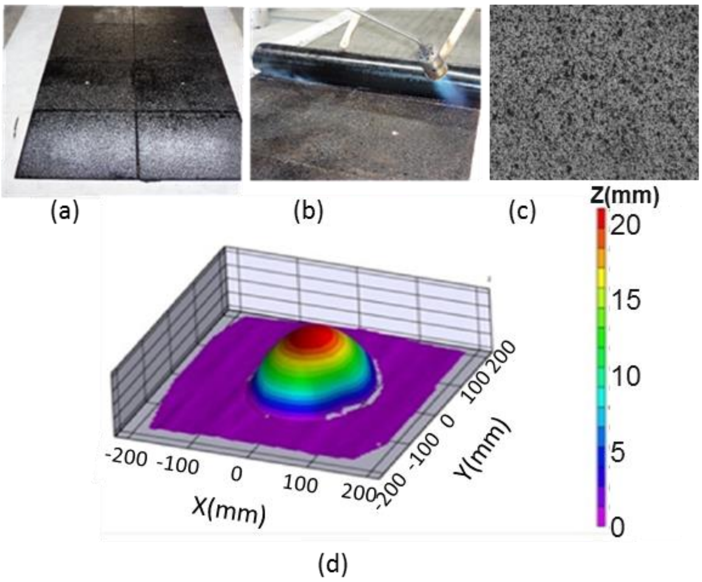

Fig. 3.3 (a) primer applied on the concrete plate (b) welding of the PBM on the concrete plate (c) speckle pattern on the surface of the PBM and (d) 3D view of the blister height

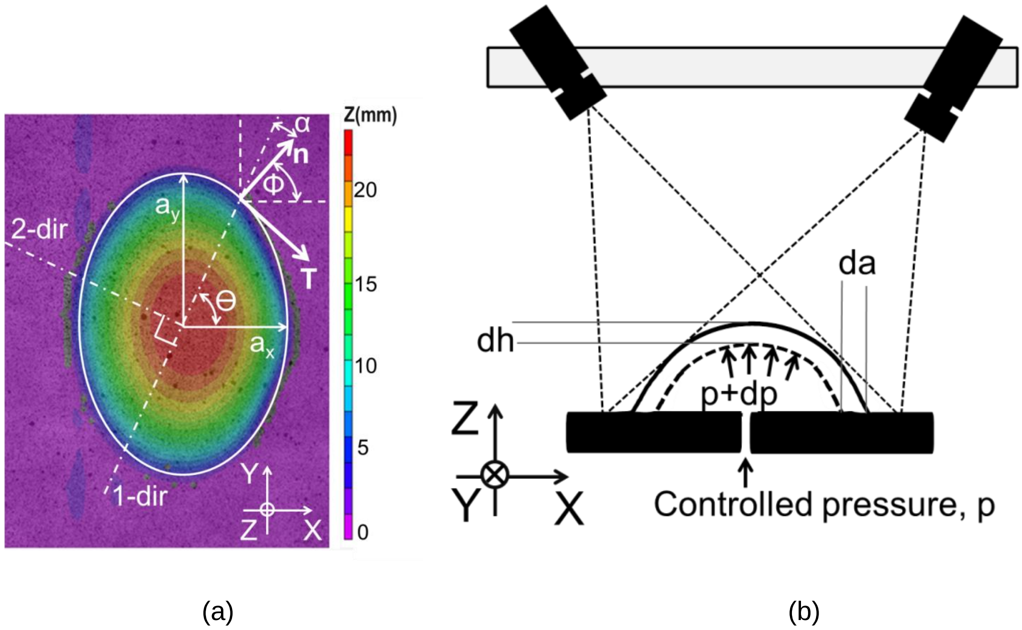

Fig. 3.4 (a) Top view of elliptical adhesive debonding contour on the membrane and (b) schematic view of 3D optical system for blister growth measurement

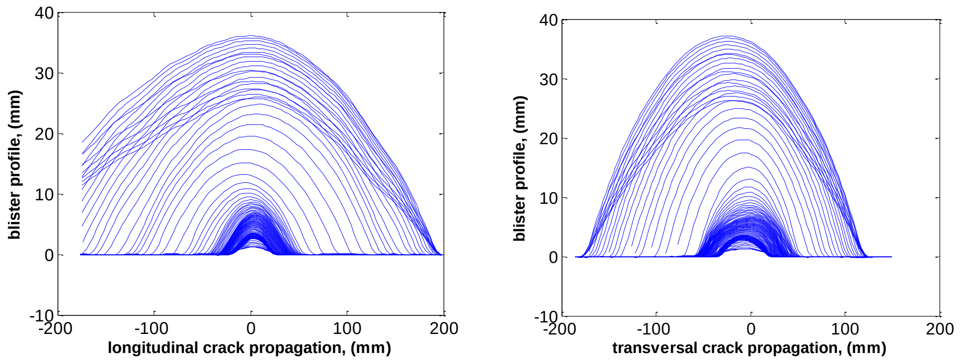

(a) (b)

Fig. 3.5 (a) Transversal and (b) Longitudinal blister propagation (digital image correlation)

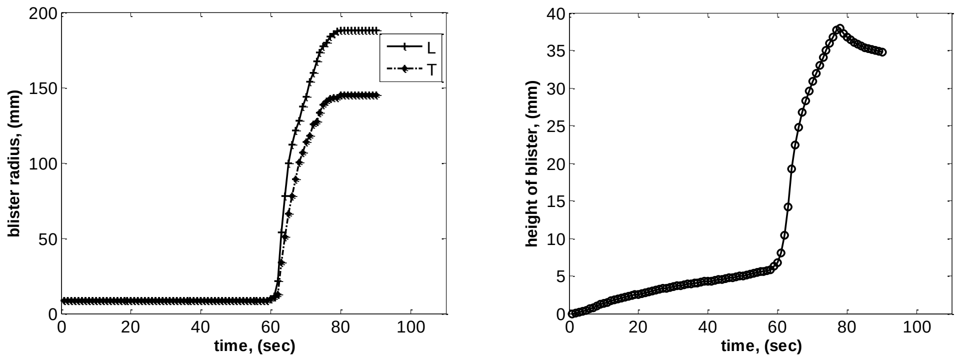

(a) (b)

Fig. 3.6 (a) Longitudinal (L) and transversal (T) blister radius with time and (b) measured blister height.

3.4 Results and discussion

As the material is assumed to be orthotropic, it must be described by two values of modulus of elasticity, one along the longitudinal direction of the production direction of the PBM and one in transversal direction. Generally, the loading direction does not match the principal direction of the material properties. Thus, the stress and the strain must transform into coordinates that coincide within the principal material direction [33]. The modulus of elasticity in the 1 and 2 direction at different angles of rotation as defined in Fig. 3.7(a) is determined with Eq. (3.2). The value of shear modulus M in the stiffness matrix D is assumed to be 3.45 MPa. This value was found through iterative process until the general orthotropic equation becomes equivalent with the elliptic equation for the tensile modulus E_{eli} in each direction θ as shown in Eq. (3.3).

$$\left[\bar{D}\right]=\left[A\right]^{-1}\left[D\right]\left[R\right]\left[T\right] \tag{3.2}$$

Where, R is 'Reuter's matrix', A is the transformation matrix, $\bar{D}$ is the transformed stiffness matrix of the material.

From the biaxial and blister test experiments, it was observed that there exists affinity between the modulus of the PBM (the biaxial loading state) and the debonding ellipse. From this similarity, it was found that Eq. (3.3) can be used instead of the general orthotropic equation (Eq.3.2) to calculate the modulus of PBM as a function of angle of rotation θ.

$$E_{eli} = \sqrt{\frac{E_x{}^2 E_y{}^2}{E_y{}^2 \cos(\theta)^2 + E_x{}^2 \sin(\theta)^2}} \tag{3.3}$$

Where, E_x and E_y are moduli of elasticity in the x and y-direction, i.e. in the principal transversal and longitudinal direction of the material properties. θ is the angle of rotation as defined in Fig. 3.4(a).

Determining the normal stress along the elliptic failure front as a function of angle of rotation θ is quite cumbersome and complicated with Eq. (3.2). The elliptical equation for the elastic modulus, Eq. (3.3) was modified to calculate the stress (σ_θ) in the direction of the rotation angle θ as shown in Eq. (3.4). The strain formulation used in Eq. (3.4) is similar to the well-known 'bulge equation' reported in literature [35, 36]. Implicit differentiation of the general ellipse equation is used to determine the normal direction of the ellipse (ϕ) shown in Fig. 3.4 (a). The difference between angle θ and ϕ gives angle α which helps to express the normal stress component of the stress in the θ direction. The stress in the normal direction is presented in Eq. (3.5) and the result is shown in Fig. 3.8 (b).

$$\sigma_\theta = \sqrt{\frac{\sigma_x^2 \sigma_y^2}{\sigma_y^2 \cos(\theta)^2 + \sigma_y^2 \cos(\theta)^2}}; \quad \sigma_x = E_x \varepsilon_x = E_x \frac{2h^2}{3a_x^2}; \quad \sigma_y = E_y \varepsilon_y = E_y \frac{2h^2}{3a_y^2} \tag{3.4}$$

The normal stress as a function of the angle θ and α around the ellipse is calculated using Eq. (3.5) and presented in Fig. 2.8(b).

$$\sigma_n = \sigma_\theta \cos(\alpha); \quad \sigma_n = \frac{2h^2 E_x k \cos(\alpha)}{3a_x^2 a_y^2 \sqrt{\frac{k^2}{a_y^4} \cos(\theta)^2 + \frac{\sin(\theta)^2}{a_x^4}}} \tag{3.5}$$

Where E_x is the moduli of elasticity in x – direction, k is defined as $k=E_y/E_x$; a_x and a_y are the minor and major axes of the blister adhesive failure front; θ is the angle of rotation; h is blister height; α is the angle difference between the normal n and the rotation angle θ according to Fig. 3.4(a).

The vertical stress component (σ_v) of the normal stress (σ_θ), shown in Fig. 3.7(b), is calculated from Eq. (3.6). Angle β is assumed to be a function varying between β_1 to β_2 elliptically. The values of β_1 and β_2 are determined iteratively and found to be β_1 =29.7° and β_2=39.8° respectively.

$$\sigma_v = \sigma_n \sin(\beta) \tag{3.6}$$

Where β is the angle between the normal and vertical stress as shown in Fig. 3.7 (b)

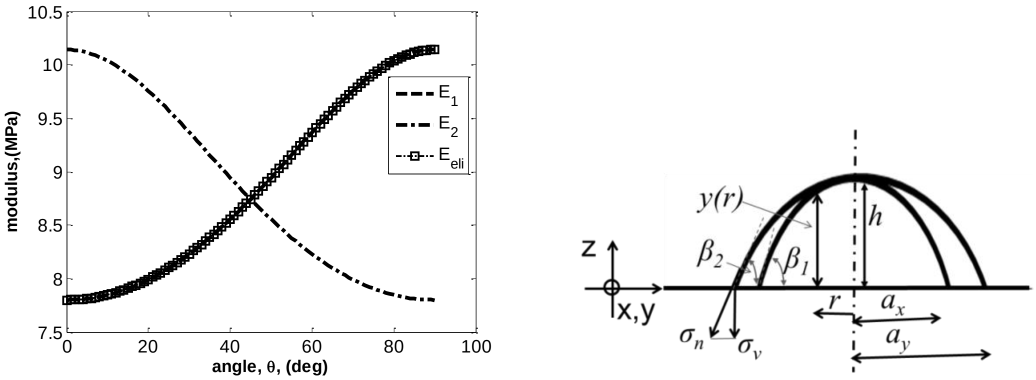

(a) (b)

Fig. 3.7 (a) Modulus as a function of angle and (b) Blister profile in x and y-axis

Substituting Eq. (3.5) in Eq. (3.6) and rearranging the equation gives the following Eq. (3.7) in terms of constant terms k, k_1 and k_2 which are a function of angle as described above. The vertical stress component determined using Eq. (3.7) is presented in Fig. 3.8(b). It is shown in Fig. 3.8(b) that the stress in the vertical direction is independent of the angle of θ. This is reasonable; otherwise elliptical adhesive blister propagation would not be possible. The vertical stress around the elliptical adhesive failure front is constant and, given the material properties in Tab. 3.1 for this calculation, the vertical stress was found to be σ_v =2.73 kPa.

Tab 3.1. Parameters used to calculate the vertical stress in the PBM around the elliptical adhesive failure front

E_x	0.078 MPa
a_x	82.65 mm
a_y	113.24 mm
h	26.7 mm
k	1.3
k_1 for θ=0°	4
k_2 for θ=0°	0

$$\sigma_v = \frac{2h^2 E_x k}{3a_x^2 a_y^2 \sqrt{\frac{k^2}{a_y^4} k_1 + \frac{k_2}{a_x^4}}} \tag{3.7}$$

$$k = \frac{E_y}{E_x}, k_1 = \frac{\cos(\theta)^2}{\cos(\alpha)^2 \sin(\beta)^2} \; and \; k_2 = \frac{\sin(\theta)^2}{\cos(\alpha)^2 \sin(\beta)^2}$$

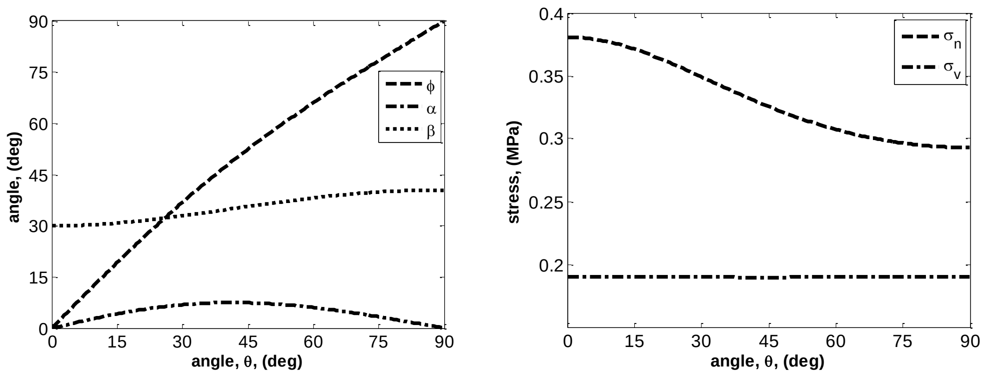

(a) (b)

Fig. 3.8 (a) Stress resolving angles around the elliptical crack front and (b) Normal and vertical component of normal stress

The total adhesive blister propagation energy is the sum of the potential energy of the external applied load (negatively defined) and the elastic strain energy stored in the membrane depending on the geometry of the adhesive failure zone [7, 9]. The work done W_{app} by the pressurized water in the blister is greater than the increase in the membrane's strain energy U_{strain}. The difference between these quantities is called fracture energy release rate G [9, 35] and thus describes the adhesive blister propagation energy release rate. G is defined per unit width along the elliptic failure front between the PMB and the concrete and has a unit of J/m^2. Hence, for an elliptical blister with an elliptic adhesive failure area A, G is given by the following Eq. (3.8).

$$G \cong -\left(\frac{\partial W_{app}}{\partial A} + \frac{\partial U_{strain}}{\partial A} \right)\Bigg|_{p} \tag{3.8}$$

If the fluid pressure is applied into the blister and assuming a thin PBM, the exact solution for the profile of circular membrane blister is determined using the Hencky series solution [7, 9]. Hencky series solution is used to determine the shape factor k_s which is determined for Poisson's ratio v = 0.35 and found to be k_s =0.543. The volume under the blister V is found from Eq. (3.9), by integrating the radius change over the circumference of the elliptic adhesive failure front.

$$V = \int_0^{2\pi} \frac{hk_s}{2} \frac{a_y^2 a_x^2}{a_y^2 \cos(\theta)^2 + a_x^2 \sin(\theta)^2} d\theta = \pi h k_s a_x a_y \tag{3.9}$$

where k_s =0.543 for v=0.35 and h is the central deflection of the blister.

Using the common equilibrium condition for pressurized thin-walled ellipse, the following equation is used to relate the pressure p and the stress σ_v as defined in Fig 3.7(b) and given by Eq. (3.7)

$$P = \sigma_v \frac{tc_{eli}}{\pi a_x a_y}; \quad c_{eli} = \pi\left(3\left(a_x + a_y\right) - \sqrt{(3a_x + a_y)(3a_y + a_x)}\right) \tag{3.10}$$

where a_x and a_y are the minor and major radius of the elliptical adhesive failure front, t is the membrane thickness and c_{eli} is the circumference of the elliptic crack front.

With the volume V of the inflated blister and the pressure applied, it is possible to calculate the strain energy to inflate the blister from initial flat state to a certain height h [7, 36] as shown in Eq. (3.11).

$$U_{strain} = \int_{h'=0}^{h'=h} P(h') \frac{dV}{dh'} dh' = \frac{2}{9} \frac{kE_x tc_{eli} k_s h^3}{a_x^2 a_y^2 \sqrt{\frac{k_1 k^2}{a_y^4} + \frac{k_2}{a_x^4}}} \tag{3.11}$$

The work done on the blister by the applied pressure p as the elliptical blister expands can be calculated using Eq. (3.12). The energy change that occurs when the elliptic adhesive failure front is increased by a differential amount of area is calculated using the derivation of the strain energy with respect to blister area at constant pressure as shown in Eq. (3.12).

$$\left(\frac{w_{app}}{\partial A}\right)_p = -\left(\frac{\partial(pV)}{\partial A}\right)_p = -phk_s; \quad \left(\frac{U_{strain}}{\partial A}\right)_p = \frac{1}{3} phk_s \tag{3.12}$$

Inserting the above equation in Eq. (3.8) and solving for adhesive blister propagation energy parameter G over the adhesive failure area A of blister results in

$$G = \frac{p^2 k_s a_x^3 a_y^3 \pi}{hkE_x tc_{eli}} \sqrt{\frac{k_1 k^2}{a_y^4} + \frac{k_2}{a_x^4}} \tag{3.13}$$

The above Eq. (3.13) can be used to calculate adhesive blister propagation energy for the whole blister which is an overall value regardless of the angle θ. Any values of angle from 0°-360° can be used for values of k_1 and k_2 . For this analysis angle θ equal to zero was used. As an example, the parameters in Tab. 3.2 were used to calculate the adhesive blister propagation energy value G, and found to be G=1.353*10^6 J/m^2. The modulus of elasticity in the x-direction, E_x, was determined from the biaxial test. From the blister test experimental data shown in Fig. 3.6 (a) and (b), the blister radii and height at measurement time of 67s was used for this analysis. a_x and a_y are the radii of the elliptic blister in the transversal and longitudinal direction found from image correlation measurements; h is the blister height; c_{eli} is the circumferential of the elliptical blister crack front. t is the thickness of the PBM; k is the ratio of the modulus of elasticity in y and x-direction. k_1 and k_2 are constants as a function of angle as shown in Eq. (3.7); k_s is the shape factor as presented in Tab. 3.2. Keeping constant parameters in Tab. 3.2 and increasing linearly the pressure from 0 up to 1MPa results in a high rate of change of blister propagation energy as indicated in Fig. 3.9.

Tab 3.2. Parameters used to calculate the adhesive blister propagation energy G

E_x	0.078 MPa
a_x	82.65 mm
a_y	113.24 mm
h	26.7 mm
c_{eli}	619.14 mm
t	5.0 mm
p	0.2MPa
k	1.3
k_1 for θ=0°	4
k_2 for θ=0°	0

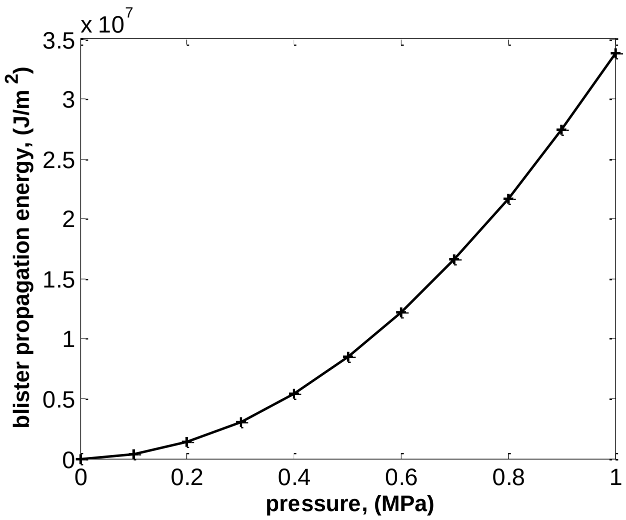

Fig. 3.9 Blister propagation energy as a function of pressure

4 Testing of Blister Propagation and Peeling of Water Proofing

4.1 Membrane Background of the blister test

It is known that blistering effects can be found on bridge decks, multistory car parks, tunnels or pedestrian areas (e.g. sidewalks). When hot mastic is applied to concrete, blisters may occur either between the dense asphalt layers and the polymer modified bitumen waterproofing membrane [6, 27], or between the waterproofing membrane and the structural concrete of the bridge deck [28]. Pressure produced by air and water vapor under the pavement is the main reason for blister formation[2]. In particular, it can be caused by the expansion of hot humid air in the concrete after torching of the membrane with open gas flame. This report focuses on blistering of orthotropic polymer modified bitumen waterproofing membranes (PBMs), which are frequently used as flexible sheets for waterproofing on concrete bridge decks to prevent water infiltration from the pavement to the concrete surface. The application process and the material properties determine functionality of PBMs and the strength of adhesion to the concrete, both having a significant impact on the life span of concrete bridges.

Generally, PBMs are composed of one or two reinforcing carrier layers that are coated on both sides with polymer-bitumen sealing material. The polymer-bitumen sealing material is a mixture of polymer modified bitumen, mineral fillers and polymers. Polymers are almost exclusively modified either with an elastomer, i.e. styrene-butadiene-styrene copolymer (SBS), or with a plastomer, i.e. atactic polypropylene (APP). A typical SBS-PBM contains 10 to 15 Mass-% SBS-copolymer and 30 to 40 Mass-% filler whereas an APP-PBM contains about 25 to 30 Mass-% APP-polymer and 10 to 30 Mass-% filler [28]. The nominal standard thickness of a PBM for waterproofing of bridge decks is 5mm. Since PBMs are normally attached to the concrete surface by heat welding with a flame or hot air, properties and functionality of the PBMs can be affected by high welding temperatures which can reach up to 400°C if hot air is used and 600-800°C if a gas torch is chosen [29]. Moreover, these high temperatures during the welding process can affect the strength of the concrete, e.g. by producing tension in the upper surface followed by cracking of the concrete. The adhesion between the concrete and the PBM can be improved by using low-viscosity epoxy resin as bonding agent after sandblasting or water jetting the concrete plate, etc. [37].

Insufficient adhesion and cohesion of the bituminous layer in the membrane and lack of strength of the concrete are the main causes for loosing adhesive bond between concrete surface and PBM. Several adhesion tests are proposed and standardized, including pull-off tests [38], pealing and shear tests[35] and others. However, these tests are generally not acknowledged to capture the risk of adhesive blister formation in a reliable and realistic way[6] specially when it comes to orthotropic material behavior of the PBM under multi axial state of stress.

If the right representation is used, for instance true stress-strain relationship in case of large deformation, very similar material behavior can be found up to the second yielding point whether uniaxial tension test or biaxial extension test is used for elastic material [19]. The fracture property G, is a 'geometric independent' material property that characterizes the energy to break the interfacial bonding forces and the energy dissipated locally ahead of the peeling front in the plastic or viscoelastic zone at crack tip [39, 40]. The energy term needs to account for the stored energy in the peeling arm, the energy dissipated during tensile deformation of the peeling arm and the energy dissipated due to bending of the peeling arm [39, 41, 42] . This approach will be used in this report for comparison with blister propagation energy [43]. Another common way of determining the fracture energy is through numerical modeling by using the cohesive zone crack propagation model via generalized 'Griffith' energy criteria, which works by limiting the maximum value of the stress in the damage zone ahead of the crack and is often used because of its physical significance [41, 44, 45].

The blister test allows characterizing the adhesive propagation of blisters under 3D testing conditions in a pressure controlled situation which is more realistic than a deformation controlled setup. The blister test behavior can be modeled as crack propagation along the interface between the welded PBM sealant and the substrate, considering the relationship between the applied pressure and blister deflection [8]. From this relationship it is possible to determine the energy dissipated during debonding of the PBM.

4.2 Objective of the study

The primary objective of the study was to implement the analytical blister propagation energy and compare it with a standard peeling test method, as described in Swiss standards, and determine the adhesive fracture energy from literature [39, 41, 42]. Three different types of polymer modified bitumen membranes (PBMs) were used for this investigation. The investigation includes the comparison between the uniaxial and biaxial test for determining the modulus of elasticity of the membranes. Influence of the displacement rate and temperature on adhesive fracture energy is also investigated for the peeling test. The other objective is to compare a new model that allows determining the corresponding adhesive blister propagation energy [43] with the fracture energy equations for peeling as proposed in literature. Finally, this helps to understand the blister crack propagation on top of the concrete surface and it's relation to the peeling test. It also helps to distinguish the adhesive properties of different types of membranes and their resistance to blister formation without conducting the time consuming and complicated pressurized blister propagation tests with digital image correlation techniques.

4.3 Material and methodology

The material used in the investigation includes three polymer modified bitumen waterproofing membranes with different components. Details of the membrane components are indicated in Tab. 4.1 based on the multilayer composition of waterproofing membranes as depicted schematically in Fig. 4.1.

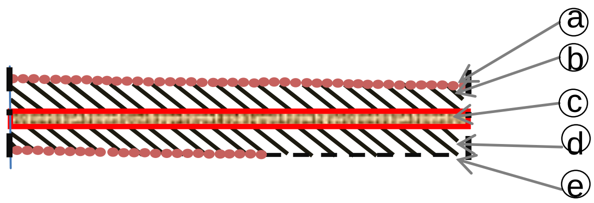

Fig. 4.1 Typical schema of the composition of polymer modified bitumen membranes: (a) top surfacing; (b) top polymer-bitumen layer with mineral filler; (c) carrier; (d) bottom polymer-bitumen layer with mineral filler; (e) bottom surfacing

Tab 4.1. Different layers if the polymer modified bitumen waterproofing membranes (MA hot mastic asphalt resistant, WF: roof resistant, EP5 and PPPV5 are condensed material designations according to Swiss standards SIA 281, PE: polyethylene)

Layer/PBM	a	b	c	d	e
SBS-1(EP5 MA)	Talcum/ Sand	Bitumen, SBS polymers and filler	Polyester	Bitumen, SBS polymers and filler	PE-film
SBS-2 (EP5 MA, WF)	Talcum/ Sand	Bitumen, SBS polymers and filler	Polyester	Bitumen, SBS polymers and filler	Sand
APP (PPV5 MA,WF)	Talcum/ Sand	Bitumen, APP polymers and filler	Polyester and glass fabric	Bitumen, APP polymers and filler	PE-film

The investigation includes testing of SBS-1 waterproofing membrane using uniaxial tension test at 23°C, 40°C and 55°C in combination with 50, 75 and 100 mm/min displacement rate in the longitudinal direction. The uniaxial test performed for SBS-1 at 23°C and 50 mm/min displacement rate is compared with biaxial test to check if the two testing condition give similar stress-strain curves and moduli of elasticity. Three specimens each were tested in a uniaxial and biaxial experiment. After this, the uniaxial test is performed for SBS-1, SBS-2 and APP waterproofing membranes at 23°C and 50 mm/min displacement rate in the longitudinal and transversal direction to determine the modulus of elasticity in the respective direction. In addition to this, peeling test is performed for SBS-1 waterproofing membrane at 23°C, 40°C and 55°C in combination with 50, 75 and 100 mm/min displacement rate in order to understand the influence of the temperature and the displacement rate on the peeling fracture energy. Peeling test is done in the longitudinal direction at 23°C for SBS-1, SBS-2 and APP water proofing membranes to determine the peeling fracture energy. Blister test is performed on SBS-1, SBS-2 and APP waterproofing membranes at 23°C by applying a controlled pressure. The pressure was set to 0.2 MPa during the testing period. Blister height and crack propagation in the longitudinal and transversal direction is measured using 3D image correlation system. Finally the blister propagation energy is compared with the fracture energy from peeling tests. A detailed description of the different tests is given below.

4.4 Biaxial tension test

In order to create a test for meaningful measuring mechanical material properties, mechanical characteristics and possible failure mechanisms of the material as well as geometrical design of the specimens must be taken into account. Cruciform specimens can be used to determine biaxial tension strength. This requires maximization of the region of the uniform biaxial strain, minimization of the shear strains in the biaxial loaded test zone as well as minimization of the strain concentration outside the test zone to create specimen failure within the biaxial loaded test zone [33]. Details of validating the biaxial test using a finite element (FE) model were presented by [43]. A cruciform shaped PBM specimen was used with a total size of 1000 mm x 1000 mm and a central part of 200 mm width. Slits were cut in each arm of the specimen to allocate a tensile deformation in the center of the specimen. Displacement at a rate of 40 mm/min was applied. Strains in longitudinal and transversal direction in the center of the cruciform specimen were measured with two needle extensometers attached to the center of the specimen. The maximum engineering strain measured was 3.9 %. All the experiments were performed with a 1:1 loading ratio at room temperature of 23°C.

The cruciform specimen was modeled using a linear elastic FE model to determine the stress causing the strain measured in the center of the specimen [43]. Due to the non-uniform stress distribution in the cruciform sample, a correction factor must be used [34]. For FE modeling of the cruciform specimen, Poisson's ratios v_{xy} and v_{yx} of 0.3 were assumed; the correction factor for the stress in the center of the specimen was found to be 0.94 [43]. Strains and forces were measured in the longitudinal and transversal direction of the PBM to determine the moduli of elasticity in the longitudinal (E_y) and transversal direction (E_x) using Eq. (4.1) as shown in Fig. 4.2.

$$\begin{bmatrix} \varepsilon_x \\ \varepsilon_y \end{bmatrix} = \begin{bmatrix} 1/E_x & -v_{yx}/E_y \\ v_{xy}/E_x & +\ 1/E_y \end{bmatrix} \begin{bmatrix} \sigma_x \\ \sigma_y \end{bmatrix} \tag{4.1}$$

where, ε_x and σ_x are strain and stress in the transversal direction, ε_y and σ_y are strain and stress in the longitudinal direction; v_{xy} and v_{yx} are the Poisson's ratios. Since both Poisson's ratios were assumed to be equal, only v without the indices is used in the following.

To compare the modulus of elasticity from the biaxial with the uniaxial experiments, equivalent stress σ_{eq} and equivalent strain ε_{eq} were calculated using Eq. (4.2). The results are presented in Fig. 4.2.

$$\sigma_{eq} = \left[\sigma_x^2 + \sigma_y^2 - \sigma_x \sigma_y \right]^{\frac{1}{2}}; \quad \varepsilon_{eq} = \frac{1}{1+v} \left[\frac{1}{2} \left[\left(\varepsilon_x - \varepsilon_y \right)^2 + \varepsilon_x^2 + \varepsilon_y^2 \right] \right]^{\frac{1}{2}} \tag{4.2}$$

where, ε_x and σ_x are strain and stress in the transversal direction, ε_y and σ_y are strain and stress in the longitudinal direction; v is the Poisson's ratio value.

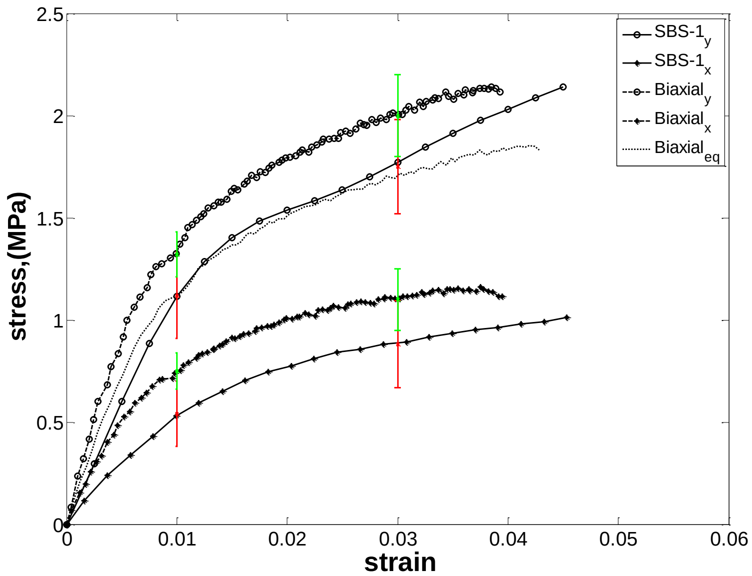

Fig. 4.2 Typical measured stress-strain curve at 23°C from biaxial (y: longitudinal, x: transversal) and uniaxial tension test

4.5 Uniaxial tension tests

Uniaxial tension tests were conducted in the longitudinal direction of the PBM to determine the influence of displacement rate and temperature. 100, 75 and 50 mm/min displacement rates were used in combination with 23°C, 40°C and 50°C temperatures. The specimens were prepared according to the Swiss testing standard, with a central part of 40 mm width and 200mm length and a nominal thickness of 5mm. Engineering stress and strain were determined instead of true stress and strain using Eq. (4.3), since the deformation of the peeling arm consider was in small range.

$$\sigma = \frac{F}{Wt} \quad ; \; \varepsilon = \frac{\Delta L}{L_0} \tag{4.3}$$

Where, F is the tension force, W is the width, t is the thickness, ΔL is the change in length and L_o is the length before deformation. Examples of the stress-strain curve performed at 23°C for SBS-1 material in the longitudinal direction are shown in Fig 4.4(a). Additional experiments were conducted on all three types of the waterproofing membranes at 23°C in both longitudinal and transversal direction as presented in Fig. 4.3(b).

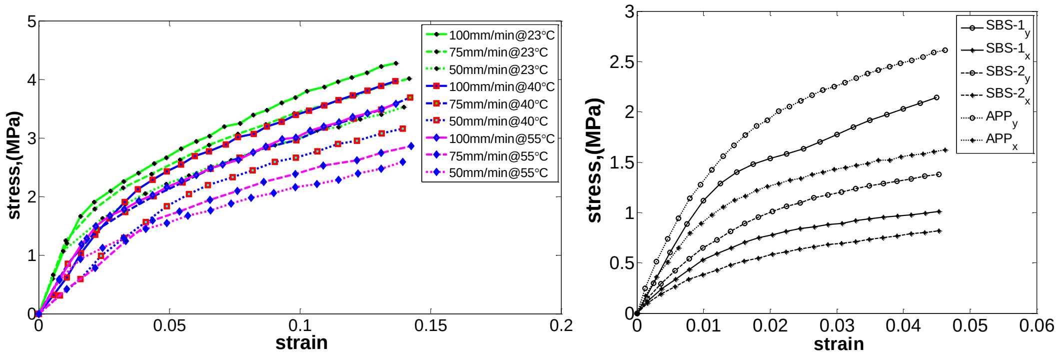

(a) (b)

Fig. 4.3 (a) Influence of temperature and displacement rate (SBS-1) (b) Uniaxial stress-strain curve for three different types of PBMs at 23°C.

4.6 Blister test

To investigate adhesive blister propagation, sand blasted square concrete plates of 500 mm*500 mm with water inlet size of 17 mm diameter were prepared and PBMs were welded on top of it as explained by [43]. The specimens were stored at 23 °C room temperature for more than 24 h and the temperature in the PBM was checked using a thermocouple prior to testing. For safety reasons water instead of gas was used to produce blisters artificially between the PBM and the concrete plate, being well aware that in reality not water but vapor would cause pressure and blister propagation. The pressure was controlled with a manometer and increased at 3.3kPa/s for 60 s until it reached 0.2MPa and then kept constant at 0.2 MPa during the blister growth for all types of the PBMs.

Digital image correlation experimental technique was used to measure the adhesive blister propagation as described by [34]. This experimental technique was found useful to measure deformation fields at the surface of objects under any kind of loading condition [19]. To generate the 3D views and contour maps of the vertical deflection of the blisters in z-direction, post processing software (Vic-3D 2009) was used. Examples of reconstructed images taken during loading are shown in Fig. 4.4 (a) and (b). Similarly the blister height and radius with time for the three different types of PBM were measured during the blister propagation as indicated in Fig. 4.5.

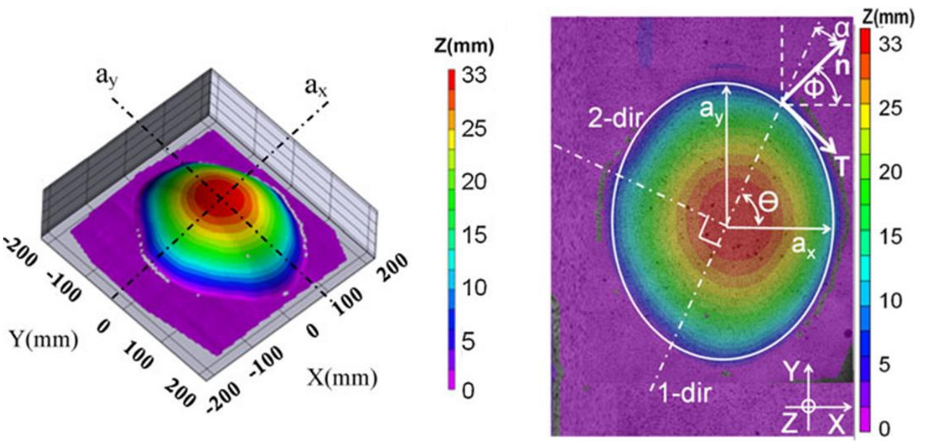

(a) (b)

Fig. 4.4 (a) 3D view of the blister (b) top view of vertical deflection in z-direction showing elliptical adhesive debonding contour on the membrane and symbols for theoretical modeling [43]

During the first 60 s of loading, bulging of the blister was detected and the change in blister radius remained zero, whereas the blister height was increasing up to 6.8, 7.1 and 2.3 mm for the SBS-1, SBS-2 and APP membranes respectively, as shown in Fig. 4.6 (a) and (b). Since the growth rate of the blister propagation was slow, one image per second was used to measure the blister growth in all experiments. The final blister height was measured using a ruler at the end of each experiment to check with the data from the digital image correlation experiment. The comparison between the digital image correlation and the measured value showed an error of about 4.25%.

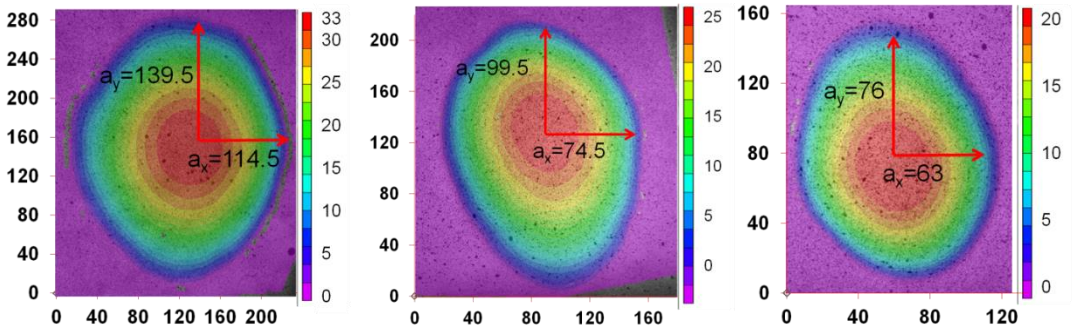

(a) (b) (c)

Fig. 4.5 Top view of elliptical blister contour and vertical deflection in z-direction of PBMs: (a) SBS-1; (b) SBS-2; (c) APP

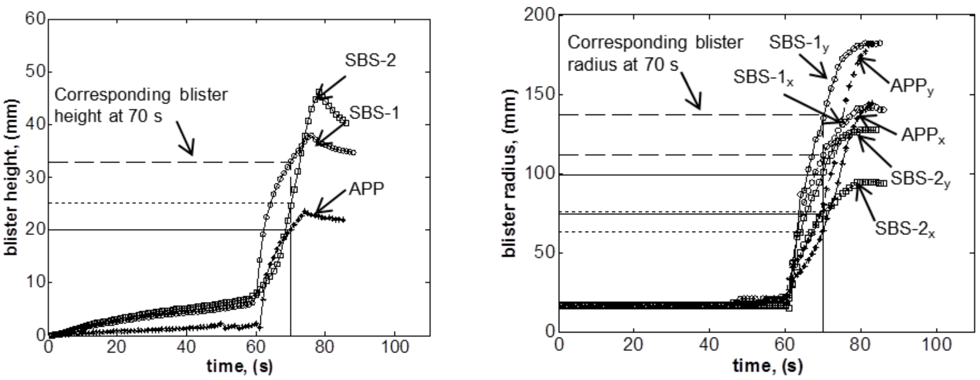

(a) (b)

Fig. 4.6 (a) Measured blister height with time (b) Blister radius in longitudinal (y) and transversal (x) direction with time. Also shown are the values at 70 s used as a reference for calculation (see Tab. 4.4)

4.7 Peeling test

Sand blasted square concrete plates of 500 mm*500 mm were prepared to investigate the peeling fracture energy. In order to increase the bond between the concrete and the PBM membrane, a primer of SBS modified bitumen dissolved in toluene was applied on the concrete surface prior to welding the PBM, as shown on Fig. 4.7 (a). The membranes were applied on each concrete plate using an open gas torch without air supply into the nozzle, as indicated in Fig. 4.7 (b). Great care was given to achieve uniform welding and reduce the most unfavorable heat effect by keeping the distance between the membrane surface and the flame as well as the speed of torching for the peeling test specimens as constant as possible. The concrete plates were cut to a size of 50*350 mm. The setup of the peeling test is shown in Fig. 4.7 (c). The specimens were conditioned at target temperature for more than 24 h and the temperature in the PBM layer was checked using a thermocouple prior to testing. The peeling crack growth was measured using string potentiometer attached to the specimen, the setup is shown in Fig. 4.7(c). The crack propagation length was measured every 0.5 s.

Peeling failure occurs from loss of interfacial bonding force. Hence, this type of failure may be related to the work of adhesion, the work of cohesion or some complicated combination of both [39]. However, note that the above terms are based on the macroscopic interpretation of the interfacial fracture process since, on microscopic scale, adhesive fracture cannot occur [39]. The peeling test is shown schematically in Fig. 4.8 (a) with symbols for theoretical modeling of the debonding, i.e. crack growth, rate and calculation of the adhesive fracture energy for peeling. The typical peeling force vs. time graph in Fig. 4.8 (b) was obtained by peeling at 100 mm/min displacement rate and 23°C conditioning temperature. The high levels of the peeling force is considered to come from a cohesive fracture in the peeling arm and the low levels from adhesive fracture between the substrate and adhesive layer [40].

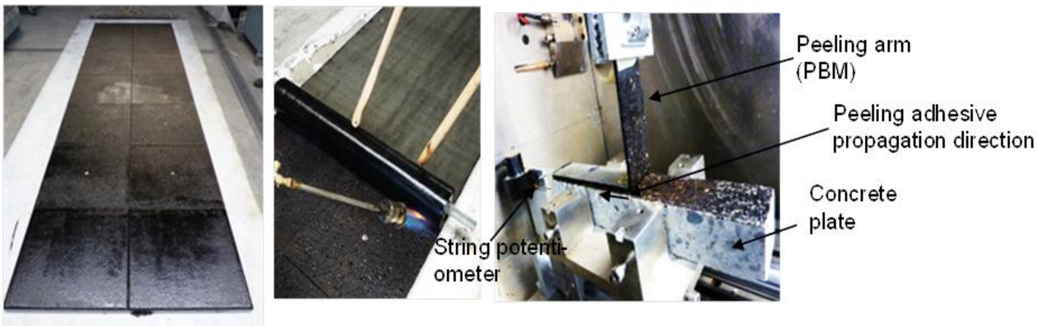

(a) (b) (C)

Fig. 4.7 (a) Primer applied on the concrete plate (b) Welding of the PBM on the concrete plate (c) Peeling test set up

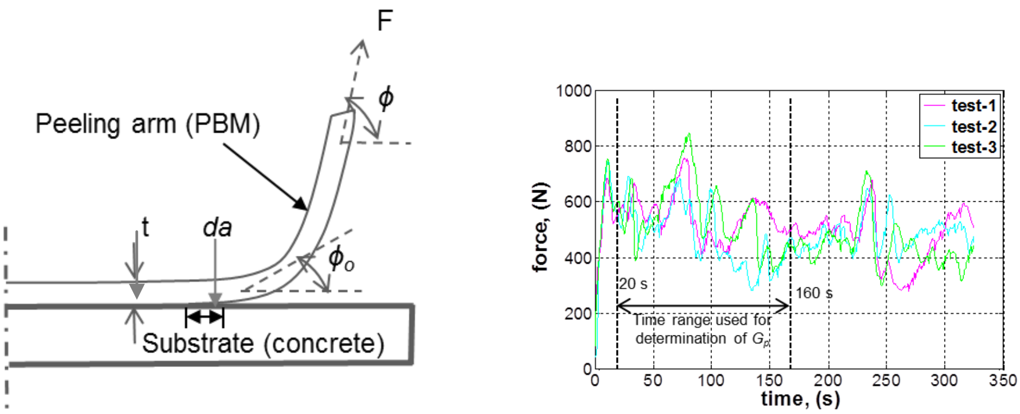

(a) (b)

Fig. 4.8 (a) Schema of peeling test with symbols for theoretical modeling (b) Typical peeling force vs. time graph

4.8 Fracture energy determination of the peeling test

In order to analyze the fracture energies of the peeling test it is necessary to conduct both the uniaxial tension test and the peeling test [39, 40]. The fracture energies of the peeling test depend on the rate of peeling force and the testing temperature. The energy balance of the system when a crack propagates between the substrate and the membrane is described in Eq. (4.5) [39, 40, 46]. This equation considers the plastic bending energy in the crack front to determine the peeling fracture energy, G_p. In order to eliminate the kinetic energy associated with moving peeling fracture, it is necessary to conduct a slow peeling test. For this reason displacement rates of 50, 75 and 100 mm/min are used. As demonstrated in Fig. 4.3, the uniaxial tests strained the waterproofing membrane beyond the yielding point and further increase in stress produces additional plastic deformation. This indicates that the waterproofing membrane follows bilinear material behavior with work hardening. Therefore, from the uniaxial test, it is possible to determine the modulus of elasticity (E), the yield strain (ε_c) and the work hardening parameter (λ) as shown in Fig. 4.9 (a). The adhesive fracture energy for peeling is calculated from Eq. (4.4),

$$G_p = G^e - G^b \tag{4.4}$$

Where G^e is the energy accounts for elastic tensile deformation and elastic bending of the peel arm and G^b accounts for plastic bending energy in the crack front.

The energy balance equation for crack propagation reads.

$$G_p = \frac{1}{W}\left(\frac{dU_{App}}{da} - \frac{dU_{strain}}{da} - \frac{dU_{dt}}{da} - \frac{dU_{db}}{da}\right) \tag{4.5}$$

Where U is an energy term, W is the width of peel arm, a is the crack length and the suffices App, strain, dt and db refer to the applied load, strain, dissipation in tensile deformation and dissipation in bending near the peel front.

The above energy terms from Eq. (4.5) which contains the elastic deformation can be rearranged as follows [40, 46].

$$G_a^{\infty E} = \frac{1}{W}\left(\frac{dU_{App}}{da}\right) = \frac{F}{W}(1-cos(\phi)); \quad G^e_{max} = \frac{1}{W}\left(\frac{dU_{dt}}{da}\right) = \frac{tE\varepsilon^2}{2}; \quad \frac{1}{W}\left(\frac{dU_{strain}}{da}\right) = \frac{F\varepsilon}{W} \tag{4.6}$$
$$G^e = \frac{F}{W}(1+\varepsilon - cos(\phi)) - \frac{tE\varepsilon^2}{2}$$

Where F is the mean peeling force, W is the width of peeling arm, ε is the strain in the peeling arm, ϕ is the angle of peeling, E is the modulus of elasticity of the membrane from the uniaxial test, t is the thickness of the membrane. The mean peeling force, F is determined as average value in the time frame between 20 s and 160 s as shown in Fig. 4.8 (b).

The deformation process on the crack front was modeled using large displacement beam theory which involves only elastic theory [47]. The peeling fracture propagation energy from the external applied force, for infinite tensile stiffens and zero bending modulus is denoted as $G_A^{\infty E}$ as shown in Eq. (4.6). The maximum elastic fracture energy which can be stored in the peeling arm is denoted as G^e_{max} as indicated in Eq. (4.6). Note that $f_1(\overline{k_o})$, in Eq. (4.7) equals to $f_2(\overline{k_o})$ defined in Eq.(4.8). The general scheme of similar modeling of the local bending was shown by references [39, 42, 47]. As it is stated in the above references, iteration needs to be performed by substituting the values of k_0 in Eq. (4.7) and (8) starting from zero until the two equations converge to the same value. As indicated in Fig. 4.9 (b) the equations converged at the value of $\overline{k_o}$, which relates the elastic maximum energy, G^e_{max} with plastic bending energy, G^b.

$$\frac{G_A^{\infty E}}{G^e_{\max}} = \frac{(1-\cos\phi)}{[1-\cos(\phi-\phi_o)]} f_1(\bar{k}_0); \quad \phi_o = \frac{4\varepsilon_c k_o}{3} \tag{4.7}$$

$$f_2(\bar{k}_0) = \frac{\lambda}{3}\left[1+4(1-\lambda)^2\right]k_o^2 + 2(1-\lambda)^2(1-2\lambda)k_o + \frac{8}{3}\frac{(1-\lambda)^4}{(1-2\lambda)k_o} - 4(1-\lambda)^3 \tag{4.8}$$

Where $G_A^{\infty E}$ is the peeling fracture propagation energy when infinite tensile stiffens and zero bending stiffness is considered, Φ_0 is the theoretical root angle at the crack front as indicated in Fig. 4.8 (a).

The parameter $\overline{k_0}$ is determined for different types of waterproofing membranes as shown in Tab. 4.6. After determining the value of $\overline{k_0}$, the strain energy which accounts for local plastic bending near the crack front of the membrane can be calculated using Eq. (4.9). In the region of plastic deformation at the crack front, the maximum elastic energy is related to plastic bending energy using f $(\overline{k_0})$ presented in Eq. (4.10) [39, 40].

$$G^b = \frac{1}{W}\left(\frac{dU_{db}}{da}\right) = G^e_{\max} f(\bar{k}_0); \quad G^e_{\max} = \frac{Et\varepsilon_c^2}{2} \qquad (4.9)$$

Where G^e_{max} is the maximum elastic fracture energy, f $(\overline{k_0})$ is a factor relating the maximum elastic fracture energy and plastic bending energy, G^b.

$$f(\bar{k}_0) = \frac{4}{3}\lambda(1-\lambda)^2\bar{k}_0^2 + 2(1-\lambda)^2(1-2\lambda)\bar{k}_0 + \frac{2}{3}\frac{(1-\lambda)}{(1-2\lambda)\bar{k}_0}\left[1+4(1-\lambda)^3\right] - (1-\lambda)[1+4(1-\lambda)^2] \qquad (4.10)$$

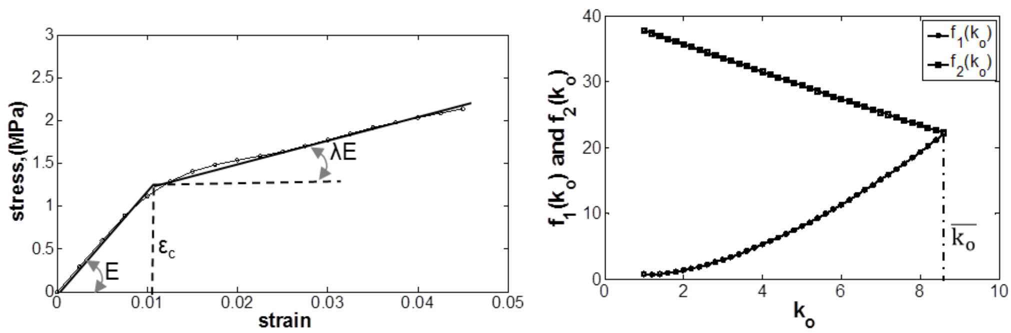

(a) (b)

Fig. 4.9 (a) Typical stress vs. strain curve of uniaxial test; (b) Convergence curve of Eq. (4.8) and (4.9)

4.9 Result and discussion

4.9.1 Blister test

When comparing between the mean values of stress-strain curve from uniaxial and biaxial test shown in Fig. 4.2, the two testing methods gave comparable results for SBS-1. The standard deviation values were determined as indicated in Fig. 4.2 close to the first yielding point for elastic deformation (at 1% strain) and at strain of 3% where plastic deformation would occur in the specimens. The standard deviation analysis showed that elastic modulus deviates from the mean value between 0.16 - 0.23 MPa for uniaxial and 0.09 - 0.2 MPa for biaxial tests as shown in Fig.4.2. The ratios E_y/E_x between the modulus of elasticity in longitudinal and transversal direction are indicated in Tab. 4.2. The result indicates that the elastic modulus ratio for SBS-1 determined in the biaxial test is comparable to the value from the uniaxial test.

Tab 4.2. Ratio of modulus elasticity of SBS and APP membranes

Loading condition		Uniaxial		Biaxial
PBM types	SBS-1	SBS-2	APP-1	SBS-1
E_y / E_x	1.44	1.34	1.35	1.43

Since for SBS-1 the ratio between the modulus of elasticity from biaxial test was found to be comparable to the uniaxial loading condition, the uniaxial test moduli were used for determining the blister propagation energy G. The uniaxial test results shown in Fig. 4.3 (b) are used to determine the moduli of elasticity E_y and E_x in the longitudinal and transversal direction as presented in Tab. 4.3 The experiments were done at conditioning temperature of 23°C and at 50 mm/min displacement rate.

Tab 4.3 Modulus of elasticity of SBS and APP membranes from uniaxial tension tests

Modulus, MPa	SBS-1	SBS-2	APP-1
E_x	57.3	38.6	62.2
E_y	82.5	51.6	84.0

According to the results of the digital image correlation measurements in Fig. 4.5, an elliptical adhesive propagation front was observed for the three different types of waterproofing membranes. However, in some cases an exact elliptical crack propagation front may not occur because of non-uniform adhesion between the concrete plate and the PBM. Since the blister propagation front resembles an elliptical shape, an elliptical adhesive propagation model was used to determine the propagation energies of these different types of the PBMs. Details of the equation are presented by [43].

The energy balance for adhesive blister propagation is described in Eq. (4.11) as the sum of the potential energies of the external applied load (negatively defined) and the elastic strain energy stored in the membrane depending on the geometry of the adhesive failure zone [7, 9].

$$G_b \cong -\left.\left(\frac{\partial W_{app}}{\partial A} + \frac{\partial U_{strain}}{\partial A}\right)\right|_p \tag{4.11}$$

Where A is elliptic adhesive failure area, W_{app} is work done and U_{strain} is membrane's strain energy

The fracture energy release rate G_b, is the difference between the work done W_{app} by the pressurized water in the blister and the membrane's strain energy U_{strain} [9, 35] and thus describes the adhesive blister propagation energy release rate [43]. G is defined per unit width along the elliptic failure front between the PBM and the concrete and has a unit of J/m^2. Hence, for an elliptical blister with an elliptic adhesive failure area A, G is given by the following Eq. (4.12).

$$G_b = \frac{p^2 k_s a_x^3 a_y^3 \pi}{hkE_x tc_{eli}} \sqrt{\frac{k_1 k^2}{a_y^4} + \frac{k_2}{a_x^4}}$$
$$k = \frac{E_y}{E_x}, k_1 = \frac{\cos(\theta)^2}{\cos(\alpha)^2 \sin(\beta)^2} \; and \; k_2 = \frac{\sin(\theta)^2}{\cos(\alpha)^2 \sin(\beta)^2} \tag{4.12}$$

Where E_x is the transversal modulus of elasticity in x – direction, E_y is the longitudinal moduli of elasticity in y – direction, a_x and a_y are the minor and major axes of the blister adhesive failure front; θ is the angle of rotation; h is the blister height; t is the thickness of the water proofing membrane; p is the applied pressure; k_s is the shape factor; C_{eli} is the circumference of the elliptical crack front; α is the angle difference between the normal n and the rotation angle θ according to Fig. 4.4(b). β is the angle between the normal and vertical stress. k, k_1 and k_2 are constant terms which are a function of angles as described above.

The adhesive blister propagation energy can be calculated using Eq. (4.12) irrespective of the angle θ. Any angle θ from 0°- 360° can be used for values of k_1 and k_2 . Angle θ equal to zero was used in this case to determine the propagation energy from Eq. (4.12). The radius a_x, a_y and the blister height h are taken at 70 s as shown in Fig. 4.6 (a) and Tab. 4.4, including other parameters to calculate the adhesive blister propagation energy for the three types of PBM. The blister propagation rate in the longitudinal direction, V_{Gb} was determined from Fig. 4.6(b), and presented in Tab. 4.4.

Tab 4.4. Parameters used to calculate the adhesive blister propagation energy G_b and blister crack propagation rate V_{Gb}

Parameters	SBS-1	SBS-2	APP
E_x, MPa	57.3	38.6	62.2
a_x, mm @70 s	114.5	74.5	63
a_y, mm @70 s	139.5	99.5	76
h, mm@70 s	33.0	25	20
c_{eli}, mm	797.56	549.5	436.5
t, mm	5.0	5.0	5.0
p, MPa	0.2	0.2	0.2
k	1.44	1.34	1.35
k_1 for θ=0°	4	4	4
k_2 for θ=0°	0	0	0
G_b, J/m^2	8626.56	4240.72	1905.46
V_{Gb}, mm/s	13.7	9.95	7.6

4.9.2 Peeling test

As shown previously in Fig. 4.3(a), the elastic modulus for a specific testing temperature and displacement rate were determined from the uniaxial tension test. From these tests it was observed that the temperature has more influence than the displacement rate on modulus of elasticity of the SBS-1 water proofing membrane. After the yielding point, the influence of the displacement rate was noticeable for all testing temperatures. As mentioned before, the mean peeling force F was used in the 20 s - 160 s time frame in Eq. (4.5) to determine the energy needed during elastic elongation of the peeling arm. To investigate the influence of temperature and displacement rate on the peeling fracture energy G_p of the SBS-1 membrane, Eq. (4.5), (4.6) and (4.10) were used. Fracture energy results for elastic deformation G^e, plastic bending deformation, G^b and adhesive fracture energy of the peeling, G_p respectively are presented in Tab. 4.5 for different temperatures and displacement rates. The adhesive fracture energy is also shown in Fig. 4.10 (a) for different temperatures and displacement rates. The results indicate that the fracture energy for peeling decreased considerably with increasing temperature whereas the influence of the displacement rate is not obvious. In addition to this, the displacement rate at the specific temperatures has insignificant influence on the fracture energy value for higher temperatures compared to lower temperatures. The crack growth rate was measeured using string potentiometer during the peeling test. The direction of the crack propagation is shown in Fig. 4.7(c). As indicated in Fig. 4.10 (b), the crack growth rate did not change significanly with increasing temperature. Neverthless, increasing the displacement rate at specific temperature increased the crack growth rate significantly. From Fig. 4.10 (a) and (b), it is obvious that the adhesive fracture energy for peeling was clearly less dependant on displacement rate than the crack growth rate.

Tab 4.5 Fracture energy values at different displacement rates and temperatures

Temperature (°C)	23			40			55		
Displacement rate, mm/min	50	75	100	50	75	100	50	75	100
G^e, J/m^2	12809.7	15840.3	16875.8	7760.6	9361.9	9750.9	5250.1	6717.5	6549.7
G^b, J/m^2	5513.2	6849	6319.2	3524.3	4757.5	4270.7	2763.4	3474	2680.5
G_p, J/m^2	8626.5	9500.3	10556.6	4236.4	4604.4	5480.3	2486.8	3243.5	3869.2
V_{Gp}, mm/s	0.86	1.21	1.62	0.73	1.19	1.53	0.72	1.07	1.48

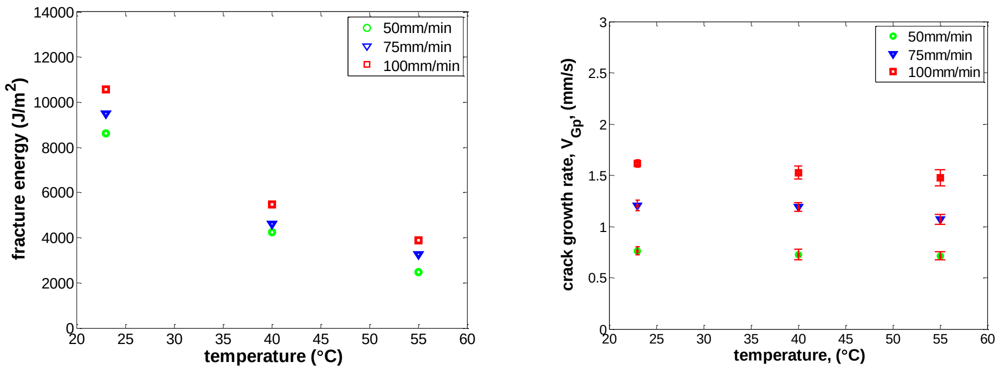

(a) (b)

Fig. 4.10 (a) Peeling Fracture energy and (b) Crack growth rate at different temperature and displacement rate

4.9.3 Comparison between the peeling and blister test

For comparing and ranking the adhesive properties of the membranes, the modulus of elasticity of SBS-1, SBS-2 and APP waterproofing membranes were determined in uniaxial tension tests at a temperature of 23°C and a displacement rate of 50mm/min (Tab. 4.3). Peeling experiments were conducted as well at 23°C and 50mm/min displacement rate. Blister tests were performed at 23°C increasing the pressure at 3.3kPa/s for 60 s until it reached 0.2MPa and then keeping it constant at 0.2 MPa during the blister growth. Comparing the blister crack propagation rate, V_{Gb} from Tab.4.4 and the peeling crack propagation rate, V_{Gp} from Tab. 4.5 (for 23°C and 50 mm/min displacement rate), the blister crack growth rate was about a factor of 15 faster than the cracking rate in the peeling test. However, as indicated in Fig. 4.10 (a) and (b) the influence of the loading speed on fracture energy according to peeling test results was found to be comparatively small, a comparison between peeling and blister test fracture energies and the corresponding ranking appeared justified.

Comparison between SBS-1, SBS-2 and APP fracture energy from blister and peeling tests indicates that SBS-1 has a higher value compared to the other types of the membranes as indicated in Tab. 4.4 and Tab. 4.6. The reason for this can be due to the presence of sand layer on the bottom of the SBS-2 membrane as presented in Tab 4.1. The reason for the lower fracture energies of APP can be attributed to the different polymer modified binder properties.

It can be seen from Fig. 4.11 (a) that the blister propagation energies G_b from the blister test Eq. (4.12) and the fracture energy G_p from the peeling test are comparable. From this, it can be concluded that, in principle, by knowing the pressure inside the blister, it is possible to use the blister propagation equations and estimate the energy required to initiate blister growth. In this way, one can also iteratively calculate back the peeling force correlated to the fracture energy. This helps to investigate susceptibility of membranes for blister formation by conducting peeling test instead of using complicated and time consuming blister tests. In order, to confirm these findings, however, further tests are needed. As indicated in Fig. 4.11 (b), the crack growth rate of blister propagation is higher compared to the peeling crack propagation, neverthless, as shown in Fig. 4.10 (b), when the crack growth rate for 23°C increased from 0.86 to 1.62 mm/s , all most dobled, the peeling fracture energy only increased by small amount as indicated in Fig. 4.10 (a). Therefore, higher crack growth rate of the blister propagation may not have significant influence on the comparison between the fracture energy of the blister and the peeling tests.

Tab 4.6. Parameters used to calculate the peeling fracture energy G_p

Parameters	SBS-1	SBS-2	APP
E_y, MPa	82.5	51.6	84.1
λ	0.18	0.40	0.29
ε, %	35.0	10.0	2.7
F, N	527.0	221.45	116.7692
]	7.3	2.0	5.6
G_p, J/m^2	8180.0	3236.0	1591.9
V_{Gp}, mm/s	0.89	0.6	0.45

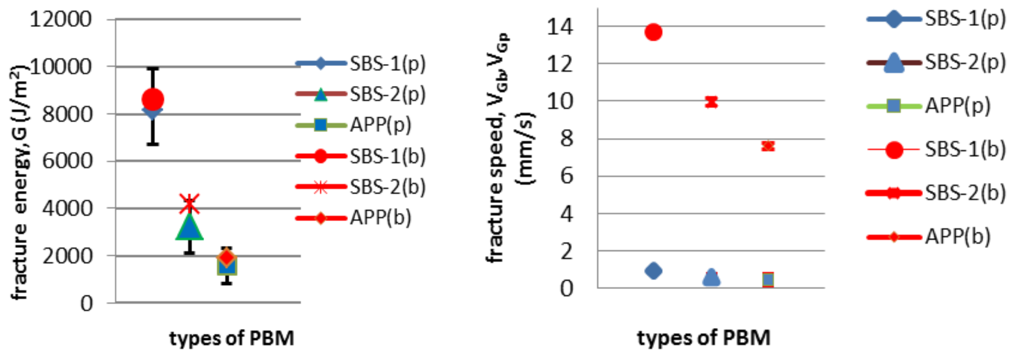

(a) (b)

Fig. 4.11 (a) Comparison of the fracture energy at 23°C between the peeling (p) and the blister test (b) for different types of PBMs; (b) Corresponding crack growth rate for different types of PBMs at 23°C temperature.

5 Schlussfolgerungen

5.1 Blasenbildung bei Gussasphalt

Die zeitabhängige vertikale Verformung von Gussasphalt-Blasen hängt von drei Faktoren ab: Den Materialcharakteristika (wie sie zur Modellierung der Blasenbildung benötigt werden), der Temperatur des Gussasphalts im Zeitpunkt der Belastung und der Geschwindigkeit der Lastaufbringung (z. B. des Blasendrucks). Es wurde festgestellt, dass die vertikale Verformung infolge Blasenbildung unter Gussasphalt deutlich stärker von der Geschwindigkeit der Temperaturänderung als vom Blasendruck beeinflusst wird. Dabei zeigten Simulationsberechnungen der Blasenbildung über einen Zeitraum von 12 Stunden, dass ein langsam aufgebrachter, gleichförmig verteilter Blasendruck und eine langsame Temperaturänderung geringere vertikale Deformationen verursachen.

Unter konstantem Blasendruck (p_0=7.12 $\cdot 10^{-06}$ MPa) wurde bei zyklischer Temperaturänderung das vertikale Blasenwachstum stark von der Temperaturabhängigkeit des Materials beeinflusst. Daraus folgt, dass bei konstantem Gasdruck im Inneren einer Blase mit steigender Temperatur deutliches Blasenwachstum auftreten kann.

Anderseits ist das Blasenwachstum unter konstanter Temperatur (T=25 °C) bei zyklischem Blasendruck geringer als im soeben beschriebenen Fall. Offenbar besitzt Gussasphalt genügend Steifigkeit, um Änderungen des Blasendruckes zu widerstehen. Tatsächlich wäre das Blasenwachstum sogar noch geringer, wenn das Gewicht des Gussasphaltes in die Simulationsberechnungen einbezogen worden wäre.

Schliesslich wurde durch Simulation aufeinanderfolgender Heiz- und Kühlzyklen festgestellt, dass sich die täglichen Temperaturschwankungen deutlich auf das Blasenwachstum in Asphaltbelägen auswirken. Während des Entlastungsvorganges, d.h. wenn Blasendruck und Temperatur abnehmen, wachsen Blasen weiter, wenngleich mit geringerer Geschwindigkeit. Tatsächlich folgt aus den Simulationsberechnungen, dass Blasen kontinuierlich unter wechselnden Belastungsbedingungen während mehrerer Tage wachsen können.

5.2 Blasenwachstum bei Dichtungsbahnen

Biaxiale Untersuchungen zur Bestimmung der mechanischen Eigenschaften von orthotropen Polymerbitumen-Dichtungsbahnen (PBM) unter mehrachsigem Spannungszustand sind nützlich, um die elastischen Baustoffeigenschaften charakterisieren zu können und die Energie der elliptischen adhäsiven Ausbreitung von Blasen zu berechnen. Die orthotropen Eigenschaften im ebenen Spannungszustand von PBM Materialien führen zu einer Blasenausbreitung mit elliptischer Rissausbreitungsfront und unterscheidet sich damit deutlich vom allgemein bekannten Fall des kreisförmigen Blasenwachstums. Wesentlich ist die Annahme einer gleichförmigen Adhäsion zwischen Betonuntergrund und PBM, wonach die vertikale Spannungskomponente an der elliptische Rissfront der Dichtungsbahn konstant sein muss, um die elliptische Form an der Blasenausbreitungsfront beizubehalten und damit eine elliptische adhäsive Blasenausbreitung zu ermöglichen.

In der Realität dürfte das Blasenwachstum auf Gasdruck unter der PBM zurückzuführen sein. Daher ist die Dichtungsbahn einer mehrachsigen Beanspruchung ausgesetzt. Im Gegensatz zum sog. Membran Adhäsion Test (MAT) der technischen Universität in Delft, wobei die Dichtungsbahn einem einachsigen Spannungszustand unterliegt und das Haftverhalten nur in einer Richtung untersucht wird, weist der Blasentest den Vorteil auf, dass die Blasenbildung unter Berücksichtigung des multiaxialen Spannungszustands simuliert wird und die Energie der Blasenausbreitung auch für orthotrope Dichtungsbahnen bestimmt werden kann. Da aber in diesen Fällen die Materialeigenschaften in Längs- und

Querrichtung unterschiedlich sind, kann somit eine Anwendung des MAT Tests zu unterschiedlichen Resultaten führen.

Blasenwachstum-Prüfungen mit konstantem Wasserdruck ergaben, dass die Blasenausbreitung in Längs- und Querrichtung proportional zum Verhältnis der Elastizitätsmoduli in den entsprechenden Richtungen ist. Die Ellipsengleichung für den Elastizitätsmodul senkrecht zur adhäsiven Bruchfront erwies sich im Falle der Blasenbildung als gute Näherung für die komplexe Orthotropie-Gleichung. Die elliptische Modulgleichung vereinfacht nämlich die Lösung des Problems ohne Verlust der orthotropen Materialeigenschaften des allgemeinen ebenen Spannungszustands. Die vertikale Komponente der Normalspannung an der Rissfront ist konstant und unabhängig von der Orientierung des Materials. Mit diesen Erkenntnissen und unter der Annahme linear elastischen Verhaltens war es möglich, eine Näherungsgleichung für die Energie der adhäsiven Rissausbreitung bei dünnen PBMs zu entwickeln.

Beim Einbau von Belägen aus Heissasphalt auf Betonbrücken oder bei extremer Sonneneinstrahlung auf die Dichtungsbahn infolge gravierender baulicher Verzögerungen, kann zwischen der Polymerbitumen-Dichtungsbahn PBM und der Betonoberfläche der Brückenplatte infolge steigendem Dampfdruck Blasenbildung entstehen. Ein solcher Druck erzeugt einen mehrachsigen Spannungszustand in der orthotropen PBM.

Vergleich und Rangierung der adhäsiven Eigenschaften der PBMs mittels analytisch ermittelter Energie der Blasenausbreitung und der standardisierten Schälzugprüfung aller drei untersuchten Dichtungsbahnen zeigen, dass die Bruchenergie der Blasenausbreitung grössenordnungsmässig jener des Schälzugs entspricht. Eine Gegenüberstellung der Bruchenergien beider Methoden bestätigt zudem, dass das erarbeitete Modell gute Resultate sowohl für das Wachstum als auch für die Ausbreitung der Blasen liefert. Allerdings kann sich die Durchführung von Blasenwachstum-Prüfungen zur Untersuchung der Hafteigenschaften von PBMs als schwierig und zeitraubend erweisen, da die Parameter des Modells sehr sorgfältig bestimmt werden müssen. Die Durchführung von Schälzug und einachsiger Prüfungen dagegen erlaubt es, die Schälzugkraft mit der Schälzug-Bruchenergie zu verknüpfen. Wegen der Korrelation zwischen der Bruchenergie der Schälzug- und Blasenwachstum-Prüfung, ist es somit möglich, die einfachere Schälzug-Prüfung als Prüfmethode zur Untersuchung des Blasenwachstums zu verwenden. Die Energie der Rissausbreitung bei Schälzug wird mehr durch die Prüftemperatur als durch die Geschwindigkeit der Rissausbreitung beeinflusst. Daraus lässt sich schliessen, dass die Vergleichbarkeit der Schälzug- und Blasenwachstums-Energie weniger durch die Verformungsgeschwindigkeit der Schälzugprüfung bzw. der Geschwindigkeit des Blasenwachstums als durch die Prüftemperatur beeinflusst wird.

Die ermittelten Elastizitätsmoduli der PBMs der vorliegenden Untersuchung weisen darauf hin, dass im Falle von SBS die biaxiale Zugprüfung und der einachsige Zugversuch im elastischen Bereich vergleichbare Spannungs-Dehnungs-Kurven liefern. Tatsächlich verlief die äquivalente Spannungs-Dehnungs-Kurve der biaxialen Prüfung ähnlich wie die einachsige Spannungs-Dehnungskurve in Längsrichtung. Daraus wurde geschlossen, dass zur Bestimmung des Materialverhaltens im elastischen Bereich biaxiale Prüfungen keinen Vorteil gegenüber einachsigen Prüfungen bieten.

Die Bildung von Blasen unter Dichtungsbahnen auf Beton-Brückenplatten wird durch einen komplexen Mechanismus verursacht, der zweifellos weitere Aufmerksamkeit und Forschungsanstrengungen erfordert. Insbesondere scheinen die in dieser Arbeit erarbeiteten und präsentierten Prinzipien vielversprechend, um als Element für eine zuverlässigere praktische Beurteilung der adhäsiven Eigenschaften von PBMs zu dienen und gleichzeitig das theoretische Verständnis samt Charakterisierung der Mechanismen jener Blasenbildung zu fördern, die bekanntlich als Auslöser für schwerwiegende und teure Langzeitschäden an Brückenplatten wirkt.

6 Conclusions

6.1 Blister formation on mastic asphalt

The time dependent vertical deflection in mastic asphalt blisters depends on three factors; material characterization of the model; temperature of the mastic asphalt at the time of loading; and the rate at which the load is applied to the material. It was found that vertical deflection of mastic asphalt is much more depending on the rate of the applied temperature than on the applied pressure. The 12 hour simulation showed that, slower applied uniformly distributed pressure and temperature produces smaller vertical deflection.

For constant pressure (p_0=7.12 $\cdot 10^{-06}$ MPa) and fluctuating temperature, the temperature dependency of the material had a great influence on the vertical deflection of the blister. This indicates that constant gas pressure inside the blister can produce significant amount of blister growth with increasing temperature.

On the other hand, for constant temperature (T=25 °C) and fluctuating pressure, the blister growth is much less than in the previous case. This is due to the fact that the mastic asphalt has enough stiffness to resist pressure changes. In fact, deflection would even be less if the weight of the mastic asphalt was incorporated in the simulation.

Finally from simulation of the consecutive cycles of heating and cooling, it was noticed that the daily temperature variations have a significant influence on blister deflection of asphalt pavements. During the unloading process, i.e. when pressure and temperature decrease, the blister still grows at a slower rate. The simulation indicates that the blister can grow continuously under repeated loading conditions over subsequent days.

6.2 Blister propagation on water proofing membrane

The biaxial tests for determining the mechanical properties of an orthotropic polymer modified bitumen membrane (PBM) in multi-axial stress state are useful to characterize the elastic material properties for calculating elliptical adhesive blister propagation energy. The plane stress orthotropic property of the PBM material creates blister crack propagation with an elliptical propagation front other than in the general well-known case of circular blister growth. Under the assumption of uniform adhesion between the concrete substrate and the PBM, the vertical stress in the membrane must be constant around the elliptical crack front in order to keep the elliptical shape of the blister propagation front, otherwise elliptical adhesive blister propagation would not be possible.

In reality, blister growth might occur due to vapor pressure created beneath the PBM, Hence, the membrane is exposed to multi axial stress state. Unlike the membrane adhesion test (MAT) of the technical University of Delft, which captures the uniaxial stress state of a membrane and adhesive bonding behavior in one dimension, the blister test has the advantage in capturing the multi axial stress state of the blister formation, thus helping to determine blister propagation energy also in orthotropic cases. Applying the MAT test for orthotropic materials could result in different results since the material properties in the longitudinal and transversal direction are different.

Blister tests with constant water pressure showed that the blister propagation in the longitudinal and transversal direction is proportional to the ratio of the modulus elasticity in the respective direction. The elliptical equation for the elastic modulus normal to the elliptic adhesive failure front is a good approximation to the complex orthotropic equation in dealing with blistering. The elliptical modulus equation simplifies the analysis of the problem without losing the general orthotropic plane stress material properties. The vertical component of the normal stress is constant and independent to the orientation of material direction. With these finding and under the assumption of linear elastic behavior it is possible to provide an approximate equation for the adhesive blister propagation energy for thin PBM's.

When placing hot mix asphalt pavements on concrete bridges or in cases of extended exposure of the waterproofing protection layer to the sun because of significant construction delays, blistering my occur between the polymer modified bitumen waterproofing membrane PBM and the concrete surface of the bridge deck, from steam pressure accumulation. Such pressure creates a multi-axial stress state in the PBM which has orthotropic material properties.

From comparing and ranking the adhesive properties of PBMs by means of the analytical blister propagation energy and its comparison with a standard peeling test method, the results from peeling fracture energy of all the three membranes indicated that the blister propagation energy is within the range of peeling fracture energy. The fracture energy comparison between the two methods indicated that the blister propagation model approach works well for modeling blister growth and propagation. Nevertheless, conducting blister test for investigating the adhesive properties of the PBMs can be difficult and time consuming, because of careful determination of the parameters for the model. By conducting peeling and uniaxial tests, it is possible to relate the peeling force to the peeling fracture energy of the PBM. Therefore, taking in to account the correlation between the fracture energies of the peeling and blister tests, it is possible to use the simpler peeling test as test method for blister propagation investigations. Peeling crack propagation energy showed only little dependancy on the crack growth rate and was more influenced by temperature. From this it was concluded that the comparison between the peeling fracture energy and blister propagation energy is less influenced by the displacement rate of peeling test and blister growth rate than by the testing temperature.

The modulus of elasticity of the PBMs determined in this study indicated that in case of SBS, the biaxial extension and standard uniaxial tension test produce comparable strain-stress curve in the elastic range. The equivalent stress-strain curve from a biaxial experiment was similar to the uniaxial stress-strain curve in the longitudinal direction. As a result, no major advantage was found in using the biaxial test over the uniaxial test to determine the material behavior in the elastic range.

Formation of blisters under waterproofing membranes on concrete bridge decks is caused by a complex mechanism which certainly needs further attention and research efforts. However, principles found and shown here appear promising and may serve as an element for both more reliable practical tools for assessing the adhesive properties of PBMs and improved theoretical understanding and characterization of the mechanisms of blister formation that are known to trigger severe and expensive long term damage of bridge deck structures.

7 Acknowledgment

The authors acknowledges the support of colleges Kienast Hans and Kato Hiroyuki, Road Engineering/Sealing Components, EMPA (Swiss Federal Laboratories for Material Science and Technology) including other group members of the Lab. and C. Galliot, Center for Synergetic Structures, EMPA, for his many interactions throughout the project.

References

[1] Partl M. N. and Hean S., "Practical Aspects of Interaction Between Mastic Asphalt and Waterproofing System in Bridge and Tunnel Construction," in *proceedings of the Fourth European Symposium on Performance of Bituminous and Hydraulic Materials in Pavements*, Nottingham, United Kingdom, 2002, pp. 58-61.

[2] Rosenberg J., "Thin Pavements With Synthetic Binder Used in Denmark," Asphalt, Ed., ed: Danish Road Institute, 2000, pp. 5-9.

[3] Alison M., Robert B., and Ralph p., "Blistering in build-up roofs: a review " in *The Fourth International Symposium on Roofing Technology*, Gaithersburg, Md. , 1999.

[4] Croll J. G. A., "Thermal Buckling of Pavement Slabs,," *The Institution of Civil Engineers,* vol. 158, pp. 115-126, 2005.

[5] Oba K. and Partl M. N., "Non-destructive IR-Thermography for Distress Detection in Asphalt Pavements and Bridge Deck Surfacings," *International Journal of Road Materials and Pavement Design, Hermes Science Publications,,* vol. 1, pp. 407-418, 2000.

[6] Partl M. N., Remy G., and Hean S., "Belagsschäden infolge Blasenbildung auf einer neuen Hängebrücke in Hongkong," Dubendorf und St. Gallen, Switzerland,2001.

[7] Hohlfelder R. J., "Bulge and Blister Testing of the Films and their Interfaces," degree of doctor of philosophy, materials science and engineering Stanford University Stanford, 1999.

[8] Fini E. H., Al-Qadi, I. L., "Development of a Pressurized Blister Test for Interface Characterization of Aggregate Highly Polymerized Bituminous Materials," *Journal of materials in civil engineering,* vol. 23, may 1 2011.

[9] Kai-Tak W., Yiu-Wing, M., "Fracture Mechanics Of a New Blister Test With Stable Crack Growth," *Acta Metall. Matter.,* vol. 43, pp. 4109-4115, 1995.

[10] Hencky H. Z., *Math. Phys,* vol. 63, 1915.

[11] Stevenson P., *Foam Engineering Fundamentals and Applications*, 2012.

[12] Partl M. N., "Deterioration Mechanisms in Polymer-modified Bitumen's Water proofing Membranes Sheets During Torching," Swiss Federal Laboratories for Material Science and Technology, Duebendorf, switzerland, 2004.

[13] "ABAQUS 6.9 User Documentation Collection," 6.91 ed: Dessault Systems, 2009.

[14] Timoshenko S. and Woinowsky-Krieger S., *Theory of Plates and Shells*, Second ed. USA: McGraw-Hill book, 1959.

[15] Reddy J. N., *Shear Deformable Beams and Plates*, First ed. New York: Elsevier, 2000.

[16] Fini E. H., Al-Qadi I. L., Masson J. F., and McGhee K. K., "Interfacial fracture energy : An indicator of the adhesion of bituminous material adhesion," in *Annual Meeting of the Association of Asphalt Paving Technologists*, Philadelphia, PA, 2008, pp. 827-850.

[17] Michalski C., "modellvorstellung zur deutung des blasewachstums im gussaphalt und anderen thermoviskosen stoffen fur den strassenbau," Appelstr. 9A, D-3000 Hannover,1992.

[18] Rogosch N., "Zur Blasenbildung in thermoviskosen Stoffen unter Berücksichtigung rheologischer Materialkennwerte und geometrischer Randbedingungen," Appelstr. 9A, D-3000 Hannover,1994.

[19] Galliot C., Luchsinger, R. H., "Uniaxial and Biaxial Mechanical Properties of ETFE Foils " *Polymer Testing,* vol. 30, pp. 356-365, Feb 13 2011.

[20] Di Benedetto H. D., Partl M. N., Franken L., and De La Roche C., "Stiffness Testing for Bituminous Mixtures," *RILEM TC 182-PEB Performance Testing and Evaluation of Bituminous Materials,* pp. 66-70, 2001.

[21] Christensen D. W. and Bonaquist R. F., "Evaluation of Indirect Tensile Test Procedures for Low-temperature Performance of Hot Mix Asphalt," 500 Fifth Street, NW, Washington, D.C, 2004.

[22] Huang Y. H., *Pavement Analysis and Design*, Second ed. New Jersey: Pearson Education, 1993.

[23] Tschoegl N. W., Wolfgang G. K., and Igor E., "poisson's ratio in linear viscoelasticity- a critical review," *Mechanics of time time-dependent materials, Kluwer Acadamic,* vol. 6, pp. 3-51, 2002.

[24] Witczak M. W., "Modification and Re-Calibration Superpave Thermal Cracking Model ", Power Road and Williams Field Road, Mesa, Ariz.December 2000.

[25] Findlay W. N., James S. L., and Onaran K., *Creep and Relaxation of Nonlinear Viscoelastic Materials*, Second ed. Mineola ,N.Y: Dover publications, 1976.

[26] Shaopeng W., Hong W., and Mingyu C., "Analysis of High Temperature Fluctuations on Asphalt Pavement of Cement Concrete Bridge," *Journal of Testing and Evaluation,* vol. 37, pp. 1-4, 2009.

[27] Hailesilassie B. W., Partl, M.N. , "Mechanisms of Asphalt Blistering on Concrete Bridges," *J. of ASTM International,* vol. 9, 2012.

[28] Hean S., Partl, M.N., "Determination of the decisive factors influencing the behaviour of bridge waterproofing systems with polymer-bitumen membranes," Federal Department of the Environment, Transport, Energy and Communications 597,2006.

[29] Hean S., Partl, M.N., "Mastic Asphalt and Waterproofing Components for Bridge and Tunnel Construction," presented at the Proceedings of 12th Int. Flexible Pavements Conference, Melbourne, 2003.

[30] Architekten-Verein S. I.-u., "prüfungen und anwendungsgebite polymerbitumen-dichtungsbahnen-schälzugprüfungen," vol. SIA 281/2, SN 564 281/2, ed. zurich, switzerland, 1999.

[31] Architekten-Verein S. I.-u., "bitumenhahnen-haftzugprüfung," vol. SIA 281/3, SN 564 281/3, ed. zurich, switzerland, 1999.

[32] X Liu A. S., J Li, G Tzimiris, "application of MAT device to characterize the adhesive bonding strength of membrane in orthotropic-steel deck bridges," in *ISAP International Symposium*, 2012.

[33] Van Hemelrijck D., Ramault, c., Makris, A., Clarke, A., Williamson, C., "Biaxial Testing of Fiber Reinforced Composites," presented at the 16th International conference on composite materials, kyoto, Japan, 2007.

[34] Galliot C. a. L., R. H., "A simple model discribing the non-linear biaxial tensile behaviour of PVC-coated polyster fabrics for use in the finite element analysis," *compos. Struct.,* vol. 90, pp. 438-447, 2009.

[35] Robert J. Hohlfelder J. J. V., William D. Nix, Huihong Luo, Christopher E. D. Chidsey, "Blister Test Analysis Methods " in *Mat. Res.* .

[36] Chao-Yu Lee M. D., Wei-Hsing Tuan., "Adhesion strength of Ag/BaTiO3 interface," *Scripta Materialia,* pp. 453–457, 2006.

[37] Partl M. N., "Deterioration Mechanisms in Polymer-Modified Bitumen's Water Proofing Membrane Sheets During Torching," Swiss Federal Laboratories for Material Science and Technology, Duebendorf, Switzerland 577,2004.

[38] "prüfungen und anwendungsgebite polymerbitumen-dichtungsbahnen-schälzugprüfungen," swiss standard SIA 281/2, SN 564 281/2, 1999.

[39] A.J. Kinloch C. C. L. a. J. G. W., "The peeling of flexible laminates," *International Journal of Fracture,* vol. 66, pp. 45-70, 1994.

[40] D.R. Moore J. G. W., "Peel Testing Of Flexiable Laminates," *Fracture Mechanics Testing Methods for Polymers, Adhesives and Composites,* vol. 28, pp. 203-223, 2001.

[41] Blackman B.R.K. H. H., Kinloch A.J., Williams J.G. , "the use of a cohesive zone model to study the fracture of fiber composites and adhesivly-bonded joints " *International Journal of Fracture,* vol. 119, pp. 25-46, 2003.

[42] H. Hadavinia L. K., A.J. Kinloch , D.R. Moore, J.G. Williams, "A numerical analysis of the elastic-plastic peel test," *Engineering Fracture Mechanics,* vol. 73, pp. 2324-2335, 2006.

[43] Hailesilassie B. W., Partl, M.N. , "Adhesive Blister Propagation under an Orthotropic Bituminous Waterproofing Membrane," *Construction & Building Materials(accepted manuscript and under review in Elsevier Editorial system),* 2013

[44] I. Georgiou H. H., A. Ivankovic, A. J. Kinloch, V. Tropsa & J. G. Williams, "Cohesive zone models and the plastically deforming peel test," *the journal of adhesion,* vol. 79, pp. 239-265, 2010.

[45] J.G. Williams H. H., "Analytical solutions for cohesive zone models," *Journal of the Mechanics and Physics of Solids,* vol. 50, pp. 809-825, 2001.

[46] Michael N. A., Beate L. B., Wolfgang G. B., "Fracture mechanics on polyethylene/polybutene-1 peel films," *Polymer Testing,* vol. 27, pp. 1017-1025, 2008.

[47] K-S. Kim N. A., "Elastoplastic Analysis Of The Peel Test," *Int. J. solids structures,* vol. 24, pp. 417-438, 1988.

Projektabschluss

Schweizerische Eidgenossenschaft
Confédération suisse
Confederazione Svizzera
Confederaziun svizra

Eidgenössisches Departement für
Umwelt, Verkehr, Energie und Kommunikation UVEK
Bundesamt für Strassen ASTRA

FORSCHUNG IM STRASSENWESEN DES UVEK

Version vom 09.10.2013

Formular Nr. 3: Projektabschluss

erstellt / geändert am: 03. Mar. 2014

Grunddaten

Projekt-Nr.: VSS 2006/515

Projekttitel: Forschungspaket Brücken: EP5- Mechanismen der Blasenbildung

Enddatum: 04. Apr. 2014

Texte

Zusammenfassung der Projektresultate:

Finite element model was developed to simulate the blister growth with focus on long term blistering of mastic asphalt. This includes investigation of blister growth in the laboratory. It was found that vertical deflection of mastic asphalt is much more depend-ing on the rate of the applied temperature than on the applied pressure. The 12 hour simulation showed that, slower applied uniformly distributed pressure and temperature produces smaller vertical deflection.

Moreover, investigation and modeling of adhesive blister propagation between an orthotropic PBM and concrete has been done. The plane stress orthotropic property of the PBM material creates blister crack propagation with an elliptical propagation front other than in the general case of circular blister growth. Under the assumption of uniform adhesion between the concrete substrate and the PBM, the vertical stress in the membrane must be constant around the elliptical crack front in order to keep the elliptical shape of the blister propagation front, otherwise elliptical adhesive blister propagation would not be possible. The analytical blister propagation energy was compared with a standard peeling test method, as described in Swiss standards, and determined the adhesive fracture energy from literature. Three different types of polymer modified bitumen membranes (PBMs) were used for this investigation. The investigation includes the comparison between the uniaxial and biaxial test for determining the modulus of elasticity of the membranes. Influence of the displacement rate and temperature on adhesive fracture energy is also investigated for the peeling test. The fracture energy comparison between the two methods indicated that the blister propagation model approach works well for modeling blister growth and propagation. By conducting the peel test and uniaxial test, it is possible to interpret the peel force in terms of peeling fracture energy of the PBM. Therefore taking in to account the correlation between the fracture energy between the peeling and blister test, it is possible to use a peeling test as investigation method for blister propagation.

Forschung im Strassenwesen des UVEK: Formular 3 Seite 1 / 3

Zielerreichung:

- The finite-element model simulation shows that the daily temperature variations may have a significant influence on blister growth in asphalt pavements.
- The material properties of SBS membranes under the in-plane complex stress state was determined from biaxial test data.
- It was found that the ratio of the longitudinal to transversal adhesive blister propagation is comparable to the ratio of the modulus of elasticity in the longitudinal to transversal direction.
- The analytical blister propagation energy approach for waterproofing membranes was compared with adhesive fracture energy from standard peeling test methods.
- The modulus of elasticity of the membranes from uniaxial and biaxial testing conditions were com-parable
- The energy calculated from tests with elliptical blister propagation showed a comparable value to the standard peeling fracture energy for similar types of PBMs.

Folgerungen und Empfehlungen:

- Vertical deflection of mastic asphalt is much more depending on the rate of the applied temperature than on the applied pressure.
- The PBM material creates blister crack propagation with an elliptical propagation front other than in the general case of circular blister growth.
- The comparison between the peeling fracture energy and blister propagation energy is less influenced by the displacement rate of peeling test and blister growth rate than by the testing temperature.
- The correlation between the fracture energies of the peeling and blister tests, it is possible to use the simpler peeling test as test method for blister propagation investigations.

Publikationen:

- Hailesilassie, B. W., Partl, M.N., 'Mechanisms of Asphalt Blistering on Concrete Bridges', J. of ASTM International, Vol. 9.DOI: 10.1520/JAI104135, 2012.
- Hailesilassie B. W. and Partl M. N., "Adhesive blister propagation under an orthotropic bituminous waterproofing membrane," Construction and Building Materials, vol. 48, pp. 1171-1178, 11// 2013.
- Hailesilassie B., Hean S., and Partl M., "Testing of blister propagation and peeling of orthotropic bituminous waterproofing membranes," Materials and Structures, pp. 1-14, 2013/11/21 2013.

Der Projektleiter/die Projektleiterin:

Name: Partl Vorname: Manfred N.

Amt, Firma, Institut: KTH, division of highway engineering

Unterschrift des Projektleiters/der Projektleiterin:

Schweizerische Eidgenossenschaft
Confédération suisse
Confederazione Svizzera
Confederaziun svizra

Eidgenössisches Departement für
Umwelt, Verkehr, Energie und Kommunikation UVEK
Bundesamt für Strassen ASTRA

FORSCHUNG IM STRASSENWESEN DES UVEK

Formular Nr. 3: Projektabschluss

Beurteilung der Begleitkommission:

Beurteilung:

Die durchgeführten Arbeiten weichen in einigen Punkten von den ursprünglich beabsichtigten ab. Insbesondere wurde zusätzlich die Schälzugprüfung untersucht. Anstelle der Untersuchung von Blasenkolonien wurde das mechanische Verhalten vertieft untersucht, denn ohne diese Informationen lässt sich die im Vergleich zu einer Blase erheblich komplexere Situation einer Blasenkolonie theoretisch nicht ausreichend gut erfassen. Im Sinne einer Gesamtschau darf festgestellt werden, dass die Arbeit die ursprünglich geplante Zielsetzung übertrifft.

Umsetzung:

Der in dieser Arbeit entwickelte Blasenbildungstest kann zur Beurteilung von Polymerbitumen Dichtungsbahnen in Hinblick auf das Risiko von Blasenbildung eingesetzt werden.

weitergehender Forschungsbedarf:

Die Ursache des Aufbaus von Druck in Blasen ist noch nicht abschliessend erforscht. Weitergehende Untersuchungen in dieser Richtung sind erwünscht. Ebenso ist es wünschenswert, das Wachstum von Blasen in Kolonien im Vergleich zu dem einer einzelnen Blase zu erforschen, denn in der Praxis, in Schadenfällen, treten Blasen oft gehäuft und so nahe beieinander auf, dass eine Wechselwirkung zwischen ihnen die Entwicklung des Schadens beeinflusst.

Einfluss auf Normenwerk:

Die Untersuchung zeigt, dass Blasenwachstum und Schälzugprüfung bezüglich ihrer Bruchenergie korrelieren. Die Schälzugprüfung nach SIA 281-2 erfasst daher wichtige Aspekte des Schadensmechanismus bei Blasenbildung auf Brücken. Sie ist weiterhin die Normprüfung der Wahl und braucht nicht durch eine komplexere Prüfung ersetzt werden.

Der Präsident/die Präsidentin der Begleitkommission:

Name: Hürzeler Vorname: Hans

Amt, Firma, Institut: Kanton Aargau, Department Bau, Verkehr und Umwelt

Unterschrift des Präsidenten/der Präsidentin der Begleitkommission:

h. hürzeler

Forschung im Strassenwesen des UVEK: Formular 3 Seite 3 / 3

Verzeichnis der Berichte der Forschung im Strassenwesen

Bericht-Nr.	Projekt Nr.	Titel	Jahr
1465	ASTRA 2000/417	Erfahrungen mit der Sanierung und Erhaltung von Betonoberflächen	2014
1462	ASTRA 2011/004	Ermittlung der Versagensgrenze eines T2 Norm-Belages mit der mobiles Grossversuchsanlage MLS10	2014
1460	SVI 2007/017	Nutzen der Verkehrsinformation für die Verkehrssicherheit	2014
1459	VSS 2002/501	Leichtes Fallgewichtsgerät für die Verdichtungskontrolle von Fundationsschichten	2014
1458	VSS 2010/703	Umsetzung Erhaltungsmanagement für Strassen in Gemeinden - Arbeitshilfen als Anhang zur Norm 640 980	2014
1457	SVI 2012/006	Forschungspaket VeSPA Teilprojekt 5: Medizinische Folgen des Strassenunfallgeschehens	2014
1456	SVI 2012/005	Fotschungspaket VeSPA Teilprojekt 4: Einflüsse des Wetters auf das Strassenunfallgeschehen	2014
1455	SVI 2012/004	Forschungspaket VeSPA Teilprojekt 3: Einflüsse von Fahrzeugeigenschaften auf das Strassenunfallgeschehen	2014
1454	SVI 2012/003	Forschungspaket VeSPA Teilprojekt 2: Einflüsse von Situation und Infrastruktur auf das Strassenunfallgeschehen: Phase 1	2014
1453	SVI 2012/002	Forschungspaket VeSPA Teilprojekt 1: Einflüsse von Mensch und Gesellschaft auf das Strassenunfallgeschehen: Phase 1	2014
1452	SVI 2012/001	Forschungspaket VeSPA: Synthesebericht Phase 1	2014
1451	FGU 2010/006	Gasanalytik zur frühzeitigen Branddetektion in Tunneln	2013
1450	VSS 2002/401	Kaltrecycling von Ausbauasphalt mit bituminösen Bindemitteln	2014
1449	ASTRA 2010/024	E-Scooter - Sozial- und naturwissenschaftliche Beiträge zur Förderung leichter Elektrofahrzeuge in der Schweiz	2013
1448	SVI 2009/008	Anforderungen der Güterlogistik an die Netzinfrastruktur und die langfristige Netzentwicklung in der Schweiz. Forschungspaket UVEK/ASTRA "Strategien zum wesensgerechten Einsatz der Verkehrsmittel im Güterverkehr der Schweiz", Teilprojekt C	2014
1447	SVI 2009/005	Informationstechnologien in der zukünftigen Gütertransportwirtschaft Forschungspaket UVEK/ASTRA "Strategien zum wesensgerechten Einsatz der Verkehrsmittel im Güterverkehr der Schweiz", Teilprojekt E	2013
1446	VSS 2005/454	Forschungspaket Recycling von Ausbauasphalt in Heissmischgut: EP3: Stofffluss- und Nachhaltigkeitsbeurteilung	2013
1445	VSS 2009/301	Öffnung der Busstreifen für weitere Verkehrsteilnehmende	2013
1444	VSS 2007/306	Verkehrsqualität und Leistungsfähigkeit von Anlagen des leichten Zweirad- und des Fussgängerverkehrs	2013
1443	VSS 2007/305	Verkehrsqualität und Leistungsfähigkeit des strassengebundenen ÖV	2013
1442	SVI 2010/004	Messen des Nutzens von Massnahmen mit Auswirkungen auf den Langsamverkehr - Vorstudie	2013
1441_2	SVI 2009/010	Zielsystem im Güterverkehr. Forschungspaket UVEK/ASTRA Strategien zum wesensgerechten Einsatz der Verkehrsmittel im Güterverkehr der Schweiz - Teilprojekt G	2013
1441_1	SVI 2009/010	Effizienzsteigerungspotenziale in der Transportwirtschaft durch integrierte Bewirtschaftungsinstrumente aus Sicht der Infrastrukturbetreiber Synthese der Teilprojekte B3, C, D, E und F des Forschungspakets Güterverkehr anhand eines Zielsystems für den Güterverkehr	2013
1440	SVI 2009/006	Benchmarking-Ansätze im Verkehrswesen	2013
1439	SVI 2009/002	Konzept zur effizienten Erfassung und Analyse der Güterverkehrsdaten Forschungspaket UVEK/ASTRA Strategien zum wesensgerechten Einsatz von Verkehrsmitteln im Güterverkehr der Schweiz TP A	2013
1438_2	SVI 2009/011	Ortsbezogene Massnahmen zur Reduktion der Auswirkungen des Güterverkehrs - Teil 2. Forschungspaket UVEK/ASTRA Strategien zum wesensgerechten Einsatz der Verkehrsmittel im Güterverkehr der Schweiz TP H	2013

Bericht-Nr.	Projekt Nr.	Titel	Jahr
1438_1	SVI 2009/011	Ortsbezogene Massnahmen zur Reduktion der Auswirkungen des Güterverkehrs - Teil 1. Forschungspaket UVEK/ASTRA Strategien zum wesensgerechten Einsatz der Verkehrsmittel im Güterverkehr der Schweiz TP H	2013
1437	VSS 2008/203	Trottoirüberfahrten und punktuelle Querungen ohne Vortritt für den Langsamverkehr	2013
1436	VSS 2010/401	Auswirkungen verschiedener Recyclinganteile in ungebundenen Gemischen	2013
1435	FGU 2008/007_OBF	Schadstoff- und Rauchkurzschlüsse bei Strassentunneln	2013
1434	VSS 2006/503	Performance Oriented Requirements for Bitumainous Mixtures	2013
1433	ASTRA 2010/001	Güterverkehr mit Lieferwagen: Entwicklungen und Massnahmen Forschungspaket UVEK/ASTRA Strategien zum wesensgerechten Einsatz der Verkehrsmittel im Güterverkehr der Schweiz TP B3	2013
1432	ASTRA 2007/011	Praxis-Kalibrierung der neuen mobilen Grossversuchanlage MLS10 für beschleunigte Verkehrslastsimulation auf Strassenbelägen in der Schweiz	2013
1431	ASTRA 2011/015	TeVeNOx - Testing of SCR-Systems on HD-Vehicles	2013
1430	ASTRA 2009/004	Impact des conditions météorologiques extrêmes sur la chaussée	2013
1429	SVI 2009/009	Einschätzungen der Infrastrukturnutzer zur Weiterentwicklung des Regulativs Forschungspaket UVEK/ASTRA Strategien zum wesensgerechten Einsatz der Verkehrsmittel im Güterverkehr der Schweiz TP F	2013
1428	SVI 2010/005	Branchenspezifische Logistikkonzepte und Güterverkehrsaufkommen sowie deren Trends Forschungspaket UVEK/ASTRA Strategien zum wesensgerechten Einsatz der Verkehrsmittel im Güterverkehr der Schweiz TP B2	2013
1427	SVI 2006/002	Begegnungszonen - eine Werkschau mit Empfehlungen für die Realisierung	2013
1426	ASTRA 2010/025_OBF	Luftströmungsmessung in Strassentunneln	2013
1425	VSS 2005/401	Résistance à l'altération des granulats et des roches	2013
1424	ASTRA 2006/007	Optimierung der Baustellenplanung an Autobahnen	2013
1423	ASTRA 2010/012	Forschungspaket: Lärmarme Beläge innerorts EP3: Betrieb und Unterhalt lärmarmer Beläge	2013
1422	ASTRA 2011/006_OBF	Fracture processes and in-situ fracture observations in Gipskeuper	2013
1421	VSS 2009/901	Experimenteller Nachweis des vorgeschlagenen Raum- und Topologiemodells für die VM-Anwendungen in der Schweiz (MDATrafo)	2013
1420	SVI 2008/003	Projektierungsfreiräume bei Strassen und Plätzen	2013
1419	VSS 2001/452	Stabilität der Polymere beim Heisseinbau von PmB-haltigen Strassenbelägen	2013
1418	VSS 2008/402	Anforderungen an hydraulische Eigenschaften von Geokunststoffen	2012
1417	FGU 2009/002	Heat Exchanger Anchors for Thermo-active Tunnels	2013
1416	FGU 2010/001	Sulfatwiderstand von Beton: verbessertes Verfahren basierend auf der Prüfung nach SIA 262/1, Anhang D	2013
1415	VSS 2010/A01	Wissenslücken im Infrastrukturmanagementprozess "Strasse" im Siedlungsgebiet	2013
1414	VSS 2010/201	Passive Sicherheit von Tragkonstruktionen der Strassenausstattung	2013
1413	SVI 2009/003	Güterverkehrsintensive Branchen und Güterverkehrsströme in der Schweiz Forschungspaket UVEK/ASTRA Strategien zum wesensgerechten Einsatz der Verkehrsmittel im Güterverkehr der Schweiz Teilprojekt B1	2013
1412	ASTRA 2010/020	Werkzeug zur aktuellen Gangliniennorm	2013
1411	VSS 2009/902	Verkehrstelematik für die Unterstützung des Verkehrsmanagements in ausserordentlichen Lagen	2013
1410	VSS 2010/202_OBF	Reduktion von Unfallfolgen bei Bränden in Strassentunneln durch Abschnittsbildung	2013
1409	ASTRA 2010/017_OBF	Regelung der Luftströmung in Strassentunneln im Brandfall	2013
1408	VSS 2000/434	Vieillissement thermique des enrobés bitumineux en laboratoire	2012
1407	ASTRA 2006/014	Fusion des indicateurs de sécurité routière : FUSAIN	2012
1406	ASTRA 2004/015	Amélioration du modèle de comportement individuell du Conducteur pour évaluer la sécurité d'un flux de trafic par simulation	2012
1405	ASTRA 2010/009	Potential von Photovoltaik an Schallschutzmassnahmen entlang der Nationalstrassen	2012
1404	VSS 2009/707	Validierung der Kosten-Nutzen-Bewertung von Fahrbahn-Erhaltungsmassnahmen	2012

Bericht-Nr.	Projekt Nr.	Titel	Jahr
1403	SVI 2007/018	Vernetzung von HLS- und HVS-Steuerungen	2012
1402	VSS 2008/403	Witterungsbeständigkeit und Durchdrückverhalten von Geokunststoffen	2012
1401	SVI 2006/003	Akzeptanz von Verkehrsmanagementmassnahmen-Vorstudie	2012
1400	VSS 2009/601	Begrünte Stützgitterböschungssysteme	2012
1399	VSS 2011/901	Erhöhung der Verkehrssicherheit durch Incentivierung	2012
1398	ASTRA 2010/019	Environmental Footprint of Heavy Vehicles Phase III: Comparison of Footprint and Heavy Vehicle Fee (LSVA) Criteria	2012
1397	FGU 2008/003_OBF	Brandschutz im Tunnel: Schutzziele und Brandbemessung Phase 1: Stand der Technik	2012
1396	VSS 1999/128	Einfluss des Umhüllungsgrades der Mineralstoffe auf die mechanischen Eigenschaften von Mischgut	2012
1395	FGU 2009/003	KarstALEA: Wegleitung zur Prognose von karstspezifischen Gefahren im Untertagbau	2012
1394	VSS 2010/102	Grundlagen Betriebskonzepte	2012
1393	VSS 2010/702	Aktualisierung SN 640 907, Kostengrundlage im Erhaltungsmanagement	2012
1392	ASTRA 2008/008_009	FEHRL Institutes WIM Initiative (Fiwi)	2012
1391	ASTRA 2011/003	Leitbild ITS-CH Landverkehr 2025/30	2012
1390	FGU 2008/004_OBF	Einfluss der Grundwasserströmung auf das Quellverhalten des Gipskeupers im Bel-chentunnel	2012
1389	FGU 2003/002	Long Term Behaviour of the Swiss National Road Tunnels	2012
1388	SVI 2007/022	Möglichkeiten und Grenzen von elektronischen Busspuren	2012
1387	VSS 2010/205_OBF	Ablage der Prozessdaten bei Tunnel-Prozessleitsystemen	2012
1386	VSS 2006/204	Schallreflexionen an Kunstbauten im Strassenbereich	2012
1385	VSS 2004/703	Bases pour la révision des normes sur la mesure et l'évaluation de la planéité des chaussées	2012
1384	VSS 1999/249	Konzeptuelle Schnittstellen zwischen der Basisdatenbank und EMF-, EMK- und EMT-DB	2012
1383	FGU 2008/005	Einfluss der Grundwasserströmung auf das Quellverhalten des Gipskeupers im Chien-bergtunnel	2012
1382	VSS 2001/504	Optimierung der statischen Eindringtiefe zur Beurteilung von harten Gussasphaltsorten	2012
1381	SVI 2004/055	Nutzen von Reisezeiteinsparungen im Personenverkehr	2012
1380	ASTRA 2007/009	Wirkungsweise und Potential von kombinierter Mobilität	2012
1379	VSS 2010/206_OBF	Harmonisierung der Abläufe und Benutzeroberflächen bei Tunnel-Prozessleitsystemen	2012
1378	SVI 2004/053	Mehr Sicherheit dank Kernfahrbahnen?	2012
1377	VSS 2009/302	Verkehrssicherheitsbeurteilung bestehender Verkehrsanlagen (Road Safety Inspection)	2012
1376	ASTRA 2011/008_004	Erfahrungen im Schweizer Betonbrückenbau	2012
1375	VSS 2008/304	Dynamische Signalisierungen auf Hauptverkehrsstrassen	2012
1374	FGU 2004/003	Entwicklung eines zerstörungsfreien Prüfverfahrens für Schweissnähte von KDB	2012
1373	VSS 2008/204	Vereinheitlichung der Tunnelbeleuchtung	2012
1372	SVI 2011/001	Verkehrssicherheitsgewinne aus Erkenntnissen aus Datapooling und strukturierten Datenanalysen	2012
1371	ASTRA 2008/017	Potenzial von Fahrgemeinschaften	2011
1370	VSS 2008/404	Dauerhaftigkeit von Betonfahrbahnen aus Betongranulat	2011
1369	VSS 2003/204	Rétention et traitement des eaux de chaussée	2012
1368	FGU 2008/002	Soll sich der Mensch dem Tunnel anpassen oder der Tunnel dem Menschen?	2011
1367	VSS 2005/801	Grundlagen betreffend Projektierung, Bau und Nachhaltigkeit von Anschlussgleisen	2011
1366	VSS 2005/702	Überprüfung des Bewertungshintergrundes zur Beurteilung der Strassengriffigkeit	2010
1365	SVI 2004/014	Neue Erkenntnisse zum Mobilitätsverhalten dank Data Mining?	2011
1364	SVI 2009/004	Regulierung des Güterverkehrs Auswirkungen auf die Transportwirtschaft Forschungspaket UVEK/ASTRA Strategien zum wesensgerechten Einsatz der Ver-kehrsmittel im Güterverkehr der Schweiz TP D	2012
1363	VSS 2007/905	Verkehrsprognosen mit Online -Daten	2011

Bericht-Nr.	Projekt Nr.	Titel	Jahr
1362	SVI 2004/012	Aktivitätenorientierte Analyse des Neuverkehrs	2012
1361	SVI 2004/043	Innovative Ansätze der Parkraumbewirtschaftung	2012
1360	VSS 2010/203	Akustische Führung im Strassentunnel	2012
1359	SVI 2004/003	Wissens- und Technologientransfer im Verkehrsbereich	2012
1358	SVI 2004/079	Verkehrsanbindung von Freizeitanlagen	2012
1357	SVI 2007/007	Unaufmerksamkeit und Ablenkung: Was macht der Mensch am Steuer?	2012
1356	SVI 2007/014	Kooperation an Bahnhöfen und Haltestellen	2011
1355	FGU 2007/002	Prüfung des Sulfatwiderstandes von Beton nach SIA 262/1, Anhang D: Anwendbarkeit und Relevanz für die Praxis	2011
1354	VSS 2003/203	Anordnung, Gestaltung und Ausführung von Treppen, Rampen und Treppenwegen	2011
1353	VSS 2000/368	Grundlagen für den Fussverkehr	2011
1352	VSS 2008/302	Fussgängerstreifen (Grundlagen)	2011
1351	ASTRA 2009/001	Development of a best practice methodology for risk assessment in road tunnels	2011
1350	VSS 2007/904	IT-Security im Bereich Verkehrstelematik	2011
1349	VSS 2003/205	In-Situ-Abflussversuche zur Untersuchung der Entwässerung von Autobahnen	2011
1348	VSS 2008/801	Sicherheit bei Parallelführung und Zusammentreffen von Strassen mit der Schiene	2011
1347	VSS 2000/455	Leistungsfähigkeit von Parkierungsanlagen	2010
1346	ASTRA 2007/004	Quantifizierung von Leckagen in Abluftkanälen bei Strassentunneln mit konzentrierter Rauchabsaugung	2010
1345	SVI 2004/039	Einsatzbereiche verschiedener Verkehrsmittel in Agglomerationen	2011
1344	VSS 2009/709	Initialprojekt für das Forschungspaket "Nutzensteigerung für die Anwender des SIS"	2011
1343	VSS 2009/903	Basistechnologien für die intermodale Nutzungserfassung im Personenverkehr	2011
1342	FGU 2005/003	Untersuchungen zur Frostkörperbildung und Frosthebung beim Gefrierverfahren	2010
1341	FGU 2007/005	Design aids for the planning of TBM drives in squeezing ground	2011
1340	SVI 2004/051	Aggressionen im Verkehr	2011
1339	SVI 2005/001	Widerstandsfunktionen für Innerorts-Strassenabschnitte ausserhalb des Einflussbereiches von Knoten	2010
1338	VSS 2006/902	Wirkungsmodelle für fahrzeugseitige Einrichtungen zur Steigerung der Verkehrssicherheit	2009
1337	ASTRA 2006/015	Development of urban network travel time estimation methodology	2011
1336	ASTRA 2007/006	SPIN-ALP: Scanning the Potential of Intermodal Transport on Alpine Corridors	2010
1335	VSS 2007/502	Stripping bei lärmmindernden Deckschichten unter Überrollbeanspruchung im Labormassstab	2011
1334	ASTRA 2009/009	Was treibt uns an? Antriebe und Treibstoffe für die Mobilität von Morgen	2011
1333	SVI 2007/001	Standards für die Mobilitätsversorgung im peripheren Raum	2011
1332	VSS 2006/905	Standardisierte Verkehrsdaten für das verkehrsträgerübergreifende Verkehrsmanagement	2011
1331	VSS 2005/501	Rückrechnung im Strassenbau	2011
1330	FGU 2008/006	Energiegewinnung aus städtischen Tunneln: Systemeevaluation	2010
1329	SVI 2004/073	Alternativen zu Fussgängerstreifen in Tempo-30-Zonen	2010
1328	VSS 2005/302	Grundlagen zur Quantifizierung der Auswirkungen von Sicherheitsdefiziten	2011
1327	VSS 2006/601	Vorhersage von Frost und Nebel für Strassen	2010
1326	VSS 2006/207	Erfolgskontrolle Fahrzeugrückhaltesysteme	2011
1325	SVI 2000/557	Indices caractéristiques d'une cité-vélo. Méthode d'évaluation des politiques cyclables en 8 indices pour les petites et moyennes communes.	2010
1324	VSS 2004/702	Eigenheiten und Konsequenzen für die Erhaltung der Strassenverkehrsanlagen im überbauten Gebiet	2009
1323	VSS 2008/205	Ereignisdetektion im Strassentunnel	2011
1322	SVI 2005/007	Zeitwerte im Personenverkehr: Wahrnehmungs- und Distanzabhängigkeit	2008
1321	VSS 2008/501	Validation de l'oedomètre CRS sur des échantillons intacts	2010

Bericht-Nr.	Projekt Nr.	Titel	Jahr
1320	VSS 2007/303	Funktionale Anforderungen an Verkehrserfassungssysteme im Zusammenhang mit Lichtsignalanlagen	2010
1319	VSS 2000/467	Auswirkungen von Verkehrsberuhigungsmassnahmen auf die Lärmimmissionen	2010
1318	FGU 2006/001	Langzeitquellversuche an anhydritführenden Gesteinen	2010
1317	VSS 2000/469	Geometrisches Normalprofil für alle Fahrzeugtypen	2010
1316	VSS 2001/701	Objektorientierte Modellierung von Strasseninformationen	2010
1315	VSS 2006/904	Abstimmung zwischen individueller Verkehrsinformation und Verkehrsmanagement	2010
1314	VSS 2005/203	Datenbank für Verkehrsaufkommensraten	2008
1313	VSS 2001/201	Kosten-/Nutzenbetrachtung von Strassenentwässerungssystemen, Ökobilanzierung	2010
1312	SVI 2004/006	Der Verkehr aus Sicht der Kinder: Schulwege von Primarschulkindern in der Schweiz	2010
1311	VSS 2000/543	VIABILITE DES PROJETS ET DES INSTALLATIONS ANNEXES	2010
1310	ASTRA 2007/002	Beeinflussung der Luftströmung in Strassentunneln im Brandfall	2010
1309	VSS 2008/303	Verkehrsregelungssysteme - Modernisierung von Lichtsignalanlagen	2010
1308	VSS 2008/201	Hindernisfreier Verkehrsraum - Anforderungen aus Sicht von Menschen mit Behinderung	2010
1307	ASTRA 2006/002	Entwicklung optimaler Mischgüter und Auswahl geeigneter Bindemittel; D-A-CH - Initialprojekt	2008
1306	ASTRA 2008/002	Strassenglätte-Prognosesystem (SGPS)	2010
1305	VSS 2000/457	Verkehrserzeugung durch Parkierungsanlagen	2009
1304	VSS 2004/716	Massnahmenplanung im Erhaltungsmanagement von Fahrbahnen	2008
1303	ASTRA 2009/010	Geschwindigkeiten in Steigungen und Gefällen; Überprüfung	2010
1302	VSS 1999/131	Zusammenhang zwischen Bindemitteleigenschaften und Schadensbildern des Belages?	2010
1301	SVI 2007/006	Optimierung der Strassenverkehrsunfallstatistik durch Berücksichtigung von Daten aus dem Gesundheitswesen	2009
1300	VSS 2003/903	SATELROU Perspectives et applications des méthodes de navigation pour la télématique des transports routiers et pour le système d'information de la route	2010
1299	VSS 2008/502	Projet initial - Enrobés bitumineux à faibles impacts énergétiques et écologiques	2009
1298	ASTRA 2007/012	Griffigkeit auf winterlichen Fahrbahnen	2010
1297	VSS 2007/702	Einsatz von Asphaltbewehrungen (Asphalteinlagen) im Erhaltungsmanagement	2009
1296	ASTRA 2007/008	Swiss contribution to the Heavy-Duty Particle Measurement Programme (HD-PMP)	2010
1295	VSS 2005/305	Entwurfsgrundlagen für Lichtsignalanlagen und Leitfaden	2010
1294	VSS 2007/405	Wiederhol- und Vergleichspräzision der Druckfestigkeit von Gesteinskörnungen am Haufwerk	2010
1293	VSS 2005/402	Détermination de la présence et de l'efficacité de dope dans les bétons bitumineux	2010
1292	ASTRA 2006/004	Entwicklung eines Pflanzenöl-Blockheizkraftwerkes mit eigener Ölmühle	2010
1291	ASTRA 2009/005	Fahrmuster auf überlasteten Autobahnen Simultanes Berechnungsmodell für das Fahrverhalten auf Autobahnen als Grundlage für die Berechnung von Schadstoffemissionen und Fahrzeitgewinnen	2010
1290	VSS 1999/209	Conception et aménagement de passages inférieurs et supérieurs pour piétons et deux-roues légers	2008
1289	VSS 2005/505	Affinität von Gesteinskörnungen und Bitumen, nationale Umsetzung der EN	2010
1288	ASTRA 2006/020	Footprint II - Long Term Pavement Performance and Environmental Monitoring on A1	2010
1287	VSS 2008/301	Verkehrsqualität und Leistungsfähigkeit von komplexen ungesteuerten Knoten: Analytisches Schätzverfahren	2009
1286	VSS 2000/338	Verkehrsqualität und Leistungsfähigkeit auf Strassen ohne Richtungstrennung	2010
1285	VSS 2002/202	In-situ Messung der akustischen Leistungsfähigkeit von Schallschirmen	2009
1284	VSS 2004/203	Evacuation des eaux de chaussée par les bas-cotés	2010

Bericht-Nr.	Projekt Nr.	Titel	Jahr
1283	VSS 2000/339	Grundlagen für eine differenzierte Bemessung von Verkehrsanlagen	2008
1282	VSS 2004/715	Massnahmenplanung im Erhaltungsmanagement von Fahrbahnen: Zusatzkosten infolge Vor- und Aufschub von Erhaltungsmassnahmen	2010
1281	SVI 2004/002	Systematische Wirkungsanalysen von kleinen und mittleren Verkehrsvorhaben	2009
1280	ASTRA 2004/016	Auswirkungen von fahrzeuginternen Informationssystemen auf das Fahrverhalten und die Verkehrssicherheit Verkehrspsychologischer Teilbericht	2010
1279	VSS 2005/301	Leistungsfähigkeit zweistreifiger Kreisel	2009
1278	ASTRA 2004/016	Auswirkungen von fahrzeuginternen Informationssystemen auf das Fahrverhalten und die Verkehrssicherheit - Verkehrstechnischer Teilbericht	2009
1277	SVI 2007/005	Multimodale Verkehrsqualitätsstufen für den Strassenverkehr - Vorstudie	2010
1276	VSS 2006/201	Überprüfung der schweizerischen Ganglinien	2008
1275	ASTRA 2006/016	Dynamic Urban Origin - Destination Matrix - Estimation Methodology	2009
1274	SVI 2004/088	Einsatz von Simulationswerkzeugen in der Güterverkehrs- und Transportplanung	2009
1273	ASTRA 2008/006	UNTERHALT 2000 - Massnahme M17, FORSCHUNG: Dauerhafte Materialien und Verfahren SYNTHESE - BERICHT zum Gesamtprojekt "Dauerhafte Beläge" mit den Einzelnen Forschungsprojekten: - ASTRA 200/419: Verhaltensbilanz der Beläge auf Nationalstrassen - ASTRA 2000/420: Dauerhafte Komponenten auf der Basis erfolgreicher Strecken - ASTRA 2000/421: Durabilité des enrobés - ASTRA 2000/422: Dauerhafte Beläge, Rundlaufversuch - ASTRA 2000/423: Griffigkeit der Beläge auf Autobahnen, Vergleich zwischen den Messergebnissen von SRM und SCRIM - ASTRA 2008/005: Vergleichsstrecken mit unterschiedlichen oberen Tragschichten auf einer Nationalstrasse	2008
1272	VSS 2007/304	Verkehrsregelungssysteme - behinderte und ältere Menschen an Lichtsignalanlagen	2010
1271	VSS 2004/201	Unterhalt von Lärmschirmen	2009
1270	VSS 2005/502	Interaktion Strasse Hangstabilität: Monitoring und Rückwärtsrechnung	2009
1269	VSS 2005/201	Evaluation von Fahrzeugrückhaltesystemen im Mittelstreifen von Autobahnen	2009
1268	ASTRA 2005/007	PM10-Emissionsfaktoren von Abriebspartikeln des Strassenverkehrs (APART)	2009
1267	VSS 2007/902	MDAinSVT Einsatz modellbasierter Datentransfernormen (INTERLIS) in der Strassenverkehrstelematik	2009
1266	VSS 2000/343	Unfall- und Unfallkostenraten im Strassenverkehr	2009
1265	VSS 2005/701	Zusammenhang zwischen dielektrischen Eigenschaften und Zustandsmerkmalen von bitumenhaltigen Fahrbahnbelägen (Pilotuntersuchung)	2009
1264	SVI 2004/004	Verkehrspolitische Entscheidfindung in der Verkehrsplanung	2009
1263	VSS 2001/503	Phénomène du dégel des sols gélifs dans les infrastructures des voies de communication et les pergélisols alpins	2006
1262	VSS 2003/503	Lärmverhalten von Deckschichten im Vergleich zu Gussasphalt mit strukturierter Oberfläche	2009
1261	ASTRA 2004/018	Pilotstudie zur Evaluation einer mobilen Grossversuchsanlage für beschleunigte Verkehrslastsimulation auf Strassenbelägen	2009
1260	FGU 2005/001	Testeinsatz der Methodik "Indirekte Vorauserkundung von wasserführenden Zonen mittels Temperaturdaten anhand der Messdaten des Lötschberg-Basistunnels	2009
1259	VSS 2004/710	Massnahmenplanung im Erhaltungsmanagement von Fahrbahnen - Synthesebericht	2008
1258	VSS 2005/802	Kaphaltestellen Anforderungen und Auswirkungen	2009
1257	SVI 2004/057	Wie Strassenraumbilder den Verkehr beeinflussen Der Durchfahrtswiderstand als Arbeitsinstrument bei der städtebaulichen Gestaltung von Strassenräumen	2009
1256	VSS 2006/903	Qualitätsanforderungen an die digitale Videobild-Bearbeitung zur Verkehrsüberwachung	2009

Bericht-Nr.	Projekt Nr.	Titel	Jahr
1255	VSS 2006/901	Neue Methoden zur Erkennung und Durchsetzung der zulässigen Höchstgeschwindigkeit	2009
1254	VSS 2006/502	Drains verticaux préfabriqués thermiques pour la consolidation in-situ des sols	2009
1253	VSS 2001/203	Rétention des polluants des eaux de chausées selon le système "infilitrations sur les talus". Vérification in situ et optimisation	2009
1252	SVI 2003/001	Nettoverkehr von verkehrsintensiven Einrichtungen (VE)	2009
1251	ASTRA 2002/405	Incidence des granulats arrondis ou partiellement arrondis sur les propriétés d'ahérence des bétons bitumineux	2008
1250	VSS 2005/202	Strassenabwasser Filterschacht	2007
1249	FGU 2003/004	Einflussfaktoren auf den Brandwiderstand von Betonkonstruktionen	2009
1248	VSS 2000/433	Dynamische Eindringtiefe zur Beurteilung von Gussasphalt	2008
1247	VSS 2000/348	Anforderungen an die strassenseitige Ausrüstung bei der Umwidmung von Standstreifen	2009
1246	VSS 2004/713	Massnahmenplanung im Erhaltungsmanagement von Fahrbahnen: Bedeutung Oberflächenzustand und Tragfähigkeit sowie gegenseitige Beziehung für Gebrauchs- und Substanzwert	2009
1245	VSS 2004/701	Verfahren zur Bestimmung des Erhaltungsbedarfs in kommunalen Strassennetzen	2009
1244	VSS 2004/714	Massnahmenplanung im Erhaltungsmanagement von Fahrbahnen - Gesamtnutzen und Nutzen-Kosten-Verhältnis von standardisierten Erhaltungsmassnahmen	2008
1243	VSS 2000/463	Kosten des betrieblichen Unterhalts von Strassenanlagen	2008
1242	VSS 2005/451	Recycling von Ausbauasphalt in Heissmischgut	2007
1241	ASTRA 2001/052	Erhöhung der Aussagekraft des LCPC Spurbildungstests	2009
1240	ASTRA 2002/010	L'acceptabilité du péage de congestion : Résultats et analyse de l'enquête en Suisse	2009
1239	VSS 2000/450	Bemessungsgrundlagen für das Bewehren mit Geokunststoffen	2009
1238	VSS 2005/303	Verkehrssicherheit an Tagesbaustellen und bei Anschlüssen im Baustellenbereich von Hochleistungsstrassen	2008
1237	VSS 2007/903	Grundlagen für eCall in der Schweiz	2009
1236	ASTRA 2008/008_07	Analytische Gegenüberstellung der Strategie- und Tätigkeitsschwerpunkte ASTRA-AIPCR	2008
1235	VSS 2004/711	Forschungspaket Massnahmenplanung im EM von Fahrbahnen - Standardisierte Erhaltungsmassnahmen	2008
1234	VSS 2006/504	Expérimentation in situ du nouveau drainomètre européen	2008
1233	ASTRA 2000/420	Unterhalt 2000 Forschungsprojekt FP2 Dauerhafte Komponenten bitumenhaltiger Belagsschichten	2009
660	AGB 2008/002	Indirekt gelagerte Betonbrücken - Sachstandsbericht	2014
659	AGB 2009/014	Suizidprävention bei Brücken: Follow-Up	2014
658	AGB 2006/015_OBF	Querkraftwiderstand vorgespannter Brücken mit ungenügender Querkraftbewehrung	2014
657	AGB 2003/012	Brücken in Holz: Möglichkeiten und Grenzen	2013
656	AGB 2009/015	Experimental verification oif integral bridge abutments	2013
655	AGB 2007/004	Fatigue Life Assessment of Roadway Bridges Based on Actual Traffic Loads	2013
654	AGB 2005-008	Thermophysical and Thermomechanical Behavior of Cold-Curing Structural Adhesives in Bridge Construction	2013
653	AGB 2007/002	Poinçonnement des pontsdalles précontraints	2013
652	AGB 2009/006	Detektion von Betonstahlbrüchen mit der magnetischen Streufeldmethode	2013
651	AGB 2006/006_OBF	Instandsetzung und Monitoring von AAR-geschädigten Stützmauern und Brücken	2013
650	AGB 2005/010	Korrosionsbeständigkeit von nichtrostenden Betonstählen	2012
649	AGB 2008/012	Anforderungen an den Karbonatisierungswiderstand von Betonen	2012
648	AGB 2005/023 + AGB 2006/003	Validierung der AAR-Prüfungen für Neubau und Instandsetzung	2011
647	AGB 2004/010	Quality Control and Monitoring of electrically isolated post- tensioning tendons in bridges	2011

Bericht-Nr.	Projekt Nr.	Titel	Jahr
646	AGB 2005/018	Interactin sol-structure : ponts à culées intégrales	2010
645	AGB 2005/021	Grundlagen für die Verwendung von Recyclingbeton aus Betongranulat	2010
644	AGB 2005/004	Hochleistungsfähiger Faserfeinkornbeton zur Effizienzsteigerung bei der Erhaltung von Kunstbauten aus Stahlbeton	2010
643	AGB 2005/014	Akustische Überwachung einer stark geschädigten Spannbetonbrücke und Zustand-serfassung beim Abbruch	2010
642	AGB 2002/006	Verbund von Spanngliedern	2009
641	AGB 2007/007	Empfehlungen zur Qualitätskontrolle von Beton mit Luftpermeabilitätsmessungen	2009
640	AGB 2003/011	Nouvelle méthode de vérification des ponts mixtes à âme pleine	2010
639	AGB 2008/003	RiskNow-Falling Rocks Excel-basiertes Werkzeug zur Risikoermittlung bei Steinschlag-schutzgalerien	2010
638	AGB2003/003	Ursachen der Rissbildung in Stahlbetonbauwerken aus Hochleistungsbeton und neue Wege zu deren Vermeidung	2008
637	AGB 2005/009	Détermination de la présence de chlorures à l'aide du Géoradar	2009
636	AGB 2002/028	Dimensionnement et vérification des dalles de roulement de ponts routiers	2009
635	AGB 2004/002	Applicabilité de l'enrobé drainant sur les ouvrages d'art du réseau des routes nationales	2008
634	AGB 2002/007	Untersuchungen zur Potenzialfeldmessung an Stahlbetonbauten	2008
633	AGB 2002/014	Oberflächenschutzsysteme für Betontragwerke	2008
632	AGB 2008/201	Sicherheit des Verkehrssystem Strasse und dessen Kunstbauten Testregion - Methoden zur Risikobeurteilung Schlussbericht	2010
631	AGB 2000/555	Applications structurales du Béton Fibré à Ultra-hautes Performances aux ponts	2008
630	AGB 2002/016	Korrosionsinhibitoren für die Instandsetzung chloridverseuchter Stahlbetonbauten	2010
629	AGB 2003/001 + AGB 2005/019	Integrale Brücken - Sachstandsbericht	2008
628	AGB 2005/026	Massnahmen gegen chlorid-induzierte Korrosion und zur Erhöhung der Dauerhaftigkeit	2008
627	AGB 2002/002	Eigenschaften von normalbreiten und überbreiten Fahrbahnübergängen aus Polymerbi-tumen nach starker Verkehrsbelastung	2008
626	AGB 2005/110	Sicherheit des Verkehrssystems Strasse und dessen Kunstbauten: Baustellensicherheit bei Kunstbauten	2009
625	AGB 2005/109	Sicherheit des Verkehrssystems Strasse und dessen Kunstbauten: Effektivität und Effizienz von Massnahmen bei Kunstbauten	2009
624	AGB 2005/108	Sicherheit des Verkehrssystems / Strasse und dessen Kunstbauten / Risikobeurteilung für Kunstbauten	2010
623	AGB 2005/107	Sicherheit des Verkehrssystems Strasse und dessen Kunstbauten: Tragsicherheit der bestehenden Kunstbauten	2009
622	AGB 2005/106	Rechtliche Aspekte eines risiko- und effizienzbasierten Sicherheitskonzepts	2009
621	AGB 2005/105	Sicherheit des Verkehrssystems Strasse und dessen Kunstbauten Szenarien der Gefahrenentwicklung	2009
620	AGB 2005/104	Sicherheit des Verkehrssystems Strasse und dessen Kunstbauten: Effektivität und Effizienz von Massnahmen	2009
619	AGB 2005/103	Sicherheit des Verkehrssystems / Strasse und dessen Kunstbauten / Ermittlung des Netzrisikos	2010
618	AGB 2005/102	Sicherheit des Verkehrssystems Strasse und dessen Kunstbauten: Methodik zur ver-gleichenden Risikobeurteilung	2009
617	AGB 2005/100	Sicherheit des Verkehrssystems Strasse und dessen Kunstbauten Synthesebericht	2010
616	AGB 2002/020	Beurteilung von Risiken und Kriterien zur Festlegung akzeptierter Risiken in Folge aussergewöhnlicher Einwirkungen bei Kunstbauten	2009